NASA Technical Memorandum 100464

Random Process Simulation For Stochastic Fatigue Analysis

Curtis E. Larsen

March 1988

NASA

Random Process Simulation For
Stochastic Fatigue Analysis

Curtis E. Larsen
Lyndon B. Johnson Space Center
Houston, Texas

TABLE OF CONTENTS

LIST OF TABLES

LIST OF FIGURES

LIST OF SYMBOLS

AR	Autoregressive
ARMA	Autoregressive Moving Average
a_t	Random variate in ARMA model
α_2	Bandwidth parameter, irregularly factor for Gaussian processes
b	2-block psd area ratio
C	Material constant
C_0	Estimate for σ_Z^2
d/d_0	Normalized damage rate
d_j	Fractional damage due to n_j cycles
d/t	Expected damage rate
$D(t)$	Total damage at time t
$E(\cdot)$	Mathematical expectation
$E[R^m]$	Rainflow stress range moment
$E[S^m]$	Theoretical stress range moment
erf(x)	Error function
erfc(x)	Complementary error function
$f_X(\cdot)$, $p_X(\cdot)$	Probability density function for X
$F_X(\cdot)$	Cumulative distribution function for X
G	Constant magnitude of psd
$G_X(\omega)$	1-sided psd, defined on $(0,\infty)$
$\Gamma(x)$	Gamma function
$\Gamma_{XX}(\tau)$	Autocovariance function, stationary processes
INT(r)	Largest integer $\leq$ r

LIST OF SYMBOLS - Con't.

$K_{XX}(t,s)$	Autocovariance function, general process
λ_j	j^{th} moment of psd
MA	Moving Average
m	Inverse of slope of logs-log N regression line
m_X, μ_X	Mean value of X
μ	Constant term in ARMA model
N	Number of cycles to failure in constant amplitude fatigue test
n_j	Number of cycles at amplitude S_j
n_p	Expected rate of peak occurrences
ν_b^+	Expected rate of up-crossings of level b
ω	Frequency, radians/second
ω_c	Cut-off frequency
P	Peak value
psd	Power spectral density
ϕ_i	Random phase angle
ϕ_p	AR parameter
$\hat{\phi}_p$	Estimate of AR parameter
$\Phi_{XX}(b,s)$	Autocorrelation function, general processes
q	Vanmarcke's bandwidth parameter
q/q_0	Frequency cut-off parameter
r	2-block psd frequency ratio
r_p	Estimate of ρ_p correlation
$R_{XX}(\tau)$	Autocorrelation function, stationary processes

LIST OF SYMBOLS - Con't.

ρ_1	Linear correlation coefficient between adjacent extrema
ρ_k	Linear correlation coefficient between extrema k time intervals apart
ρ_{PV}	Largest negative valued peak-to-valley correlation
S	Stress range in constant amplitude fatigue test
$S_{XX}(\omega)$	2-sided psd, defined on $(-\infty, \infty)$
σ_X^2	Variance of X
T	Time to failure
θ_q	MA parameter
u	Normalized cut-off frequency
V	Valley value
$X(t)$, Z_t	Random process value at time t
$\{X(t)\}$	Random process
$\{\dot{X}(t)\}$	First derivative process
$\{\ddot{X}(t)\}$	Second derivative process

CHAPTER 1

INTRODUCTION

Stochastic theory is a useful tool in the fatigue design of structures subject to erratic loads from environments such as wind, waves, earthquakes, etc. The random stress processes which result from such loads can be described by statistical parameters in models which characterize the material behavior based on laboratory fatigue tests. These models provide a probabilistic estimate of the number of cycles, or length of time, to failure of the structure.

Two approaches have been used in applying probability theory to fatigue life prediction. In the first, simplifying assumptions are made about the distribution of the extrema of the random stress process which results in a closed-form solution for the expected number of cycles or length of time to failure. The second approach computes the necessary statistics of the extrema distribution using a computer simulated random process which is statistically similar to the expected service stress time history.

In the past, the design engineer has typically chosen to use the first approach because it is an inexpensive, simple calculation which is generally thought to result in a conservative prediction of fatigue life. However, recent studies (5,21,41,43) have shown that this approach can often be very overconservative and uneconomical, and may even be unconservative for some cases.

The simulation technique is thought to give a more accurate prediction of fatigue life and generally to result in a more economical struc-

tural design, but it requires expensive computer time during the design and analysis.

This thesis is an investigation of a technique for more efficiently simulating a random stress time history for fatigue analysis. Current simulation techniques synthesize the complete random stress time history, while for fatigue analysis only statistics of the extrema are required. Thus, a significant reduction in computation time and cost could be realized if the correctly distributed extrema could be generated directly, without the need for superfluous intermediate values. Previous research by others (43) in this area resulted in such improved techniques applicable to simple, idealized cases. The present work examines an extrema generating technique which can be applied to a wider variety of more realistic cases. The development of this technique has led to new insights about which characteristics of a random stress process are important to the fatigue problem.

Chapter 2 is a brief review of some of the theory of stochastic processes and fatigue theory as it relates to this investigation. The most popular current simulation technique and the general theory behind the proposed technique are also discussed. The results of an extensive simulation study of extrema correlations and power spectral density truncation effects are presented in Chapter 3. A proposed extrema simulation technique for random processes having a unimodal power spectral density is discussed in Chapter 4. The adaptation of this technique to bimodal power spectral densities is described in Chapter 5. Chapter 6 summarizes the important results of this study.

CHAPTER 2

BACKGROUND

This chapter presents the background material in probability, fatigue, and simulation which relates to this investigation. Section 2.1 reviews the fundamentals of stochastic processes and the statistics which pertain to fatigue studies. Section 2.2 presents the concept of accumulated damage and the extension of constant amplitude fatigue theory to random fatigue. Section 2.3 introduces the simulation of stochastic processes, and section 2.4 presents the basic theory of the simulation technique studied in this investigation.

2.1 Stochastic Processes

A stochastic or random process $\{X(t)\}$ is a family or set of ordered random variables $X(t)$. The parameter t often denotes time in physical processes, but can also denote distance or location, or any parameter which orders the occurrence of the random variables. A random process is partially described by the probability density function (PDF) of $X(t)$, $p_X(t;u)$. The first two moments of $p_X(t;u)$ are the mean, $\mu_X(t)$, and variance, $\sigma_X^2(t)$, of the process. A more complete description of the process would include the joint distribution of $X(t)$ and $X(s)$, $p_{XX}(t,s;u,v)$, from which one can find the autocorrelation function, $\Phi_{XX}(t,s) \equiv E[X(t)X(s)]$, and the autocovariance function, $K_{XX}(t,s) \equiv \Phi_{XX}(t,s) - \mu_X(t)\mu_X(s)$. In general, a random process can only be completely described by knowledge of an infinite number of multivariate distributions.

A more intuitive definition of a random process is that it is the collection or ensemble of all the possible time histories one might

observe of a randomly varying quantity. An example would be the set of 5 minute wave records observed at an offshore platform. A single record from this set is but one realization from the infinite ensemble of possible records.

A random process is said to be stationary if the choice of the "time" origin can be made arbitrarily without effecting the statistics of interest. A particularly useful type of stationarity often assumed is covariant stationarity, defined by the conditions:

a) $\mu_X(t) = \mu_X = $ constant $\qquad\qquad$ (2-1)

b) $K_{XX}(t,s) = \Gamma_{XX}(s-t) = \Gamma_{XX}(\tau)$ $\qquad\qquad$ (2-2)

The second condition above describes a "shift" property for the autocovariance: the value of the autocovariance depends only on the time interval between points, $s-t = \tau$, and not on the individual times of occurrence. These two conditions imply that the autocorrelation function also exhibits the "shift" property:

c) $\Phi_{XX}(t,s) = R_{XX}(s-t) = R_{XX}(\tau)$ $\qquad\qquad$ (2-3)

A stationary random process is referred to as being ergodic if averages taken in the time domain for a single realization converge to the corresponding statistical averages taken across the entire ensemble. That is, one infinite length realization of the process completely describes the entire ensemble. A stationary process is usually assumed to be ergodic, unless it is obviously not ergodic.

The information contained in the autocorrelation function, $R_{XX}(\tau)$, of a mean-zero, covariant stationary process is often expressed in

4

a different form as the power spectral density, (psd), of the process (20,22). The psd $S_{XX}(\omega)$ is the Fourier transform of $R_{XX}(\tau)$:

$$S_{XX}(\omega) = \frac{1}{2\pi} \int_{-\infty}^{\infty} R_{XX}(\tau)e^{-i\omega\tau} \, d\tau \tag{2-4}$$

The inverse transformation is:

$$R_{XX}(\tau) = \int_{-\infty}^{\infty} S_{XX}(\omega)e^{i\omega\tau} \, d\omega \tag{2-5}$$

Note that in these equations and those which follow, $S_{XX}(\omega)$ is the two-sided psd defined on $(-\infty, +\infty)$, while the one-sided psd, defined on $(0, +\infty)$, is given by $G_X(\omega) = 2S_{XX}(\omega)$. The variance of the process, σ_X^2, is given by the autocorrelation at $\tau = 0$, or the area under the psd:

$$\sigma_X^2 = E[X^2] = R_{XX}(0) = \int_{-\infty}^{\infty} S_{XX}(\omega)d\omega \tag{2-6}$$

The variance of the first two derivatives of $\{X(t)\}$ are given by:

$$\sigma_{\dot{X}}^2 = \int_{-\infty}^{\infty} \omega^2 S_{XX}(\omega)d\omega \tag{2-7}$$

$$\sigma_{\ddot{X}}^2 = \int_{-\infty}^{\infty} \omega^4 S_{XX}(\omega)d\omega \tag{2-8}$$

The expected number of up-crossings per unit time of the level b by $\{X(t)\}$ was derived by S.O. Rice (32) as:

$$\nu_b^+ = \int_0^{\infty} v \, p_{X\dot{X}}(b,v)dv \tag{2-9}$$

in which $p_{X\dot{X}}(u,v)$ is the joint PDF of $\{X(t)\}$ and $\{\dot{X}(t)\}$ at time t.

The rate of up-crossings of the mean (or zero up-crossings) is then:

$$\nu_0^+ = \int_0^{\infty} v p_{X\dot{X}}(0,v)dv \tag{2-10}$$

5

The above result leads to an expression for the expected number of valleys (or peaks) per unit time of $\{X(t)\}$ as:

$$n_p = \int_0^\infty w p_{\dot{X}\ddot{X}}(0,w)\,dw \tag{2-11}$$

The ratio of the rate of zero up-crossings to the rate of peak occurrences, ν_0^+/n_p, is a common measure of bandwidth known as the irregularity factor. The value of the irregularity factor is always between 0 and 1 (because $n_p \geq \nu_0^+$), and approaches 1 for a very narrowband process as the number of peaks approaches the number of zero up-crossings.

A random process $\{X(t)\}$ is said to be Gaussian (or normal) if the set $\{X(t_1), X(t_2), \cdots X(t_n)\}$ is a set of jointly normal random variables for any choice of n and $(t_1, t_2, \cdots t_n)$. This implies that a Gaussian random process is completely described by its mean, $\mu_X(t)$, and autocovariance, $K_{XX}(t,s)$. Further, it can be shown that $\{\dot{X}(t)\}$ will also be a normal process and that $\{X(t)\}$ and $\{\dot{X}(t)\}$ are jointly normal processes. If the Gaussian process $\{X(t)\}$ is also assumed to be covariant stationary, then $X(t)$ and $\dot{X}(t)$ are independent random variables.

Random processes are often assumed to be Gaussian or normal in random vibration problems because analytical manipulations are relatively easy and many actual excitations can be well approximated as being Gaussian.

Assuming that $\{X(t)\}$ is Gaussian (in addition to mean-zero, covariant stationary) enables one to evaluate the expressions for ν_0^+ and n_p as (7,20,23):

6

$$\nu_o^+ = \frac{1}{2\pi} \frac{\sigma_{\dot{X}}}{\sigma_X} \tag{2-12}$$

$$n_p = \frac{1}{2\pi} \frac{\sigma_{\ddot{X}}}{\sigma_{\dot{X}}} \tag{2-13}$$

This yields an expression for the irregularity factor of a Gaussian process:

$$\frac{\nu_o^+}{n_p} = \frac{\sigma_{\dot{X}}^2}{\sigma_X \, \sigma_{\ddot{X}}} \tag{2-14}$$

The irregularity factor, as defined by ν_o^+/n_p, is a time domain measure of the bandwidth of a random process. A set of frequency domain bandwidth parameters may be defined by the equation:

$$\alpha_j = \frac{\lambda_j}{[\lambda_o \lambda_{2j}]^{1/2}} \tag{2-15}$$

in which λ_j is the jth moment of the psd:

$$\lambda_j = \int_{-0}^{\infty} \omega^j G_X(\omega) d\omega \tag{2-16}$$

It can be shown that for any $j > 0$, $0 \leq \alpha_j \leq 1$, with α_j approaching 1 for the limiting narrowband case. Recalling equations (2-6), (2-7) and (2-8), the bandwidth parameter α_2 from this family is given by:

$$\alpha_2 = \frac{\lambda_2}{[\lambda_o \lambda_4]^{1/2}} = \frac{\sigma_{\dot{X}}^2}{\sigma_X \sigma_{\ddot{X}}} \tag{2-17}$$

Thus, for a covariant stationary, Gaussian process, $\alpha_2 = \nu_o^+/n_p$, and the irregularity factor has both a time and a frequency domain definition.

Another commonly used bandwidth parameter related to the α_j family is the parameter q proposed by Vanmarcke (40):

$$q = [1 - \alpha_1^2]^{1/2} = [1 - \frac{\lambda_1^2}{\lambda_0 \lambda_2}]^{1/2} \tag{2-18}$$

The values of q are also bounded by [0,1], but q approaches zero for the limiting narrowband case. Vanmarcke showed that this parameter also has a time domain interpretation. Based on the definition of the envelope of a random process used by Cramer and Leadbetter (6) and S.O. Rice (32), q can be defined in the time domain as:

$$q = \frac{\sigma_{\dot{R}}}{\sigma_{\dot{X}}} \tag{2-19}$$

in which:

$\sigma_{\dot{X}}$ = The rms of the slope of the process

$\sigma_{\dot{R}}$ = The rms of the slope of its envelope

Thus, q is the ratio of the rate of change of the envelope to the rate of change of the process. This interpretation breaks down for wideband processes as the envelope is no longer physically recognizable.

For a Gaussian random process, the probability density function (pdf) and cumulative distribution function (cdf) of the extrema (peaks or valleys) were derived by S.O. Rice (32) as:

$$\text{PDF: } f_p(u) = \frac{u\alpha_2}{2\sigma_X^2} [1 + \text{erf} (\frac{u\alpha_2}{\sigma_X(2 - 2\alpha_2^2)^{1/2}})] \exp(\frac{-u^2}{2\sigma_X^2})$$

$$+ (\frac{1-\alpha_2^2}{2\pi\sigma_X^2})^{1/2} \exp(\frac{-u^2}{2\sigma_X^2(1-\alpha_2^2)}) \qquad -\infty < u < \infty \tag{2-20}$$

8

$$\text{CDF: } F_p(u) = \frac{1}{2} \, erfc\left[\frac{-u}{(2-2\alpha_2^2)^{1/2}\sigma_X}\right]$$

$$- \frac{\alpha_2}{2} \, exp\left(\frac{-u^2}{2\sigma_X^2}\right) erfc\left[\frac{-u\,\alpha_2}{(2-2\alpha_2^2)^{1/2}\sigma_X}\right] \tag{2-21}$$

in which erf is the error function:

$$erf(u) = \frac{2}{\sqrt{\pi}} \int_0^u e^{-t^2} \, dt \tag{2-22a}$$

$$erf(\infty) = 1.0 \tag{2.22b}$$

and erfc is the complementary error function:

$$erfc(u) = 1 - erf(u) \tag{2-23}$$

The S.O. Rice distribution is a function of only the standard deviation of the process, σ_X, and the bandwidth of the process as defined by the irregularity factor, α_2. The cumulative distribution function (cdf), $F_p(u)$, gives the fraction of all peaks which have values less than u, including negative as well as positive peaks. The fraction of positive peaks is $(1 + \alpha_2)/2$ and the rate at which they occur is:

$$n_p^+ = n_p\left(\frac{1 + \alpha_2}{2}\right) = \frac{(1 + \alpha_2)}{4\pi} \frac{\sigma_{\ddot{X}}}{\sigma_{\dot{X}}} \tag{2-24}$$

In the limiting narrowband case $(\alpha_2 \to 1)$ all of the peaks are positive and the S.O. Rice distribution reduces to the Rayleigh distribution:

$$f_p(u) = \frac{u}{\sigma_X^2} \, exp\left(\frac{-u^2}{2\sigma_X^2}\right) \qquad o < u < \infty \tag{2-25}$$

For the limiting wideband process $(\alpha_2 \to 0)$ only one-half of the peaks are positive and the S.O. Rice distribution reduces to the Gaussian distribution:

$$f_p(u) = \frac{1}{(2\pi)^{1/2}\sigma_X} \exp(\frac{-u^2}{2\sigma_X^2}) \qquad -\infty < u < \infty \qquad (2\text{-}26)$$

2.2 Concepts in Fatigue

The results of a laboratory constant amplitude fatigue test are usually presented in the form of a plot of the logarithm of the stress range, S, versus the logarithm of the number of cycles to failure, N, as in Figure 2.1. The test data is usually best fit by a straight line, the S-N curve, given by the equation:

$$N = CS^{-m} \qquad (2\text{-}27)$$

in which C and m are material constants. The S-N curve for ferrous materials tails off at some low stress range known as the endurance limit. This is the stress range at or below which the material is treated as having an infinite fatigue life. Non-ferrous materials generally do not exhibit an endurance limit.

The Palmgren-Miner hypothesis (26,27) gives one technique for extending the constant amplitude results to the variable amplitude case. Each single cycle of stress range S_j is assumed to cause damage equal to the average damage per cycle in the constant amplitude test, $1/N(S_j)$. A number of cycles, n_j, at amplitude S_j then use a fraction of the fatigue life or cause the fractional amount of damage, d_j:

$$d_j = \frac{n_j}{N(S_j)} \qquad \text{at stress range } S_j \qquad (2\text{-}28)$$

The total fraction of damage at time t, D(t) due to all the cycles in a variable amplitude time history is then found by summing over all the stress ranges:
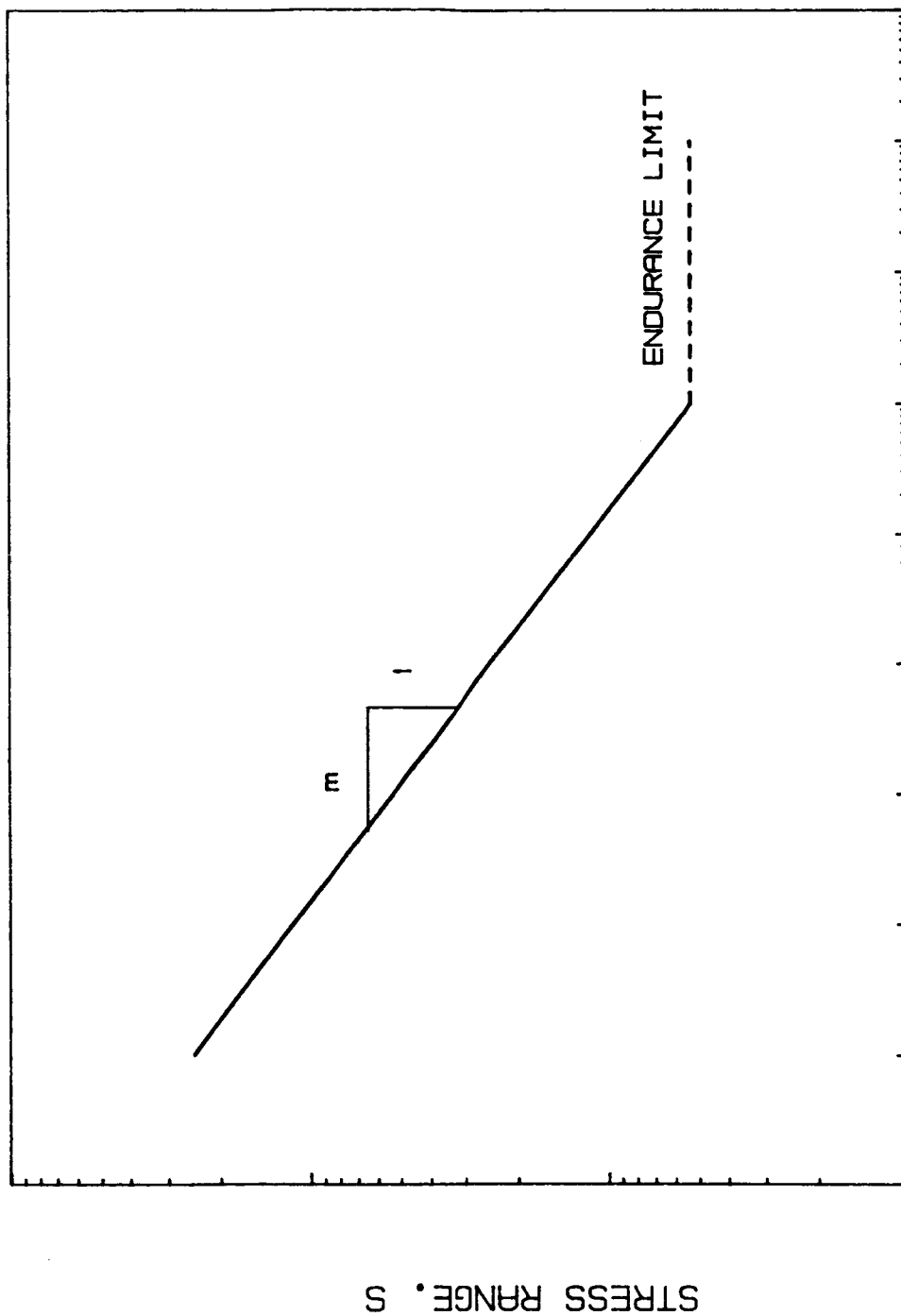
CYCLES TO FAILURE. N

Figure 2.1 Typical S-N Curve

STRESS RANGE. S

11

$$D(t) = \sum_j \frac{n_j}{N(S_j)} \tag{2-29}$$

in which $D(T) = 1$ at failure, T being the time to failure. Extending this to the continuous case, the expected damage at the time t is given by:

$$E[D(t)] = N^*(t) \int_0^\infty \frac{p_s(u)du}{N(u)} \tag{2-30}$$

in which $N^*(t)$ denotes the expected total number of cycles in time t in a random fatigue test, and $N^*(t)p_s(u)du$ denotes the number of cycles in the stress range $[u, u + du]$. Assuming that $N(u) = Cu^{-m}$ from the constant amplitude S-N curve, equation 2-30 may be written as:

$$E[D(t)] = \frac{N^*(t)}{C} \int_0^\infty u^m p_s(u)du \tag{2-31}$$

$$= \frac{N^*(t)}{C} E[S^m]$$

in which $E[S^m]$ is the mth moment of the random stress range distribution.

The Rayleigh approximation (25) assumes that a stress range can be defined as twice a Rayleigh distribution amplitude. This assumption, which is strictly correct only in the limiting narrowband case, leads to a closed form solution given by:

$$E[D(t)] = \frac{N^*(t)}{C} (2\sqrt{2} \, \sigma_X)^m \Gamma (1 + m/2) \tag{2-32}$$

$$= 1 \text{ at failure, } t = T$$

in which $\Gamma(x)$ denotes the Gamma function.

The expected time to failure, $E[T]$, is calculated by defining a cycle as the time between zero up-crossings of the stress process. This may be written as:

$$E[T] = \frac{N^*(T)}{\nu_0^+} = \frac{C}{\nu_0^+} \frac{1}{(2\sqrt{2}\sigma_x)^m \Gamma (1 + m/2)} \tag{2-33}$$

in which ν_0^+ = expected rate of zero up-crossings.

If an actual time history of the random stress process is available (as from field data or simulation) various cycle-identification techniques exist from which one can directly estimate the stress range moment, $E[S^m]$. One of the most widely accepted of these techniques is the rainflow method proposed by Matsuishi and Endo (24). An illustration of the technique is shown in Figure 2.2. The time history may be visualized as a cross-section or profile through a water filled reservoir. The lowest valley is drained, identifying the 2 largest half-cycles [7-10,10-13], and leaving two smaller valleys full. The next lowest valley is drained, identifying two half-cycles [1-4,4-7]. Continuing in this manner, the next lowest valleys are drained, and full cycles [2-3] and [8-9], [11-12] and [5-6] are identified, followed by half-cycles [0-1], and [13-14] respectively. It can be shown that the rainflow technique essentially identifies stress cycles as closed hysteresis loops for a material satisfying the Masing hypothesis. Several algorithms are available for performing rainflow analysis (8,9,24), either on an entire time history in a single pass, or sequentially in "real time" as the time history is generated or observed. The algorithm used in this study was a real-time scheme developed by Lutes and first employed by Zimmerman (43).

In the following, $E[R^m]$ denotes the stress range moment determined by rainflow analysis.
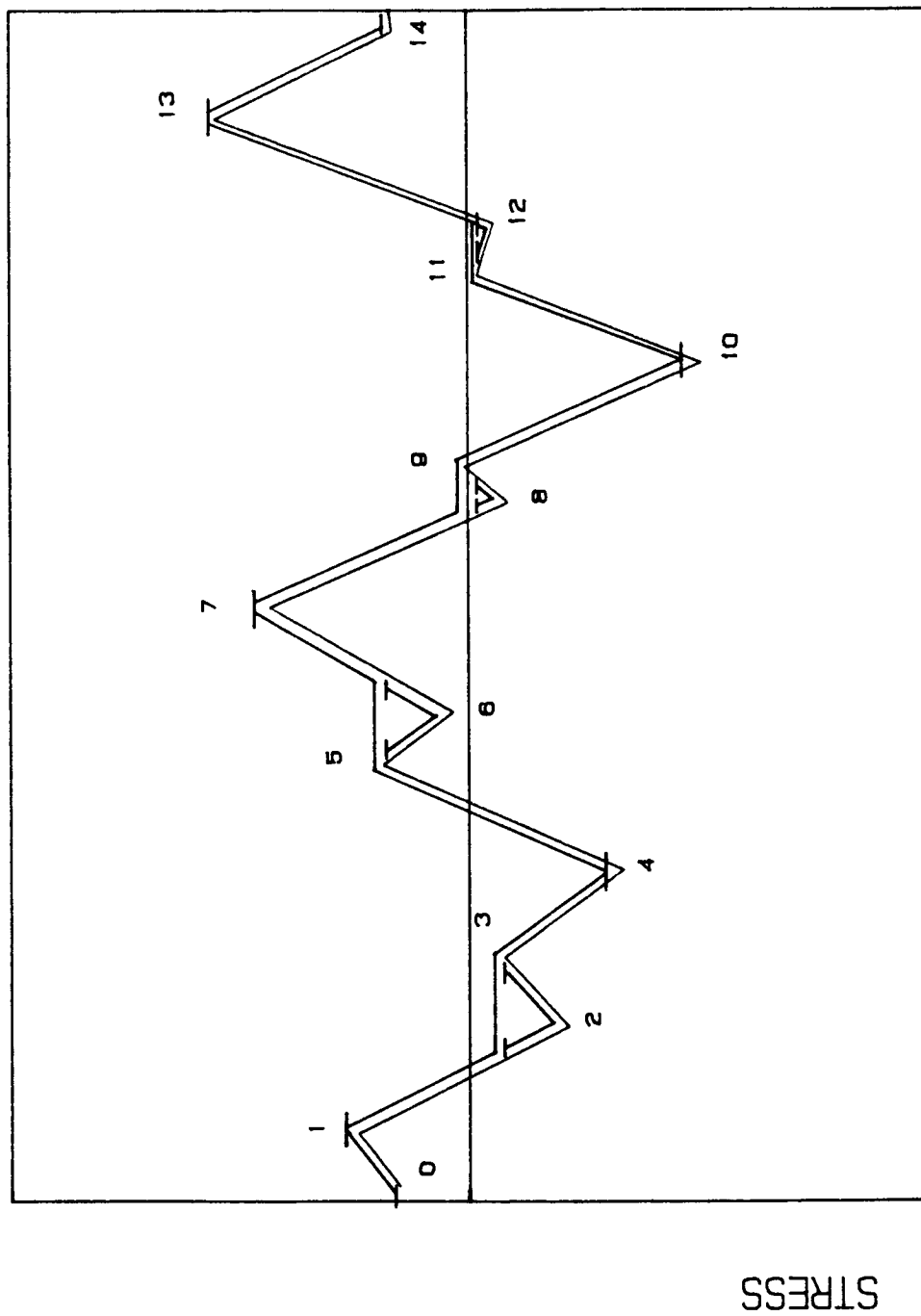
Figure 2.2 Rainflow Cycle-Identification

TIME

STRESS

14

2.3 Gaussian Process Simulation

A technique for the simulation of a stationary random process, herein referred to as the Gaussian technique, was first indicated by S.O. Rice (32). The Gaussian technique is well known in the literature and has become a standard method of simulating stationary, Gaussian random processes (2,5,35,36,41). The technique synthesizes a realization of the random process $\{X(t)\}$ from the one-sided psd $G_X(\omega)$ according to the equation:

$$X(t) = \sum_{i=1}^{M} [2\Delta\omega G_X(\omega_i)]^{1/2} \sin(\omega_i t - \phi_i) \qquad (2\text{-}34)$$

in which:

$\Delta\omega$ = frequency interval

$G_X(\omega_i)$ = ordinate of one-sided psd at ω_i

ω_i = midpoint of frequency interval

ϕ_i = independent, identically distributed (i.i.d.) random phase angles, uniform on $[0,2\pi]$

$X(t)$ is approximated as the sum of M sine wave components having random phase angles ϕ_i and of amplitude $[2\Delta\omega G_X(\omega_i)]^{1/2}$. The normality of $X(t)$ is ensured for large N by the Central Limit Theorem (1,28,29). For a constant frequency interval, $\Delta\omega$, $X(t)$ will be periodic with period $T = 2\pi/\Delta\omega$. This periodicity may be avoided by using a randomly varying $\Delta\omega$ or by selecting a new set of random phase angles $\{\phi_i\}$ at the end of each period.

The process formed by the extrema of $\{X(t)\}$, the envelope process, is usually of more interest than the process itself for problems in the analysis of first excursion probability, fatigue, and crack propaga-

15

tion. Simulation of the extrema (peaks and valleys) by the Gaussian technique can be very laborious because the exact location of the extrema is not known and an extremely large number of sample points must be generated to accurately define the peaks and valleys. For fatigue analysis this technique becomes even more inefficient because the rain-flow cycle identification technique discards all sample points but the peaks and valleys, which are necessary to define the stress ranges.

Yang (42) recognized this inefficiency and proposed a technique for simulating a random envelope process which utilized the Fast Fourier Transform. Yang's technique, however, is best suited to narrowband processes which have a well defined period, T_o, at which the envelope process is sampled to generate the extrema. For wideband processes, the problem is again one of knowing the location of the extrema, or of knowing at what times to sample the envelope process.

Zimmerman (43) also recognized the inefficiency of the Gaussian simulation technique for fatigue analysis and studied three alternate techniques which produced correlated sequences of extrema having either the Rayleigh or the S.O. Rice distributions. His work avoided the uncertainty about the time of occurrence of the extrema and when to sample the process by looking directly at the extrema as a correlated sequence of random variables. This approach introduced the parameter ρ_k, the correlation between extrema k steps apart, and the problem of determining how the extrema correlations relate to the more commonly used statistics of a random process. Zimmerman empirically related ρ_1, the peak-valley correlation, to bandwidth as described by α_2 and with this information was successful in directly simulating correlated sequences of Rayleigh (Zimmerman's Technique III) or S.O. Rice (his

16

Technique IV) distributed extrema. Simulation Technique IV was found to be three to four times faster than the Gaussian technique and gave comparable rainflow analysis results. These techniques were applied by Sarkani (34) to generate random loadings for an experimental study of fatigue in welded joints.

Zimmerman's techniques are only valid for the special case of unimodal (or "1-block") psd's which are sufficiently described by the parameter ρ_1. Attempts to extend his techniques to bimodal (or "2-block") psd's were frustrated by the unsolved problem of relating the behavior of the extrema correlations to any spectral parameters. For bimodal psd's, ρ_1 is insufficient to describe the relationship between extrema and Zimmerman's techniques are not applicable.

2.4 Autoregressive (AR) Processes and Simulation

A very versatile set of models for scalar (univariate and one-dimensional) random processes, known as Autoregressive Moving Average (ARMA) models, is described by Box and Jenkins (3) and Jenkins and Watt (19). These time series models have found wide application outside of structural engineering, primarily in economic or business forecasting. ARMA models have only recently been applied to structural engineering problems (33). Gersch (10,11,12,13,14,15,16,17) used ARMA time series techniques to synthesize the response of linear structural systems to stationary random excitation. Reed and Scanlan (31) modeled cooling tower wind loadings, and others have utilized the method to model sea waves (37,38) and earthquake ground motions (4,18,30).

The general ARMA(p,q) model of a stationary random process is given by:

$$Z_t = \phi_1 Z_{t-1} + \phi_2 Z_{t-2} + \cdots + \phi_p Z_{t-p}$$

$$+ a_t + \theta_1 a_{t-1} + \theta_2 a_{t-2} + \cdots + \theta_q a_{t-q} + \mu \qquad (2\text{-}35)$$

in which the present value of the random process, Z_t, is expressed as a weighted sum of the past p values of the process, $\{Z_{t-1}, Z_{t-2}, \cdots, Z_{t-p}\}$, a weighted sum of the q + 1 random variables $\{a_t, a_{t-1}, a_{t-2}, \cdots, a_{t-q}\}$ and a constant term μ. The sequence $\{a_k\}$ is generally assumed to be of i.i.d., mean-zero, normal variates. The ARMA(p,q) model has p + q + 2 parameters $(\phi_1, \phi_2, \cdots, \phi_p, \theta_1, \theta_2, \cdots, \theta_q, \mu, \sigma_a^2)$ which must be estimated from data on the process to be modeled. Box and Jenkins (3) note that in practice the number of unknown coefficients usually need not be greater than 2 for either p or q. The random variables $\{a_k\}$ are sometimes known as the residuals because they represent the residual, random factor that is not accounted for in the deterministic part of the model (the relationship between the current value, Z_t, and the past values, $\{Z_{t-k}\}$).

A special form of the ARMA(p,q) model is the autoregressive, AR(p), model (q = 0):

$$Z_t = \phi_1 Z_{t-1} + \phi_2 Z_{t-2} + \cdots + \phi_p Z_{t-p} + a_t + \mu \qquad (2\text{-}36)$$

in which the current value of the process is expressed completely by a weighted sum of past values, $\{Z_{t-1}, Z_{t-2}, \cdots, Z_{t-p}\}$, a random variate a_t, and a constant μ. The AR(p) model has p + 2 unknowns $(\phi_1, \phi_2 \cdots, \phi_p, \mu, \sigma_a^2)$ which must be estimated.

The autocorrelation, ρ_k, between Z_t and the value Z_{t+k}, separated by k intervals of time, is defined as:

$$\rho_k = \frac{E[(Z_t - \mu)(Z_{t+k} - \mu)]}{E[(Z_t - \mu)^2]} \qquad\qquad (2\text{-}37)$$

The autocorrelation function for an AR(p) process is given by the difference equation:

$$\rho_k = \phi_1 \rho_{k-1} + \phi_2 \rho_{k-2} + \cdots + \phi_p \rho_{k-p} \qquad\qquad (2\text{-}38)$$

Note that this equation is analogous to the difference equation satisfied by the process itself. By successively substituting $k = 1, 2, \cdots p$ into this equation, a set of linear equations is obtained for $\phi_1, \phi_2, \cdots, \phi_p$ in terms of $\rho_1, \rho_2, \cdots \rho_p$. Replacing the theoretical $\{\rho_k\}$ by their estimates obtained from the data, $\{r_k\}$, gives the Yule-Walker estimates for the $\{\hat{\phi}_k\}$:

$$[\hat{\phi}] = [R_p]^{-1}[r_p] \qquad\qquad (2\text{-}39)$$

in which

$$[\hat{\phi}] = \begin{bmatrix} \hat{\phi}_1 \\ \hat{\phi}_2 \\ \vdots \\ \hat{\phi}_p \end{bmatrix}$$

$$[R_p] = \begin{bmatrix} 1 & r_1 & r_2 & \cdots & r_{p-1} \\ r_1 & 1 & r_1 & \cdots & r_{p-2} \\ \vdots & \vdots & \vdots & \cdots & \vdots \\ r_{p-1} & r_{p-2} & r_{p-3} & \cdots & 1 \end{bmatrix}$$

$$[r_p] = \begin{bmatrix} r_1 \\ r_2 \\ \vdots \\ r_p \end{bmatrix}$$

Box and Jenkins (3) show that these estimates approximate the fully efficient maximum likelihood estimates.

For the most common AR(1) and AR(2) processes, the parameter estimates are:

$$\text{AR(1):} \quad \hat{\phi}_1 = r_1 \tag{2-40}$$

$$\text{AR(2):} \quad \hat{\phi}_1 = \frac{r_1(1 - r_2)}{1 - r_1^2} \tag{2-41}$$

$$\hat{\phi}_2 = \frac{r_2 - r_1^2}{1 - r_1^2}$$

The variance of an AR(p) process is:

$$\sigma_Z^2 = \frac{\sigma_a^2}{1 - \rho_1\phi_1 - \rho_2\phi_2 - \cdots - \rho_p\phi_p} \tag{2-42}$$

Substituting $\{r_k\}$ for $\{\rho_k\}$ and the estimate C_0 for σ_Z^2, the variance of the residuals $\{a_k\}$ is estimated by:

$$\hat{\sigma}_a^2 = C_0(1 - \hat{\phi}_1 r_1 - \hat{\phi}_2 r_2 - \cdots - \hat{\phi}_p r_p) \tag{2-43}$$

For the AR(1) and AR(2) process, this becomes:

$$\text{AR(1):} \quad \hat{\sigma}_a^2 = C_0(1 - r_1^2) \tag{2-44}$$

$$\text{AR(2):} \quad \hat{\sigma}_a^2 = C_0 \left[1 - \frac{r_1^2(1 - r_2)}{1 - r_1^2} - \frac{r_2(r_2 - r_1^2)}{1 - r_1^2} \right] \tag{2-45}$$

One can show that the AR(1) process is a Markov process. Zimmerman's techniques III and IV (43) are of the AR(1) type, although they are not expressed explicitly in this form. The present work is intended to extend the concept of modeling the extrema of a random process as a sequence of correlated random variables, as used by Zimmerman for 1-block psd's, to a more general technique adapted from the ARMA(p,q) or AR(p) family of stochastic models. Chapters 4 and 5 discuss the details of parameter estimation and the modifications to the AR(p) model necessary to synthesize correlated extrema.

CHAPTER 3

GAUSSIAN SIMULATION RESULTS

Chapter 3 presents the results of a study of four psd types for which time histories were simulated using the Gaussian technique of Section 2.3. The psd's studied are shown in Figure 3.1.

The psd of Figure 3.1a is a band-limited white noise approximation to a unimodal psd, herein referred to as a 1-block psd. It is characterized by a constant squared amplitude, G, over the frequency range ω_1 to ω_2. Bimodal psd cases were formed by the superposition of two 1-block psd's, as in Figure 3.1b. These cases, referred to as 2-block psd's, are characterized by the squared amplitude levels G_1 and G_2, and the frequency ranges ω_1 to ω_2 and ω_3 to ω_4. These parameters are related through the frequency ratio:

$$r = \omega_3/\omega_1 = \omega_4/\omega_2 \tag{3-1}$$
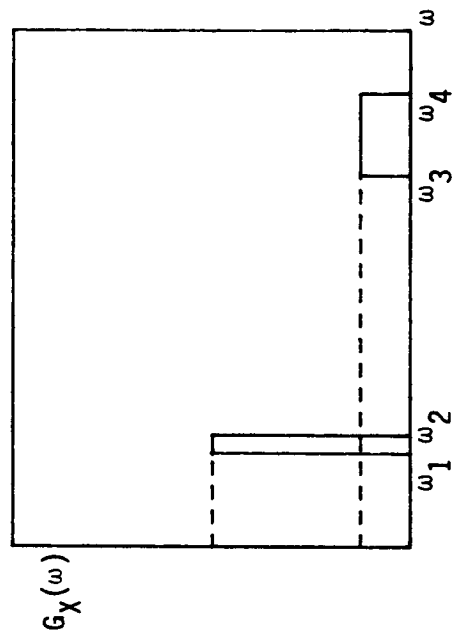
and the area ratio:

$$b = A_2/A_1 \tag{3-2}$$
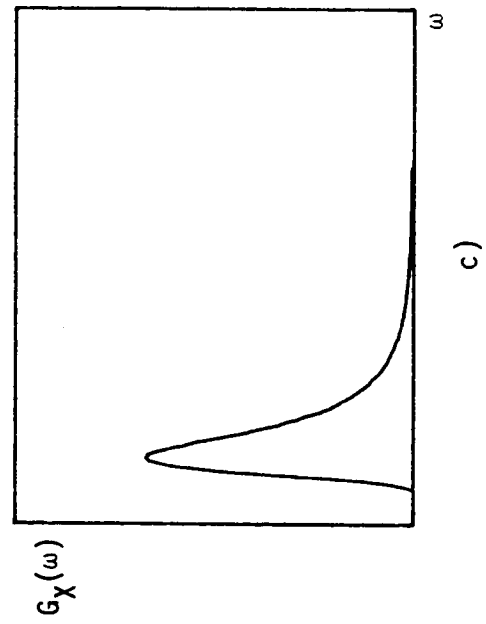
in which A_1 = area of block 1

A_2 = area of block 2

A more realistic unimodal psd shape was investigated using a form previously studied by Wirsching and Light (41), shown in Figure 3.2c. This psd has a form given by:
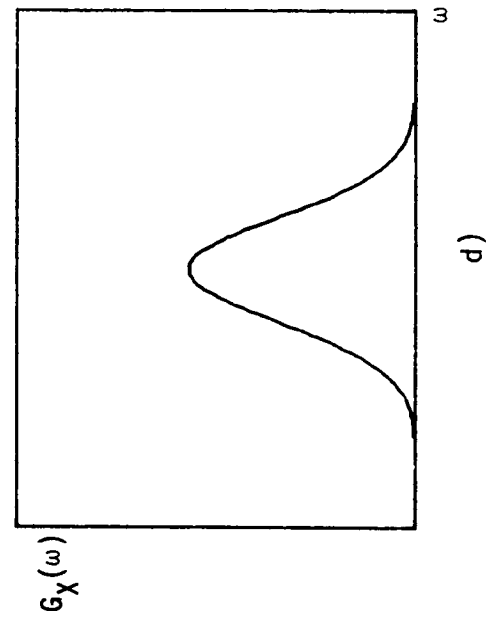
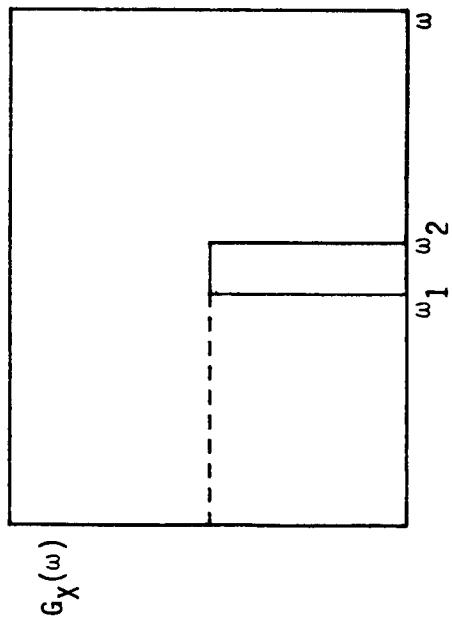$$G_X(\omega) = \frac{K}{\omega^4} \exp(-\beta/\omega^3) \tag{3-3}$$

Figure 3.1 PSD Types Studied

in which K = 3β for $E[X^2]$ = 1. This form presents some analytical difficulties because its fourth moment, λ_4, is not finite, so the irregularity factor for this psd is zero (α = 0). In addition, this psd does not have a known Fourier transform, so an analytical expression for the autocorrelation function, $R_{XX}(\tau)$, is not known. Because of these difficulties, the unimodal psd of Figure 3.1d was also studied. It has a convenient form given by:

$$G_X(\omega) = \frac{1}{c\sqrt{2\pi}} \exp[-(\omega - u)^2/2c^2] \qquad (3-4)$$

in which: u = center frequency

c = a shape factor

This form is analogous to a Gaussian or normal probability density function (pdf), for which λ_4 is finite and for which the Fourier transform is well known.

Parameter values for the specific psd cases studied are tabulated in Appendix A.

The simulation results of interest in these studies were the expected damage per unit time and the extrema correlations. For bimodal psd's, the relative contributions by the modes to the damage rate are discussed in Section 3.1. In Section 3.2, results are presented for unimodal psd's on the effect of high frequency psd truncation on the damage rate. Finally, the characteristics of the extrema correlations are presented in Section 3.3, providing a basis for the autoregressive models described in Chapters 4 and 5.

3.1 PSD Component Contributions to Damage

The effect of truncating high and low frequency psd components was studied for the 2-block type bimodal psd's. The goal of this study was to determine empirical limits beyond which a sufficiently accurate rainflow damage prediction may be obtained by considering the psd to be unimodal.

The expected damage rate is defined as:

$$d/t = n_p E[R^m](1 + b)^{m/2} \qquad (3-5)$$

For this study, the additional factor $(1 + b)^{m/2}$ has been added to normalize the results such that the psd's all have a low frequency component of unit area.

The normalized damage rate, d/d_o, is defined as:

$$\frac{d}{d_o} = \frac{d/t}{d_o/t} \qquad (3-6)$$

in which: d_o/t is the d/t for $b = 0$ (1-block psd).

A normalized area ratio, $br^{2/m}$, is also defined in which:

$$b = A_2/A_1$$

$$r = \omega_3/\omega_1 = \omega_4/\omega_2$$

$$m = \text{material constant from Equation (2-27)}$$

The normalized damage rate, d/d_o, is shown as a function of $br^{2/m}$ for $m = 3$ in Figure 3.2. Corresponding plots for $m = 5$ and $m = 7$ are given by Figures 3.3 and 3.4, respectively.

The two asymptotic limits shown in these figures are evaluated as follows.
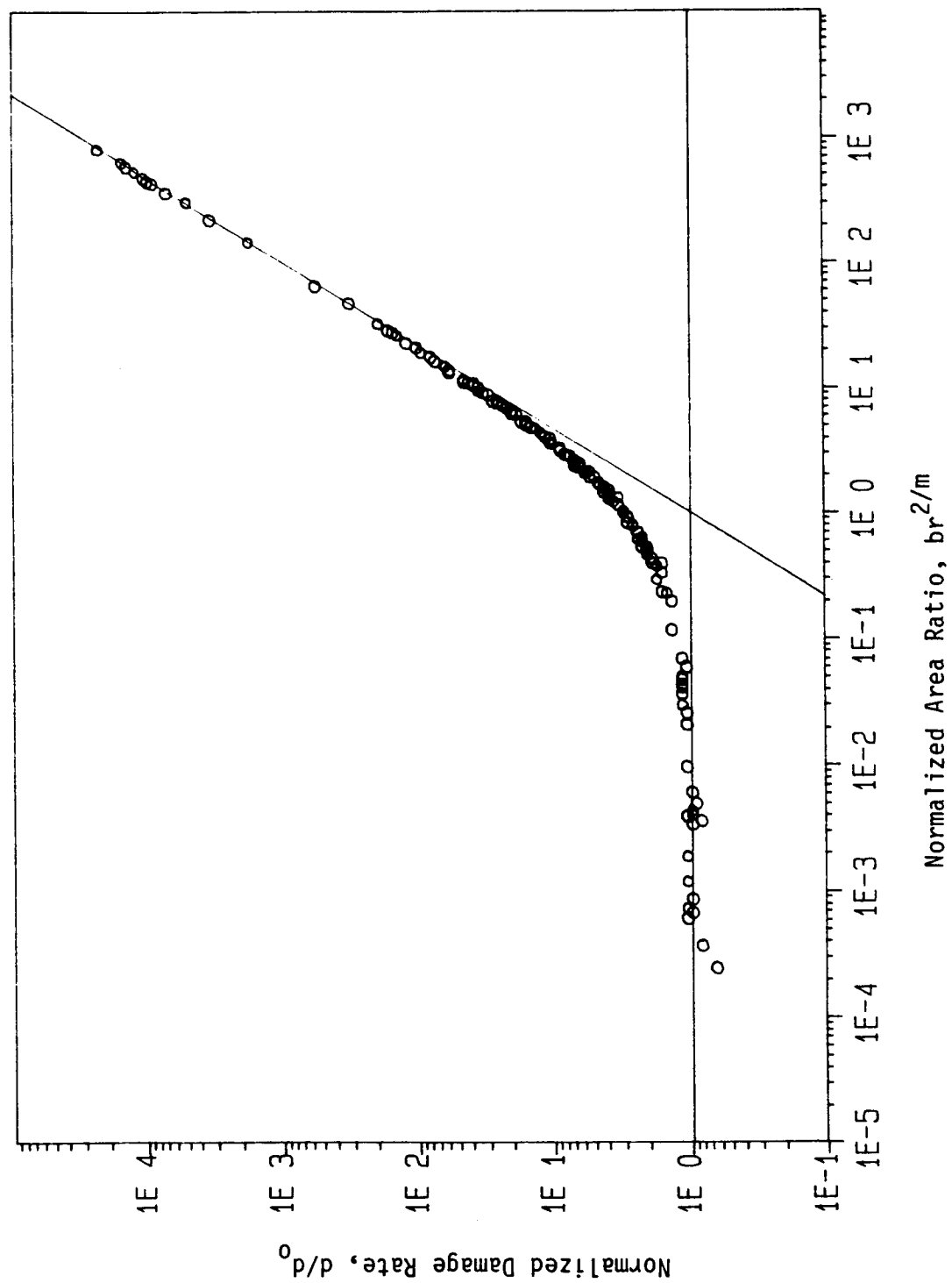
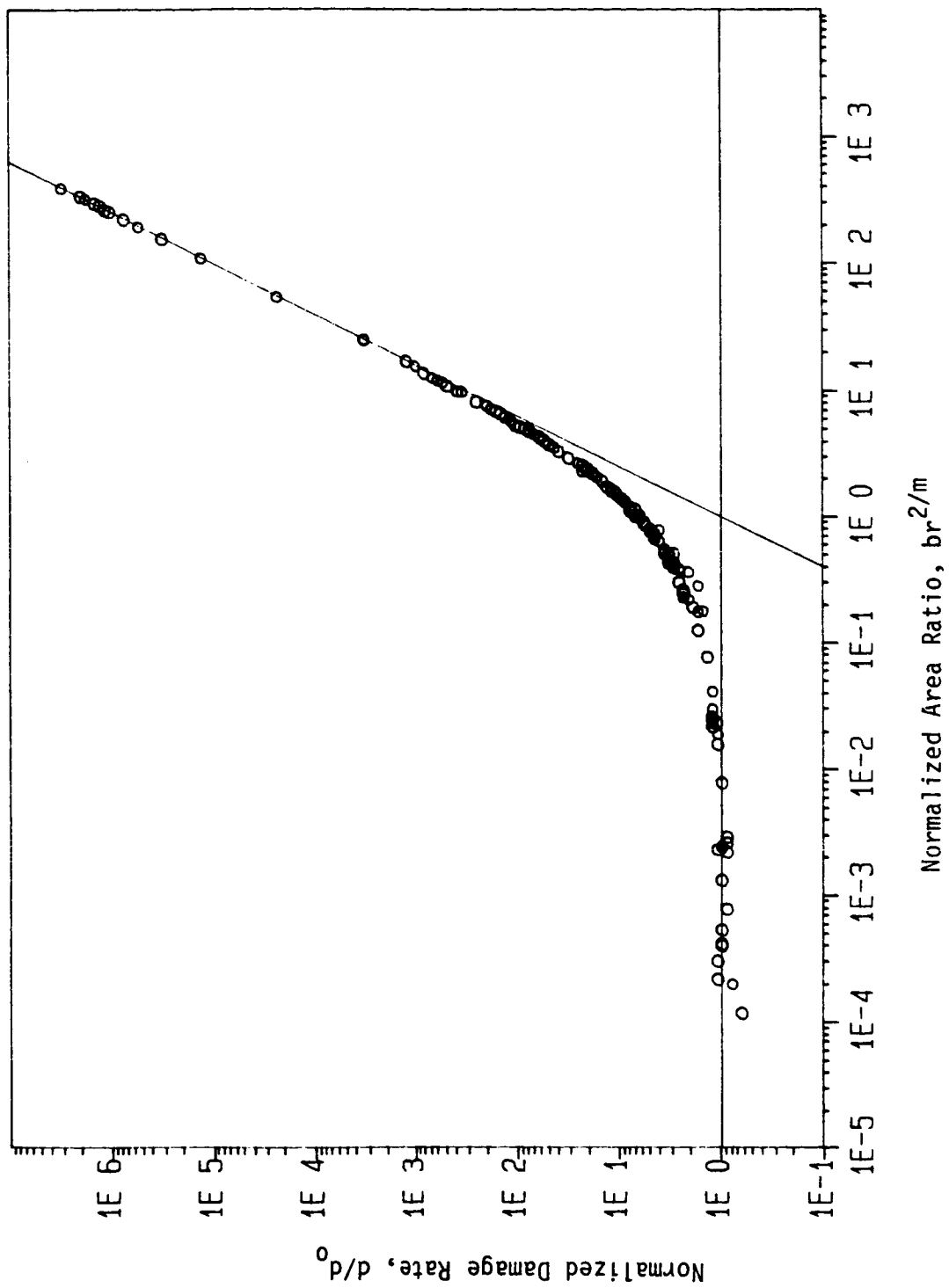Figure 3.2 Normalized Damage Rate vs Normalized Area Ratio: m = 3

26

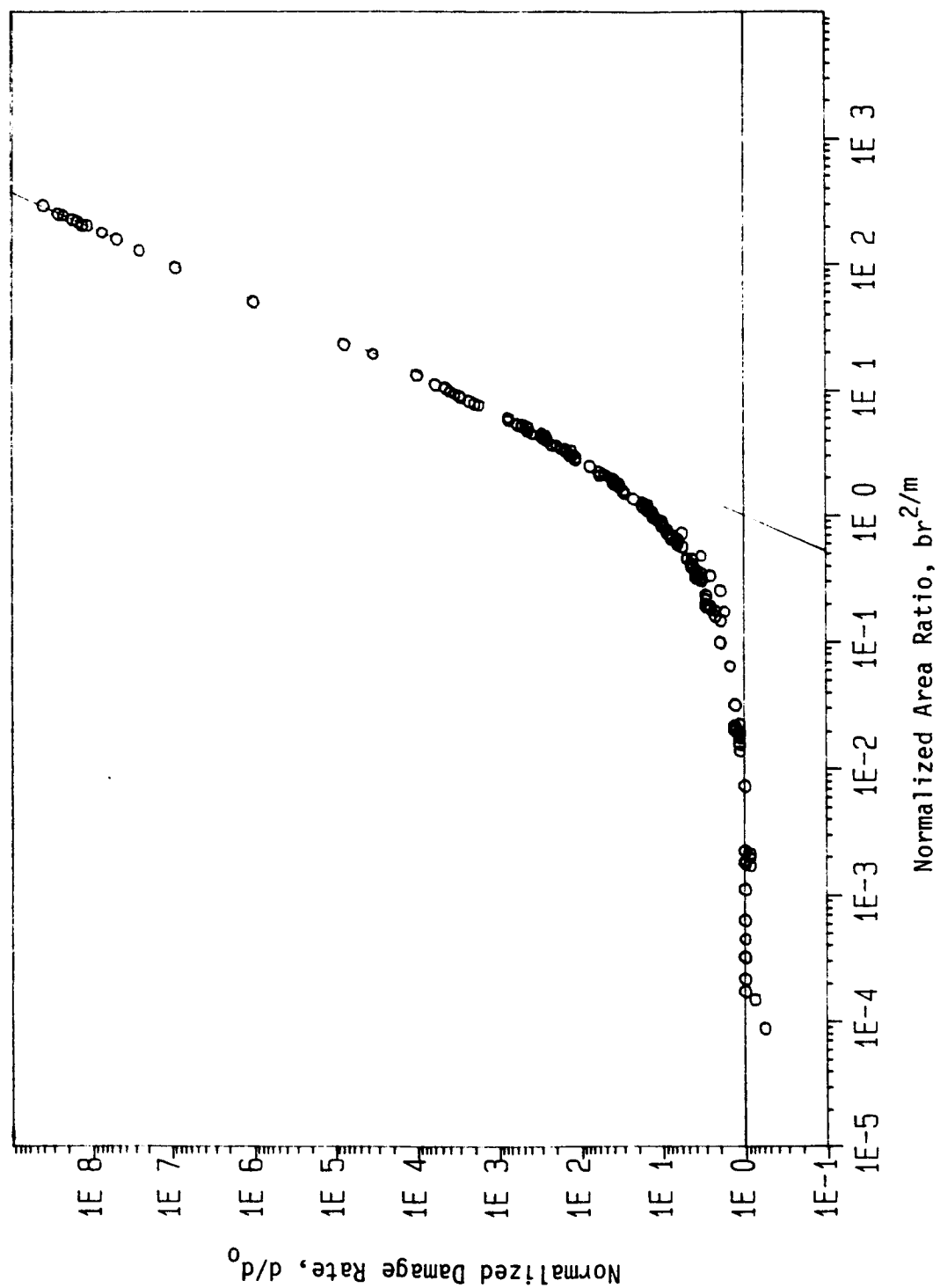Figure 3.3 Normalized Damage Rate vs Normalized Area Ratio: m = 5

27

Figure 3.4 Normalized Damage Rate vs Normalized Area Ratio: m = 7

For b = 0, the bimodal psd reduces to a unimodal psd corresponding to the low frequency block of the bimodal psd. For the particular psd's studied, using Equation 2-13 to evaluate n_p gives:

$$n_p = \frac{1}{2\pi} \left(\frac{3.06006}{3.01}\right)^{1/2} \tag{3-7}$$

The value of the range moment, $E[R^m]$, was determined from unimodal simulations as:

$$E[R^m] = \begin{cases} 29.79 & \text{for } m = 3 \\ 593.9 & \text{for } m = 5 \\ 16,550 & \text{for } m = 7 \end{cases} \tag{3-8}$$

The low frequency asymptotic limit (b = 0) for the damage rate is then:

$$\frac{d_o}{t} = \begin{cases} 4.781 & \text{for } m = 3 \\ 95.30 & \text{for } m = 5 \\ 2,656 & \text{for } m = 7 \end{cases} \tag{3-9}$$

Evaluating n_p for the general bimodal psd case gives:

$$n_p = \frac{1}{2\pi} \left[\frac{3.06006}{3.01} \frac{(1+br^4)}{(1+br^2)}\right]^{1/2} \tag{3-10}$$

and Equation 3-5 gives the damage rate as:

$$\frac{d}{t} = \frac{E[R^m]}{2\pi} \left[\frac{3.06006}{3.01} \frac{(1+br^4)}{(1+br^2)}\right]^{1/2} (1+b)^{m/2} \tag{3-11}$$

Recognizing that for a 1-block psd (b = 0):

$$\frac{d_o}{t} = \frac{E[R^m]}{2\pi} \left(\frac{3.06006}{3.01}\right)^{1/2} \tag{3-12}$$

Equation 3-11 may be rewritten as:

$$\frac{d}{d_o} = \left[\frac{(1+br^4)}{(1+br^2)}\right] (1+b)^{m/2} \tag{3-13}$$

29

Now as b tends to infinity, the bimodal psd reduces to its high frequency, unimodal component. Thus, for large b:

$$[\frac{(1+br^4)}{(1+br^2)}]^{1/2} \simeq (\frac{br^4}{br^2})^{1/2} = r \tag{3-14}$$

and $(1 + b)^{m/2} \simeq b^{m/2}$ (3-15)

The high frequency (large b) asymptotic limit is thus:

$$\frac{d}{d_o} = rb^{m/2} \tag{3-16}$$

Errors in the rainflow damage estimate as large as 20% are often acceptable in practical fatigue analysis. Using this accuracy level, the limiting area ratio below which the high frequency component mode may be neglected was estimated to be in the range of b = 0.1 to b = 0.01 for r = 1.5 to 15, respectively. Similarly, the limiting area ratio above which the low frequency component mode may be neglected was estimated to be from about b = 10 to b = 2 for r = 1.5 to 15, respectively. The region for which bimodal effects may not be neglected is also illustrated in Figure 3.5. This figure gives Vanmarcke's bandwidth parameter, q, as a function of b and r for 2-block psd's. The central region bounded by the dashed lines for m = 3,5,7 denotes the combinations of b and r for which the bimodal effect is significant. Overall limits for the region for which bimodal effects are important, bounding the effects due to m and r, are from b = 0.01 to b = 10. Psd's with area ratios outside this range can be considered to be unimodal for practical purposes.
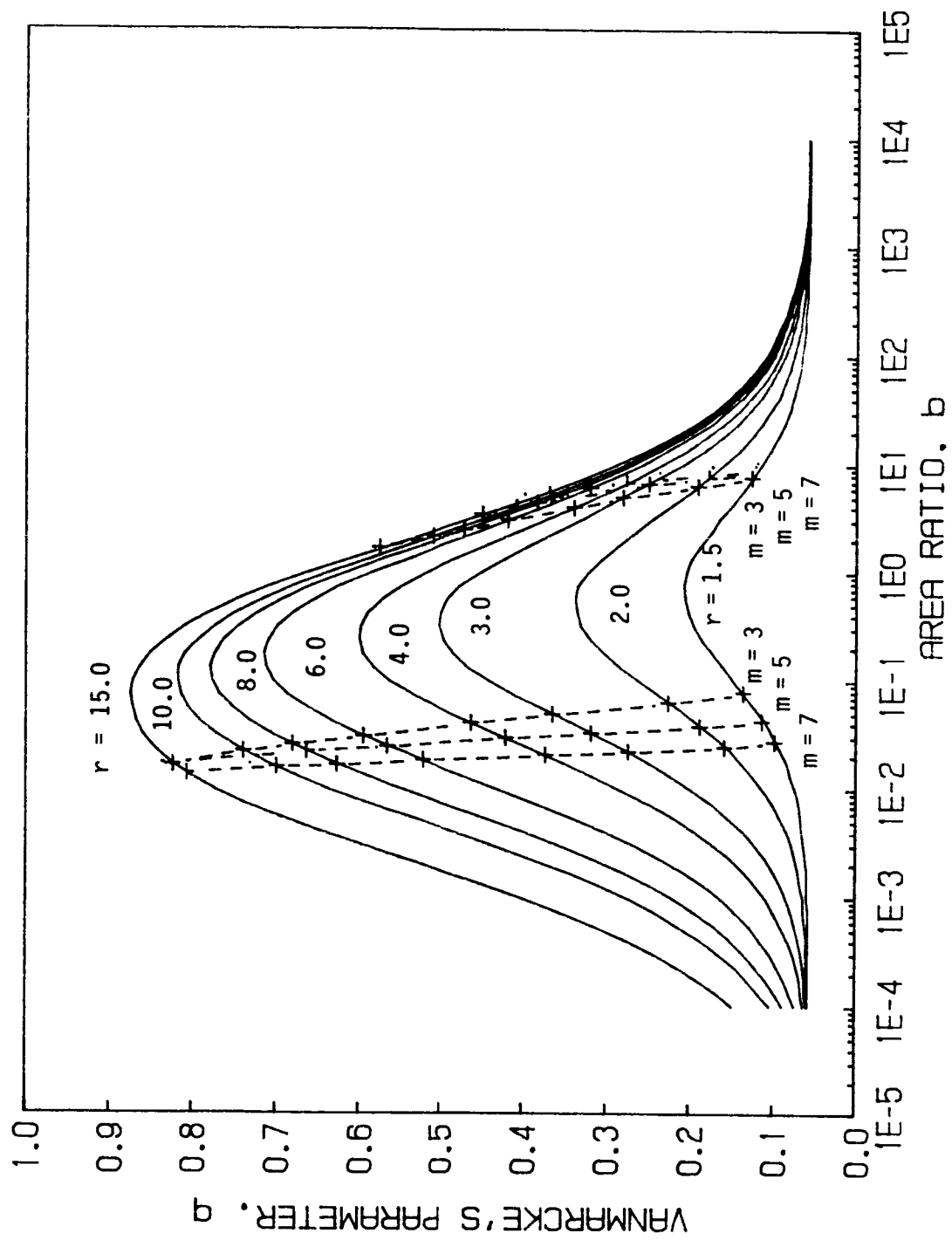
Figure 3.5 Vanmarcke's Parameter vs Area and Frequency Ratios: Bimodal Region

31

3.2 High Frequency Truncation Effect

The effect of high frequency psd truncation on the rainflow damage rate was also studied for the two unimodal psd types of Figure 3.1c and d. A rainflow analysis was performed using various high frequency cut-off levels. Average results for m = 3,5,7 are plotted in Figure 3.6 as normalized damage per unit time, d/d_0, versus a normalized cut-off frequency parameter, u. The expected damage per unit time is defined as:

$$d/t = n_p E[R^m] \tag{3-17}$$

in which: n_p = expected rate of peak occurrences

$E[R^m]$ = the mth moment of the rainflow ranges

The normalized damage per unit time is defined as:

$$d/d_0 = \frac{d/t}{d_0/t} \tag{3-18}$$

in which: d_0/t = d/t for u_{max}.

The normalized cut-off frequency is defined as:

$$u = \frac{\omega_c - \lambda_1}{(\lambda_2 - \lambda_1^2)^{1/2}} \tag{3-19}$$

in which: ω_c = cut-off frequency

λ_1 = 1st moment of psd about ω = 0

λ_2 = 2nd moment of psd about ω = 0.

Note that u is analogous to the standardized variate for a normal distribution, $U = (X - \mu)/\sigma$.

Figure 3.6 Normalized Damage Rate vs Normalized Cut-Off Frequency

33

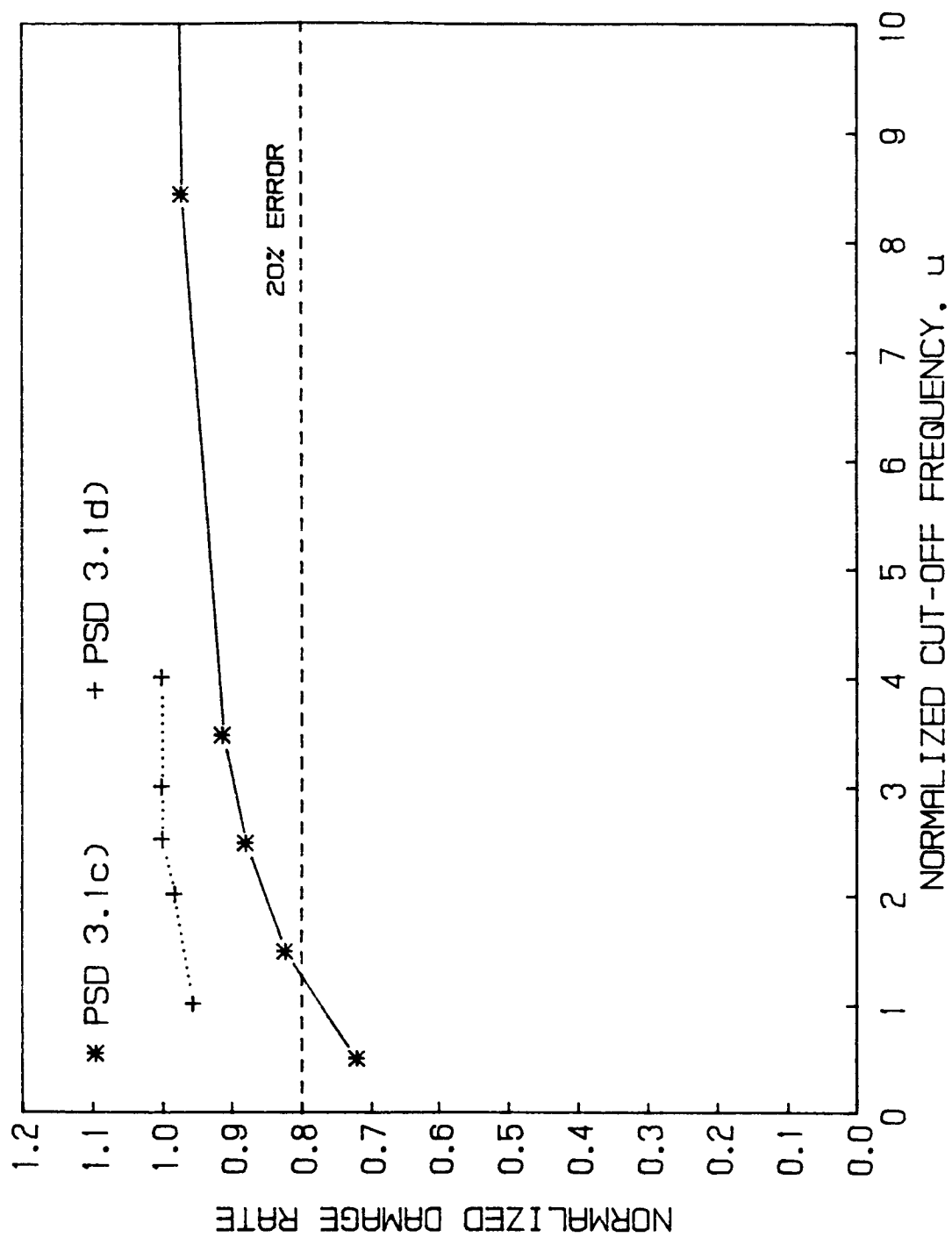Assuming again that as much as a 20% error is acceptable in the rainflow damage estimate, a high frequency cut-off of about $u = 2.0$ can be used with the psd defined by Equation 3-3. For the "normal" form psd (Equation 3-4), which decays much faster (as $e^{-\omega^2}$), a cut-off of $u = 1.0$ is sufficient for a rainflow damage estimate accurate to 5%.

It was found that these results could be presented in a more uniform manner, such that the data for both psd types defined approximately a single curve, by using a frequency cut-off parameter q/q_o, in which q is Vanmarcke's bandwidth parameter (Equation 2-18) for the psd with high frequency cut-off ω_c, and q_o is the theoretical q for the psd with $\omega_c = \infty$. For the psd defined by Equation 3-3, $q_o = 0.5613$, while $q_o = 0.1961$ for the psd given by Equation 3-4. The average (for $m = 3,5,7$) normalized damage rate, d/d_o, as a function of q/q_o, is shown in Figure 3.7. These results indicate that truncation of a unimodal psd at a ratio of $q/q_o = 0.6$ or greater should result in less than a 20% error in the rainflow damage estimate.

3.3 Extrema Correlations

Modeling the extrema (peaks and valleys) of a random stress time history as an autoregressive (AR) process requires knowledge of the pdf of extrema and the extrema correlations. The pdf for the extrema is given by the result due to S.O. Rice, equation 2-20. At this time, however, no analytical result exists which describes the extrema correlations.

Empirical estimates of the extrema correlations were computed as part of the simulation studies previously described. For modeling
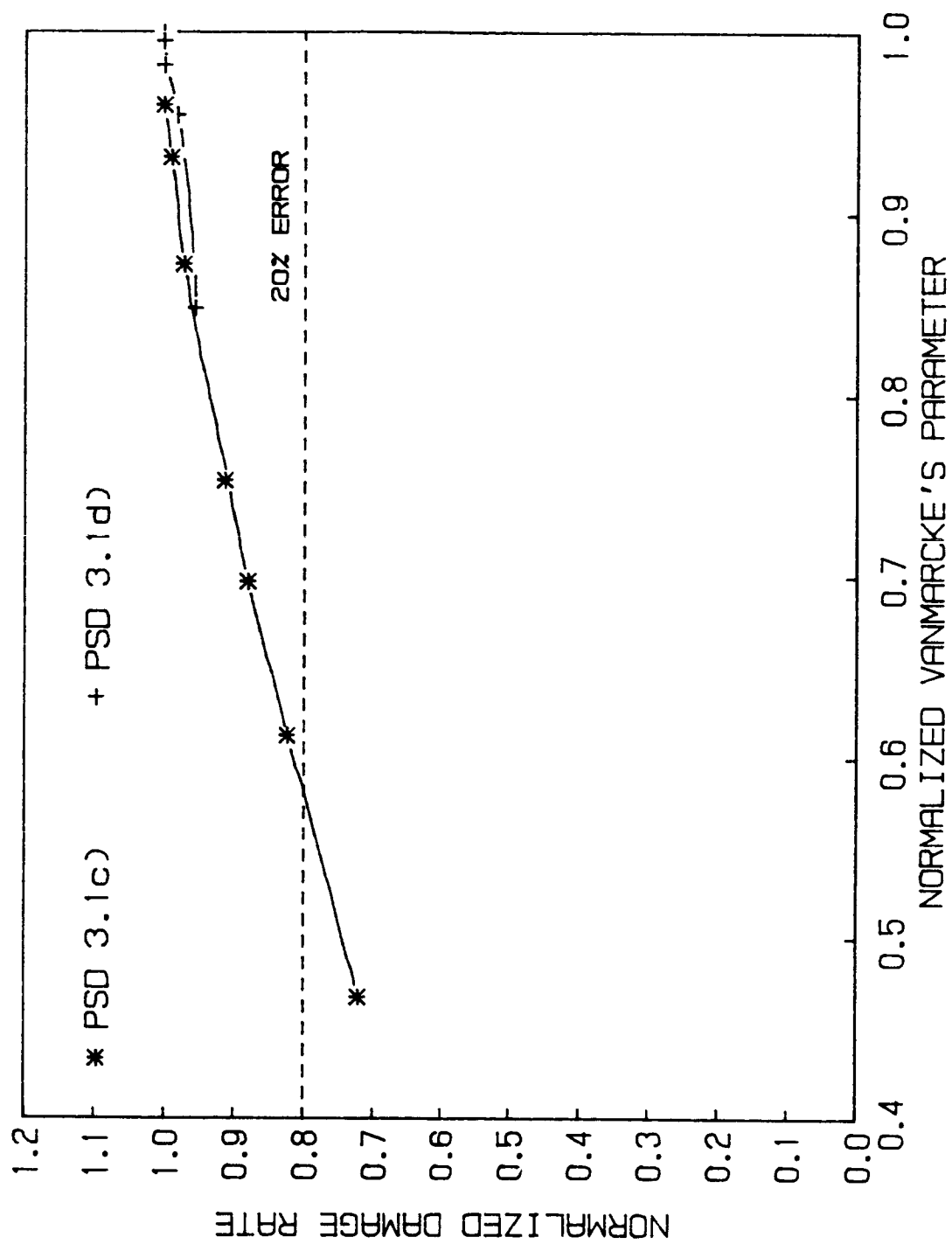
Figure 3.7   Normalized Damage Rate vs Normalized Vanmarcke's Parameter

the extrema as an AR process, the correlation of prime importance is the peak-to-valley or 1-step correlation, ρ_1. But in many cases the greatest peak-to-valley (P-V) correlation does not occur at one time step apart, or lag one, but occurs several time steps or lags later. This most significant P-V correlation will be denoted as ρ_{PV}.

Figure 3.8 presents ρ_1 plotted versus Vanmarcke's bandwidth parameter, q, for bimodal psd's. Several trends are evident. First, ρ_1 tends to -1 as q tends to zero, as expected for the limiting narrowband case. The apparent scatter in the data is the result of two effects. If data points of constant frequency ratio, r, are connected, a shift downward (decreasing ρ_1) can be identified with increasing r, as shown in Figure 3.9. A second trend becomes evident if for a constant r the data points are connected in order of decreasing area ratio, b, as shown in Figure 3.10. Starting in the lower left (with the limiting narrowband case), ρ_1 increases nearly linearly with q as b decreases, until some limiting value is reached beyond which further reductions in b reduce both q and ρ_1. This latter portion of the curve, however, does not return back along the initial path, but loops back at a higher ρ_1 for a given q.

These trends indicate that q is not the ideal spectral parameter to use to describe the variation of correlation with bandwidth. Ideally, one would use a parameter which was insensitive to changes in r and for which ρ_1 was uniquely determined. What this ideal parameter may be is unknown at this time.

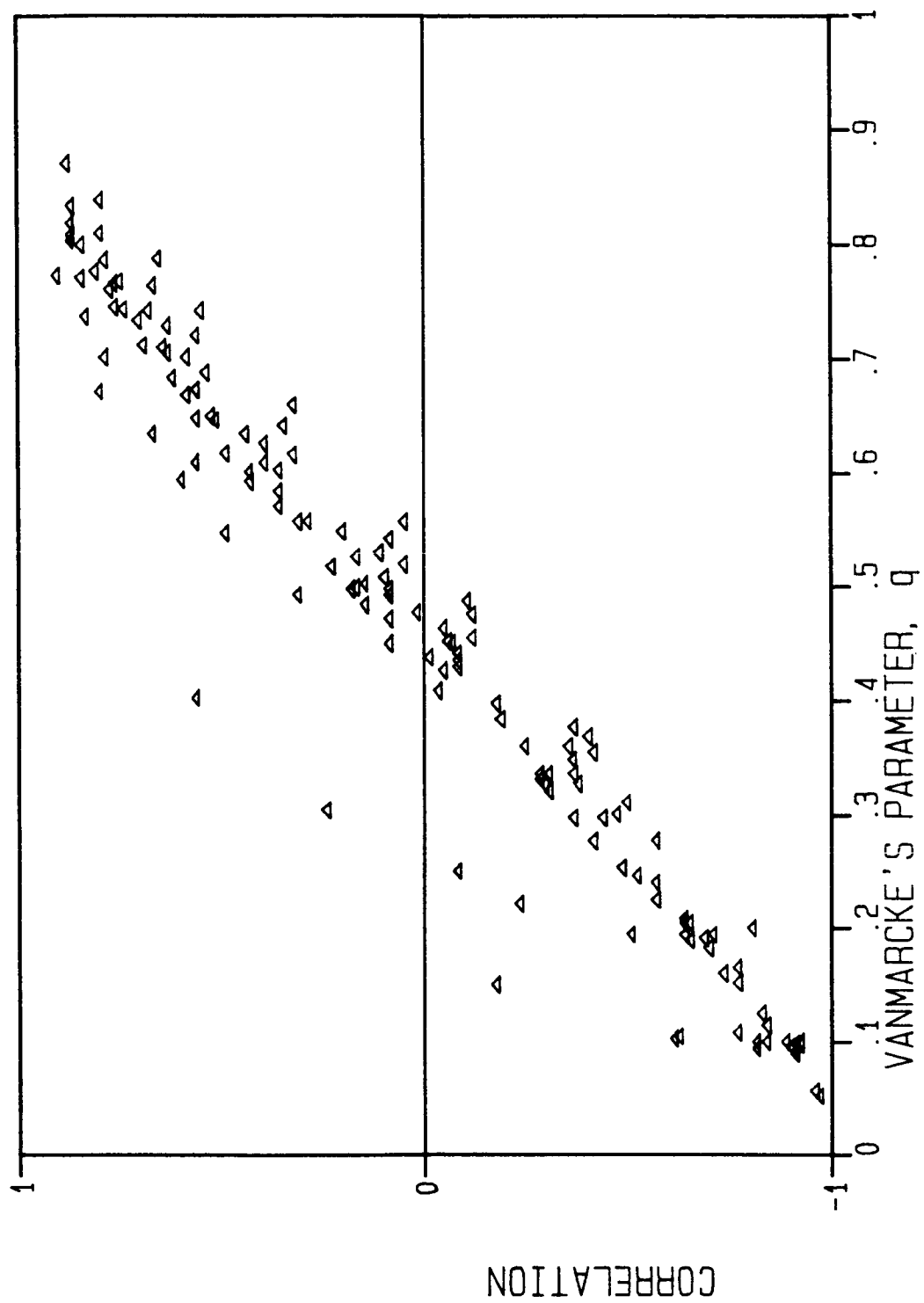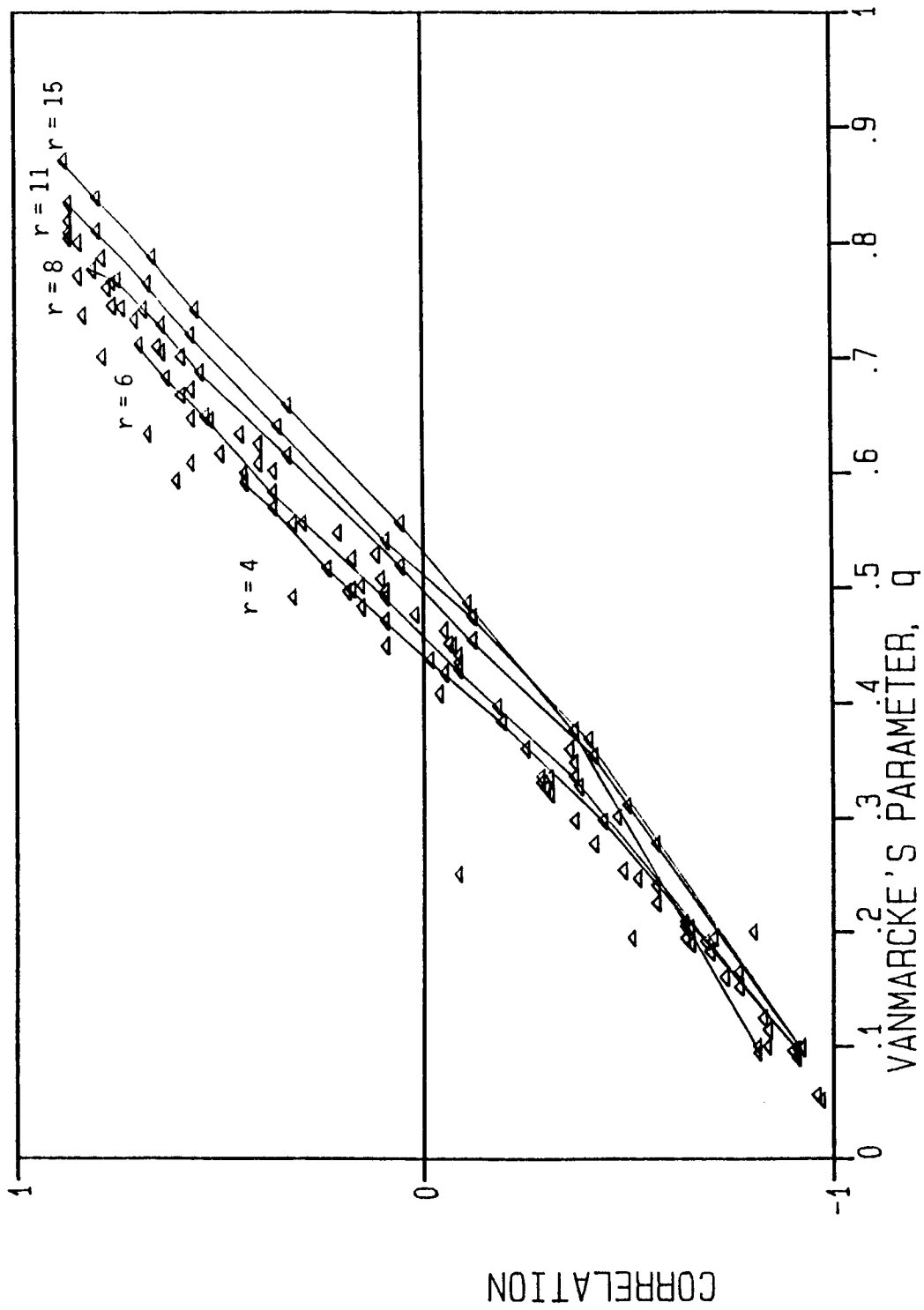Figure 3.8 Correlation ρ_1 vs Vanmarcke's Parameter: Scattergraph

37

Figure 3.9 Correlation ρ_1 vs Vanmarcke's Parameter: Frequency Ratio Effect
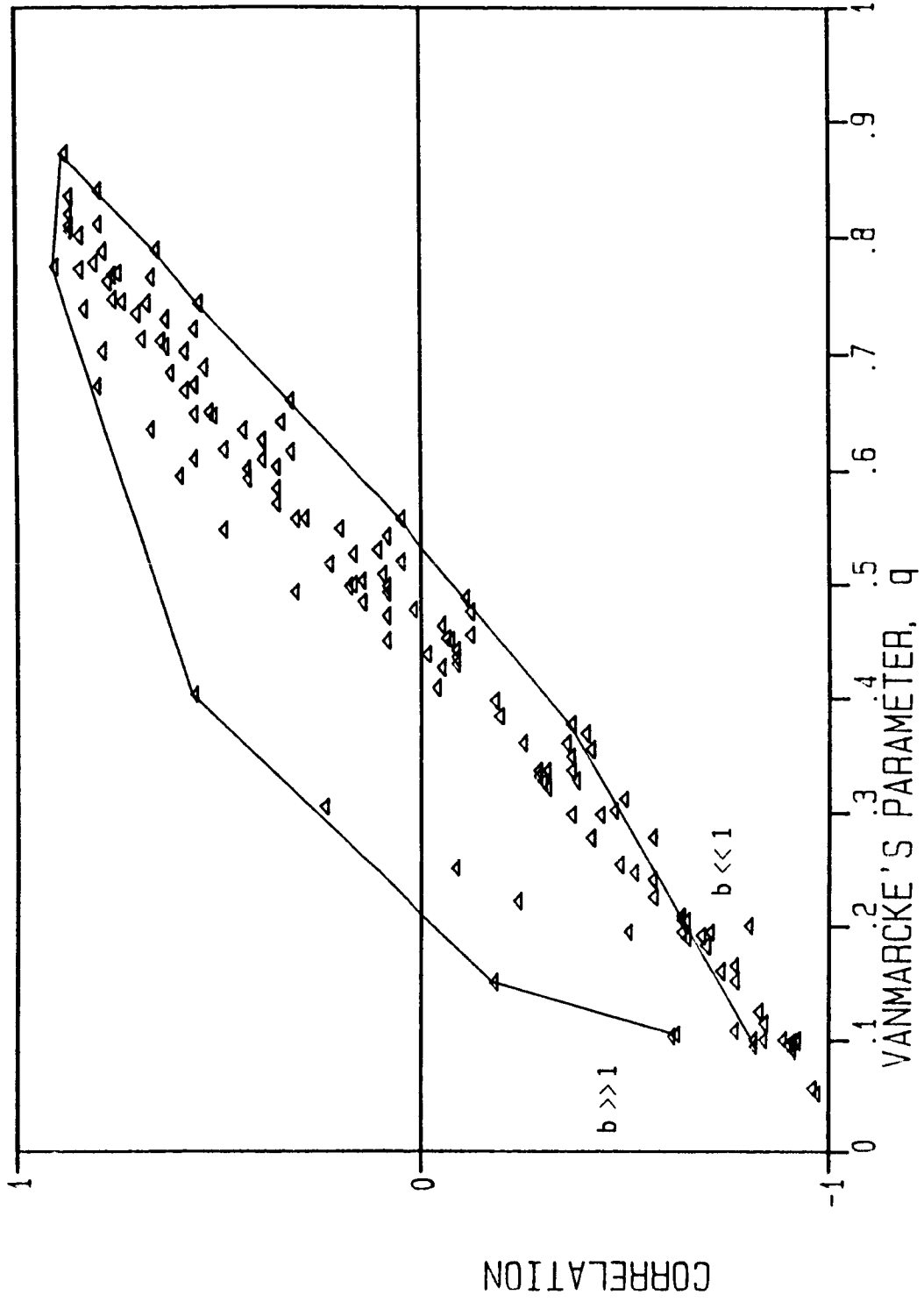
38

Figure 3.10 Correlation ρ_1 vs Vanmarcke's Parameter Area Ratio Effect, r = 15

The relation between ρ_1 and q can be used, however, if the relatively weak dependence on r is neglected and if only practical ranges of b are considered. The return portion of the correlation curve is essentially eliminated if the only values considered are those corresponding to area ratios (b) for which bimodal effects may not be neglected, as determined in the Section 3.1. (See Figure 3.5) The resulting relationship between ρ_1 and q is shown in Figure 3.11 and is given by the following equation:

$$\rho_1 = 2.45q - 1.14, \qquad 0.057 < q < 0.873 \qquad\qquad (3\text{-}20)$$

which is a linear regression of ρ_1 on q. Although the fit is imperfect, it is good for practical purposes, especially for unimodal psd's.

The extrema correlations for random processes having unimodal psd's are well behaved, as shown in Figure 3.12. In this figure and those which follow, the expected time of occurence for the kth extremum is $k/2n_p$. The most significant peak-to-valley correlation (ρ_{PV}) occurs at lag one (k=1), and the other correlations decay rapidly in an alternating manner. This makes it possible to model the extrema with an AR process based only on the lag one correlation, ρ_1. This will be discussed in more detail in Chapter 4.

The extrema correlations for bimodal psd processes are not as well behaved. For example, Figures 3.13 through 3.15 illustrate how the first 10 extrema correlations change as a function of b for a 2-block psd having r = 7. Note that in many cases ρ_1 is not the most significant peak-to-valley correlation (ρ_{PV}) and may even be positive. Which P-V correlation is most significant appears to be a function of both b and r. As b is increased from zero, the lag at which ρ_{PV} occurs
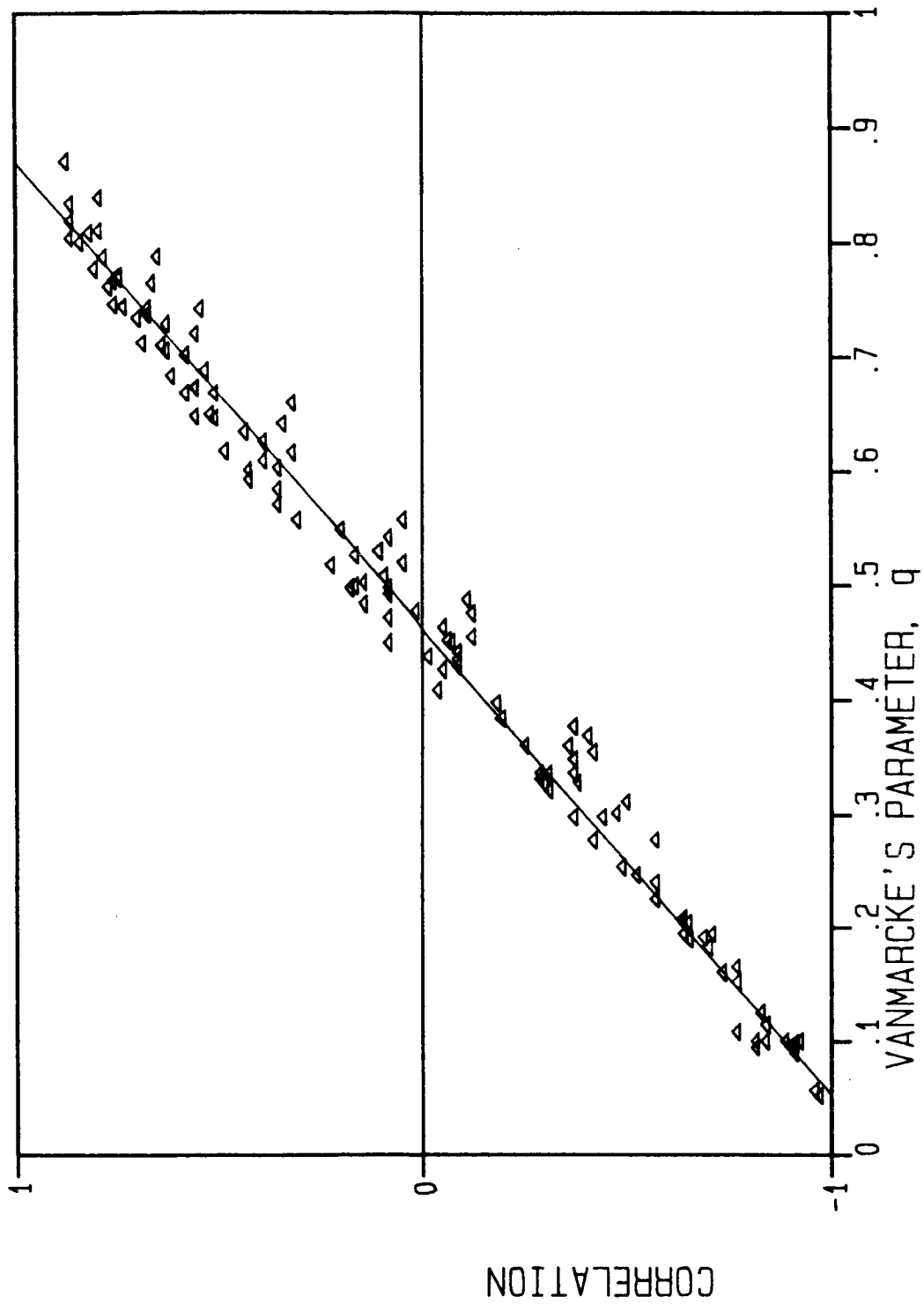
40

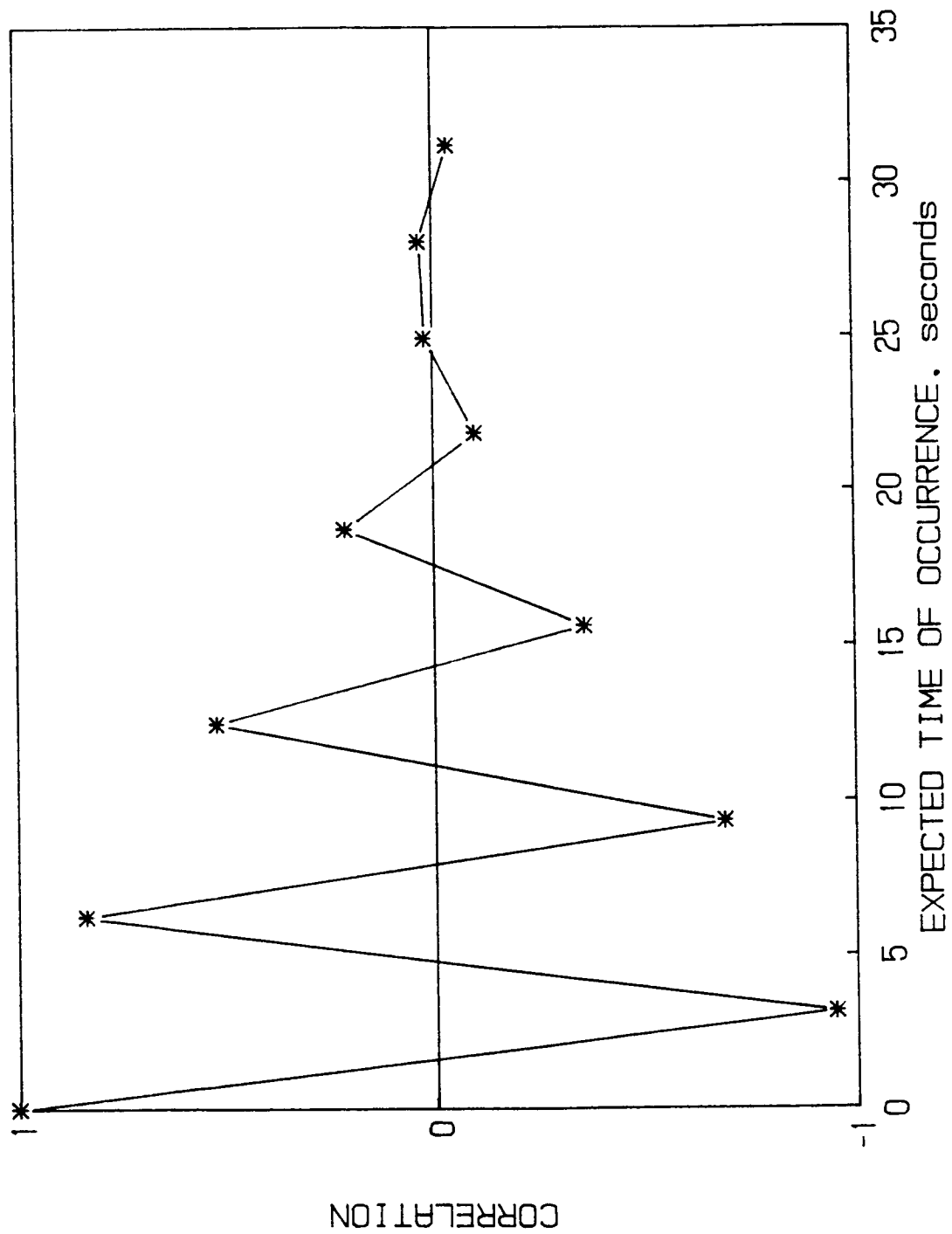Figure 3.11 Correlation ρ_1 vs Vanmarcke's Parameter: Linear Regression
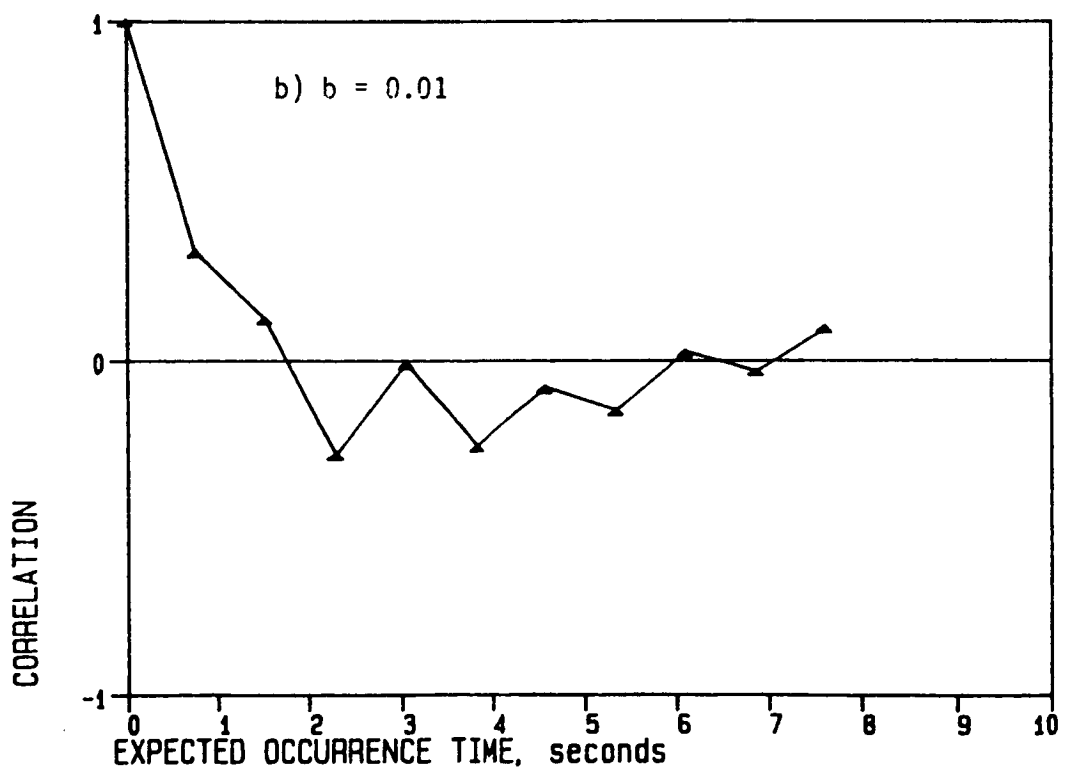
Figure 3.12 Typical Extrema Correlations: Unimodal PSD
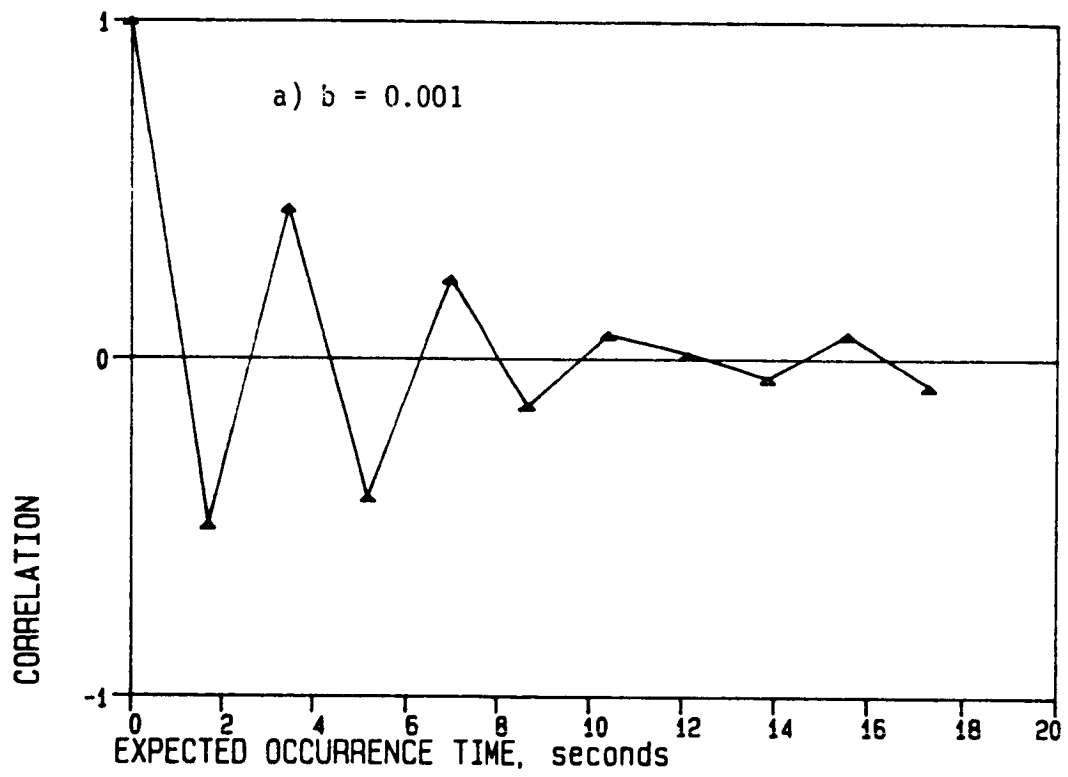
Figure 3.13 Extrema Correlations: r = 7

a) b = 0.1

b) b = 1.0
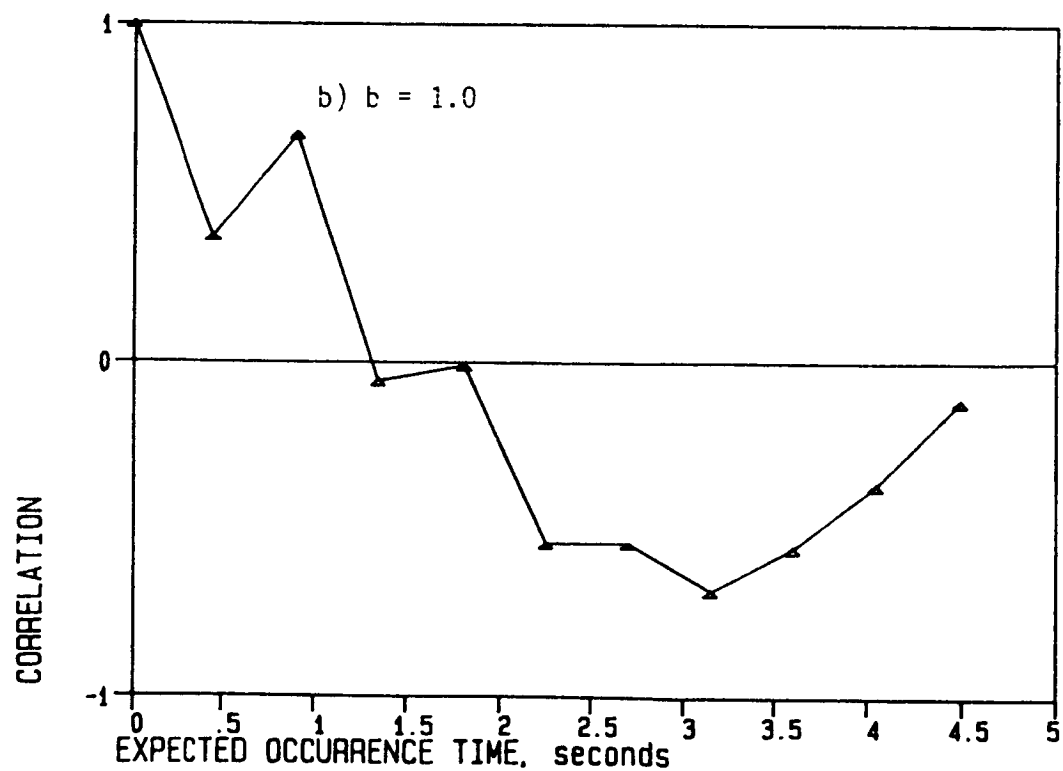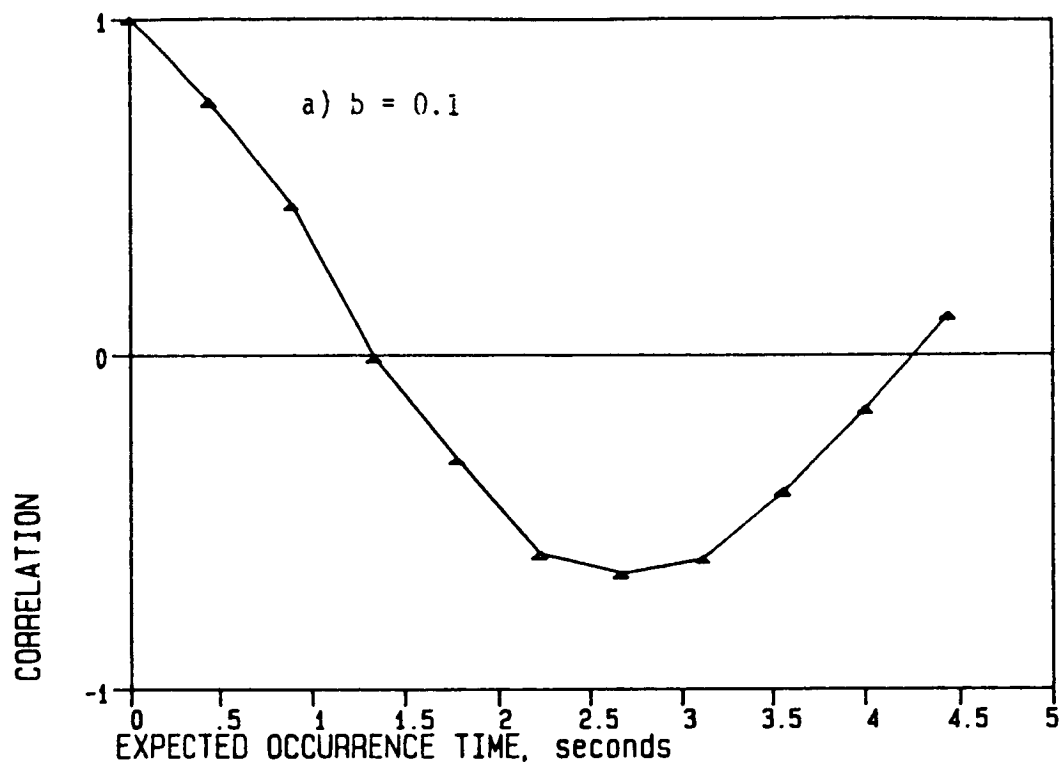
Figure 3.14   Extrema Correlations: r = 7

44
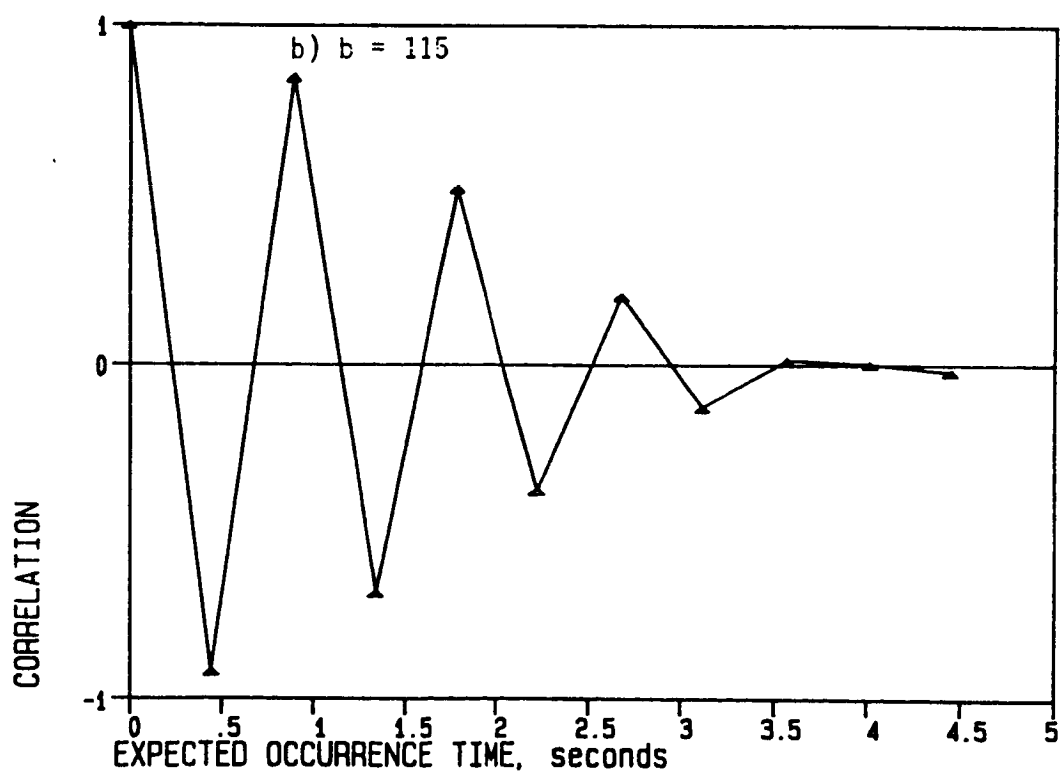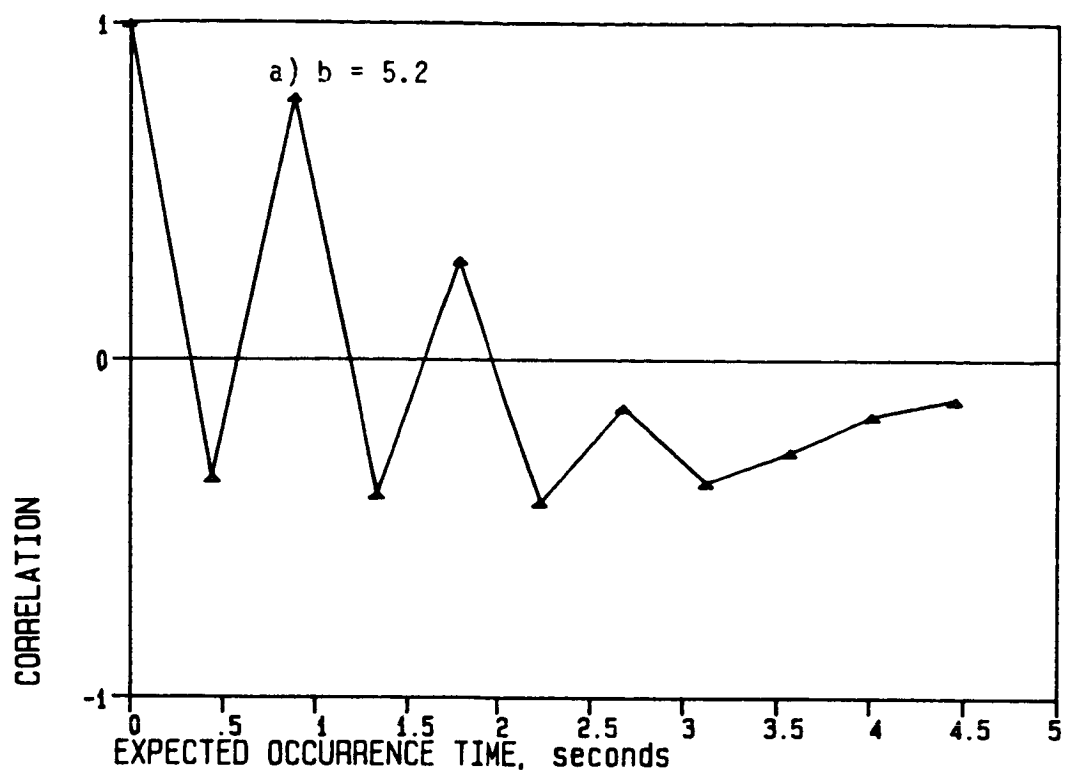
Figure 3.15 Extrema Correlations: r = 7

changes from k = 1 to k = 3, to k = 5,···until a limiting value of k = r is reached at about b = 1. As b is increased further the lag at which ρ_{PV} occurs decreases, finally coming back to k = 1 at large b values.

This behavior seems reasonable if the random process is visualized as the superposition of two narrowband processes. For very small values of b, the low frequency component is dominant, with only a low level of the high frequency component superimposed as a "noise" in the signal. The significant extrema will be the peaks and valleys of the low frequency component, and ρ_1 will be the dominant correlation. (See Figure 3.16.) At higher b values, the high frequency component becomes increasingly significant, so that the most significant valley following a large peak (and thereby giving a large rainflow range) no longer occurs immediately after that peak, but comes some n lags later. (See Figure 3.17.) At still higher b values, the high frequency component dominates and the low frequency component only appears as a slow wander about the mean. The most significant extrema correlation (and rainflow range) again occurs between adjacent peaks and valleys. (See Figure 3.18.)

This phenomenon is difficult to observe directly from a psd, but is easily seen in the autocorrelation function. As an example, Figures 3.19 through 3.24 show the $R_{XX}(\tau)$ corresponding to the extrema correlation cases presented in Figures 3.13 through 3.15. Note that in Figures 3.19 through 3.24 the upper figures are all to the same time scale to indicate how the change in area ratio, b, effects $R_{XX}(\tau)$ and the frequency content of {X(t)}. The time scale in the lower figures has been adjusted so that about the first 10 extrema of $R_{XX}(\tau)$ appear,

46
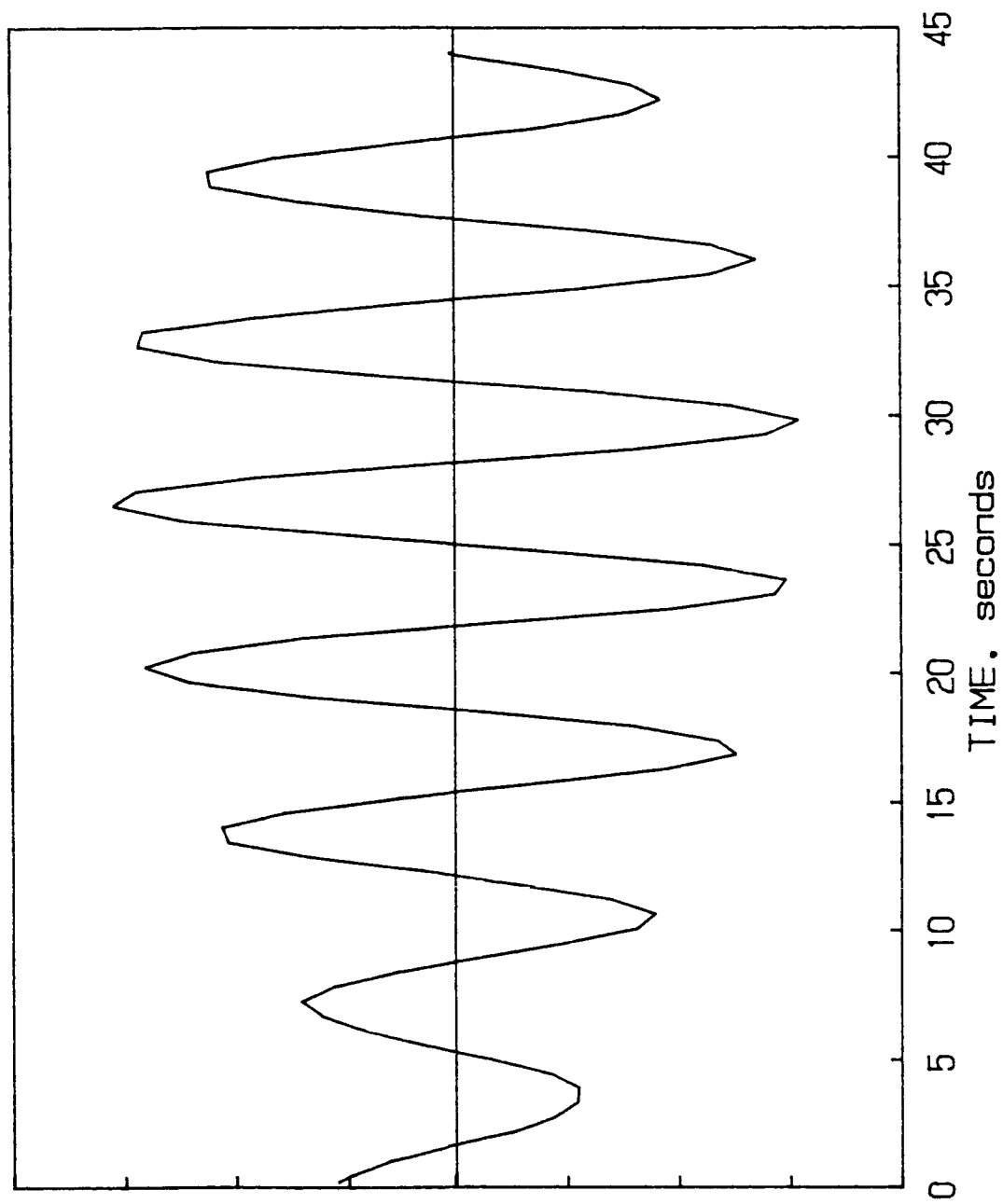
Figure 3.16 Typical Time History: Bimodal PSD, r = 3, b = 0.0016
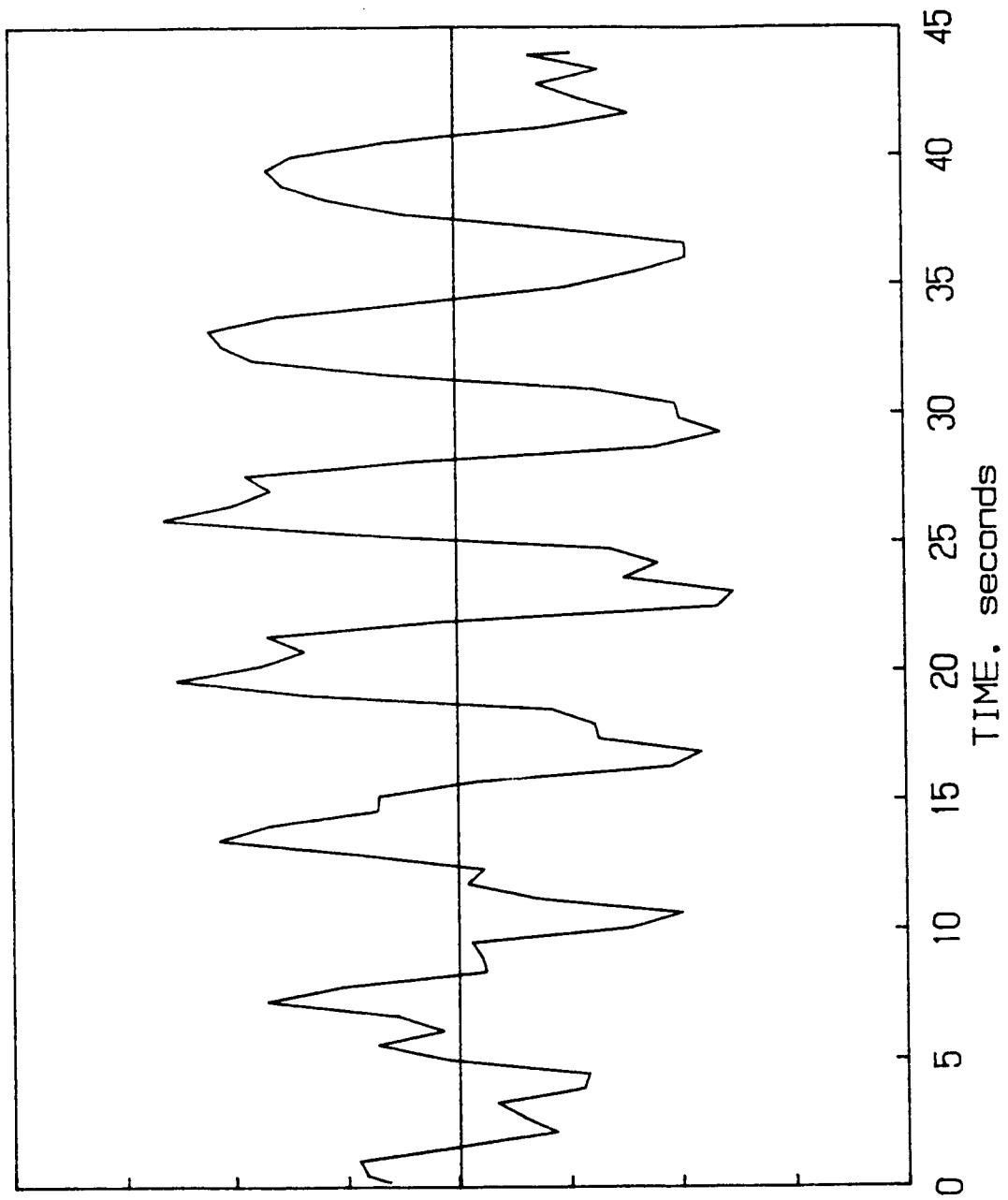
Figure 3.17 Typical Time History: Bimodal PSD, r = 3, b = 0.63
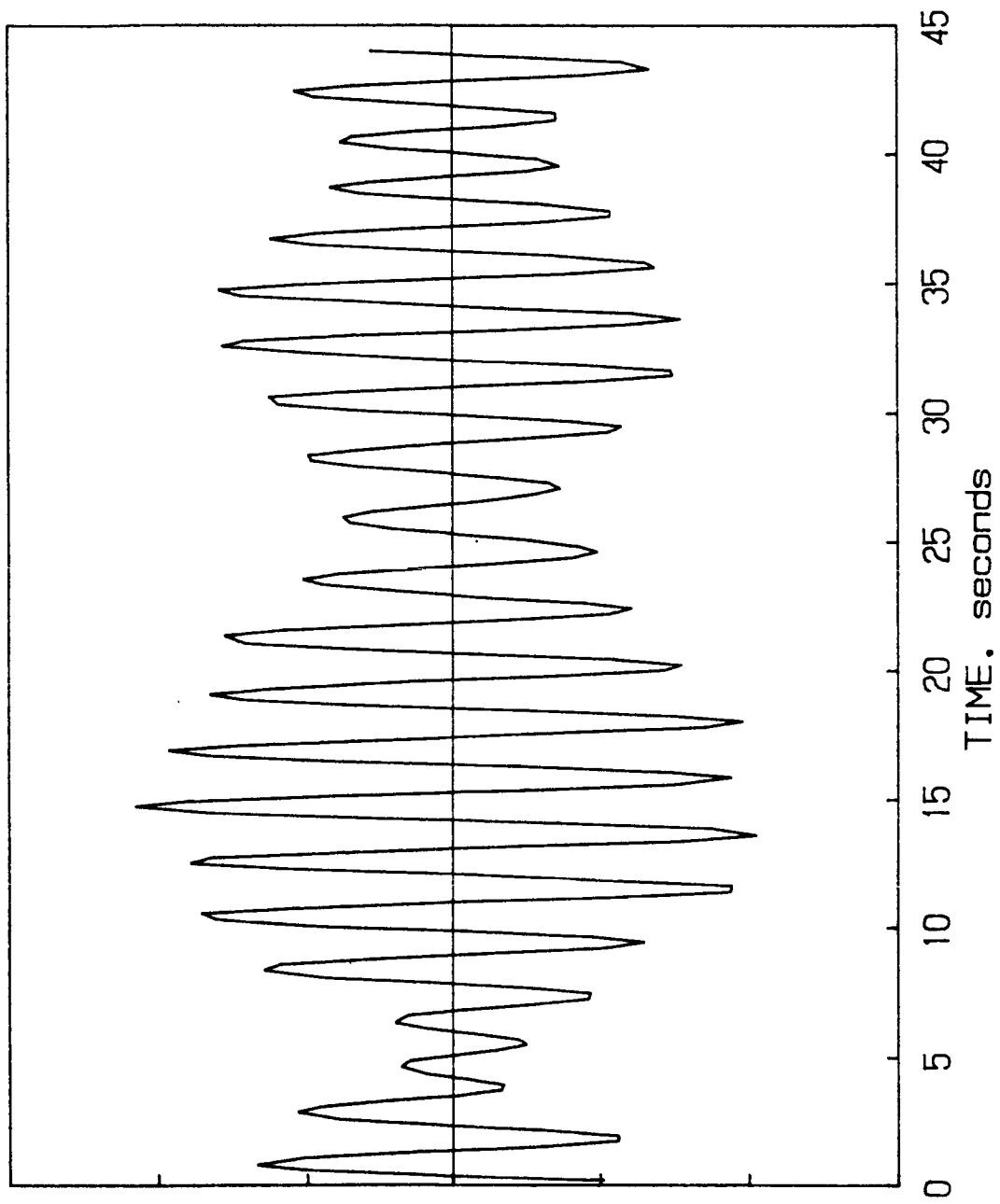
Figure 3.18 Typical Time History: Bimodal PSD, r = 3, b = 70
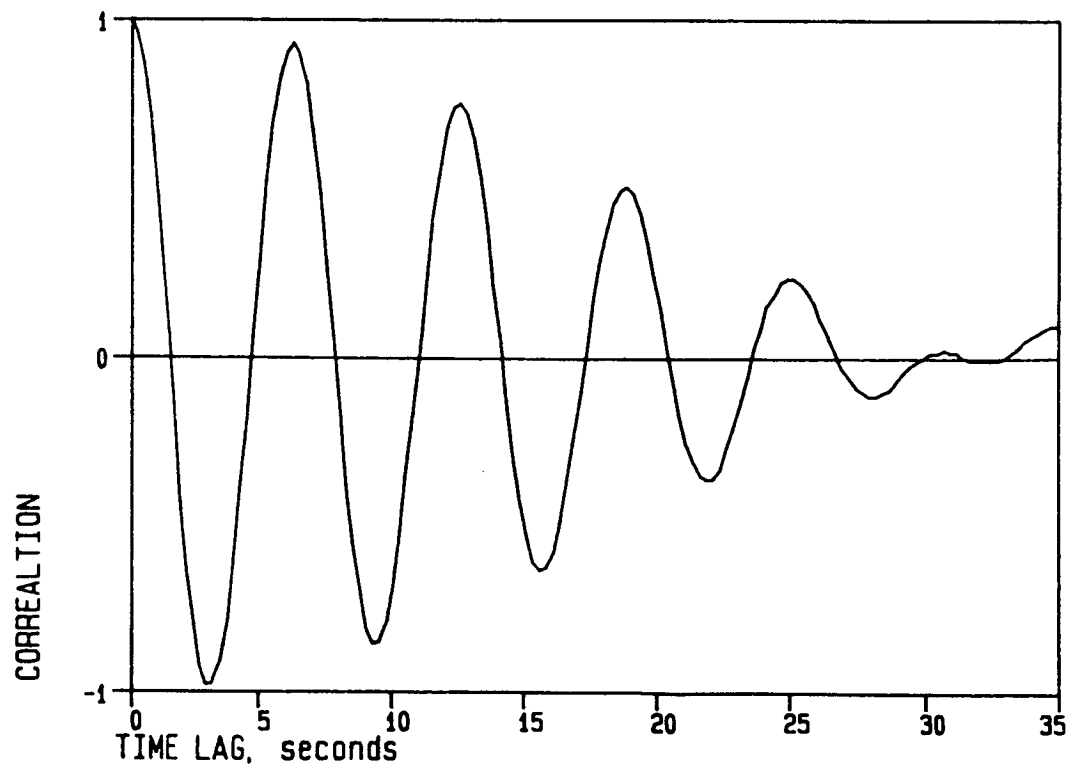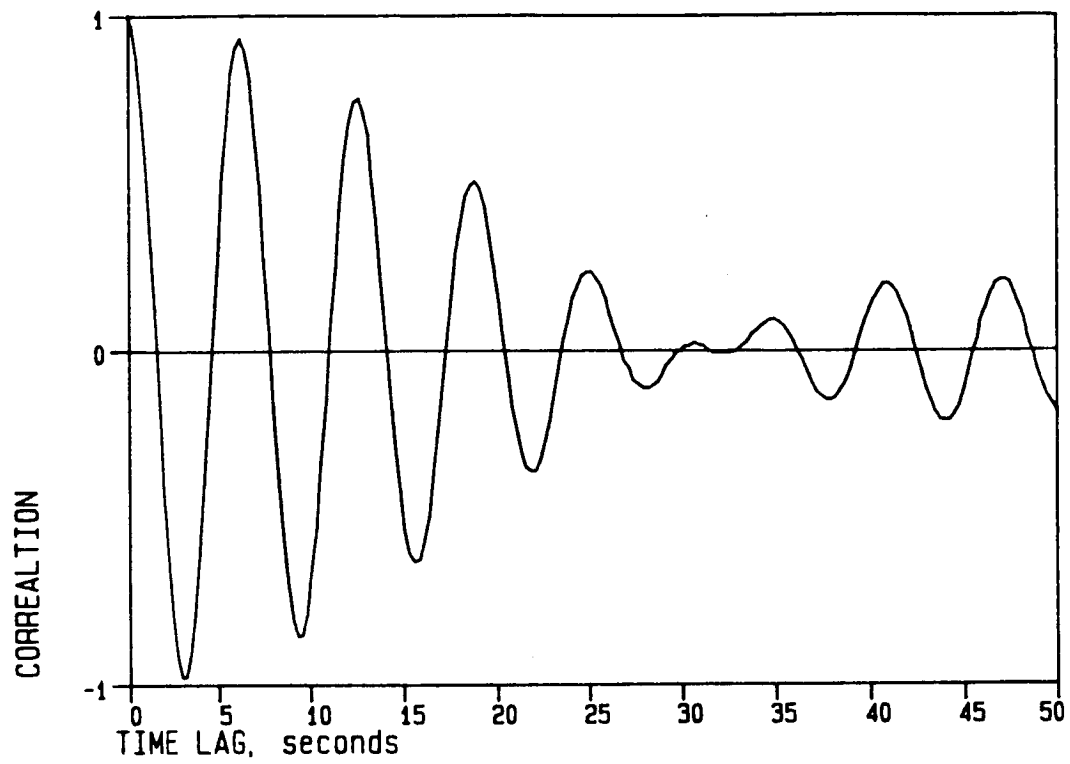
Figure 3.19   Autocorrelation Function: r = 7, b = 0.001
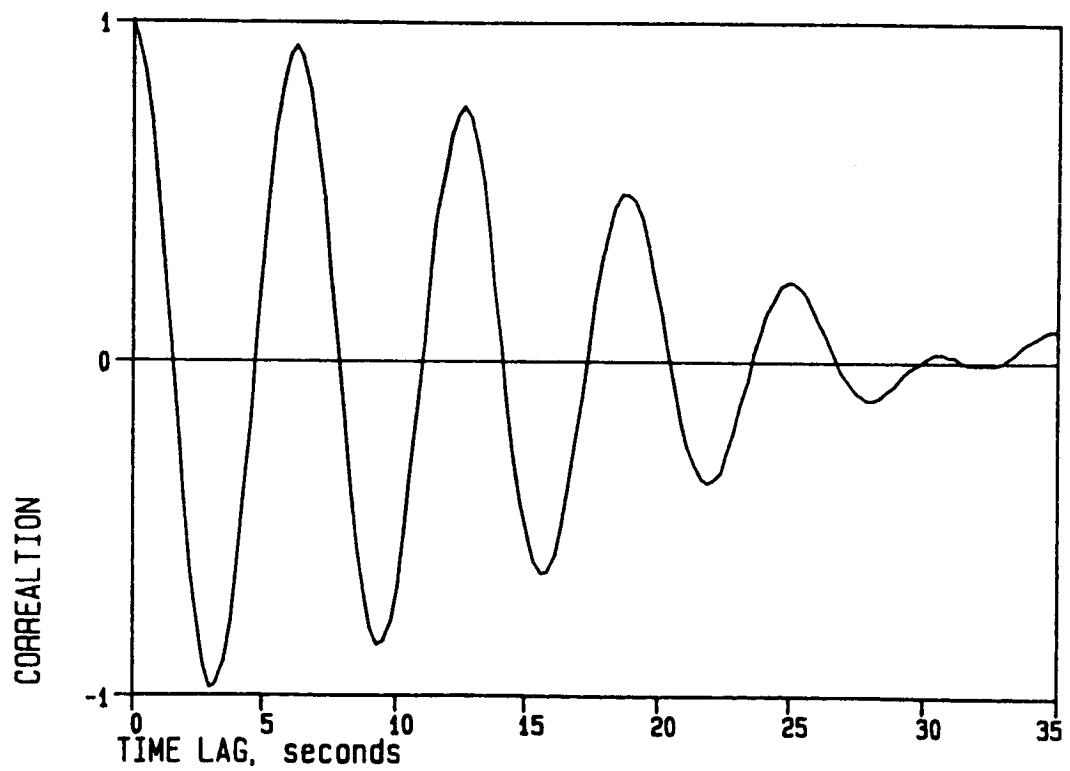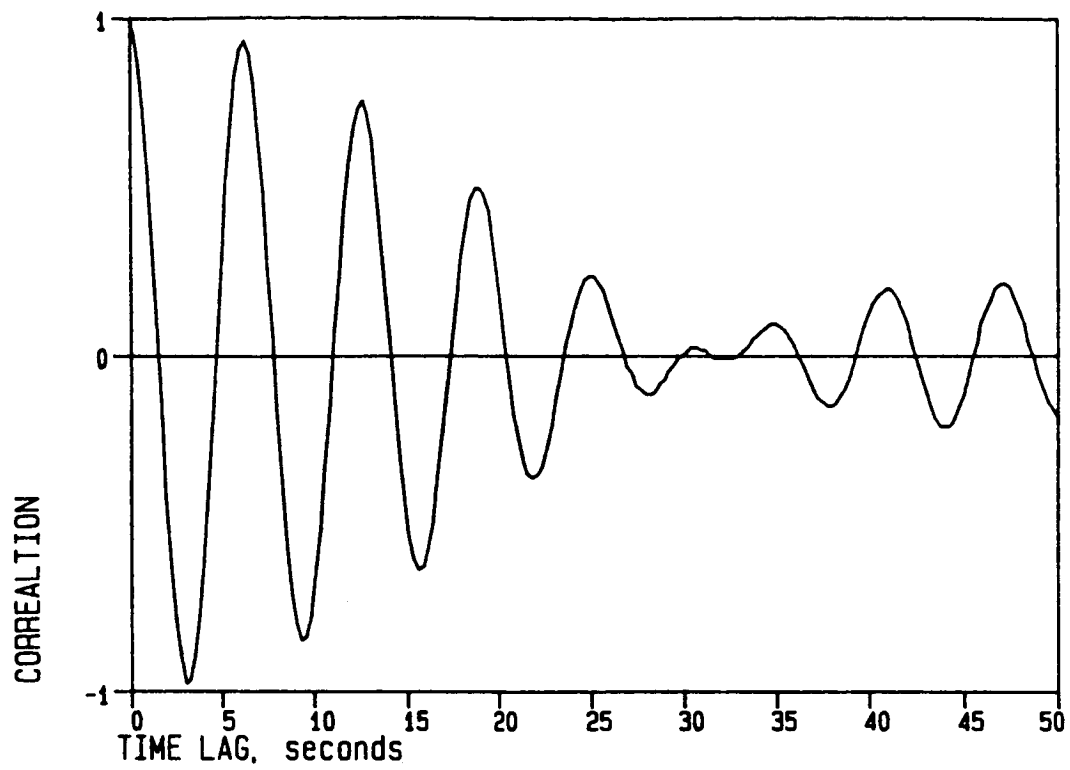
Figure 3.20   Autocorrelation Function: r = 7, b = 0.01
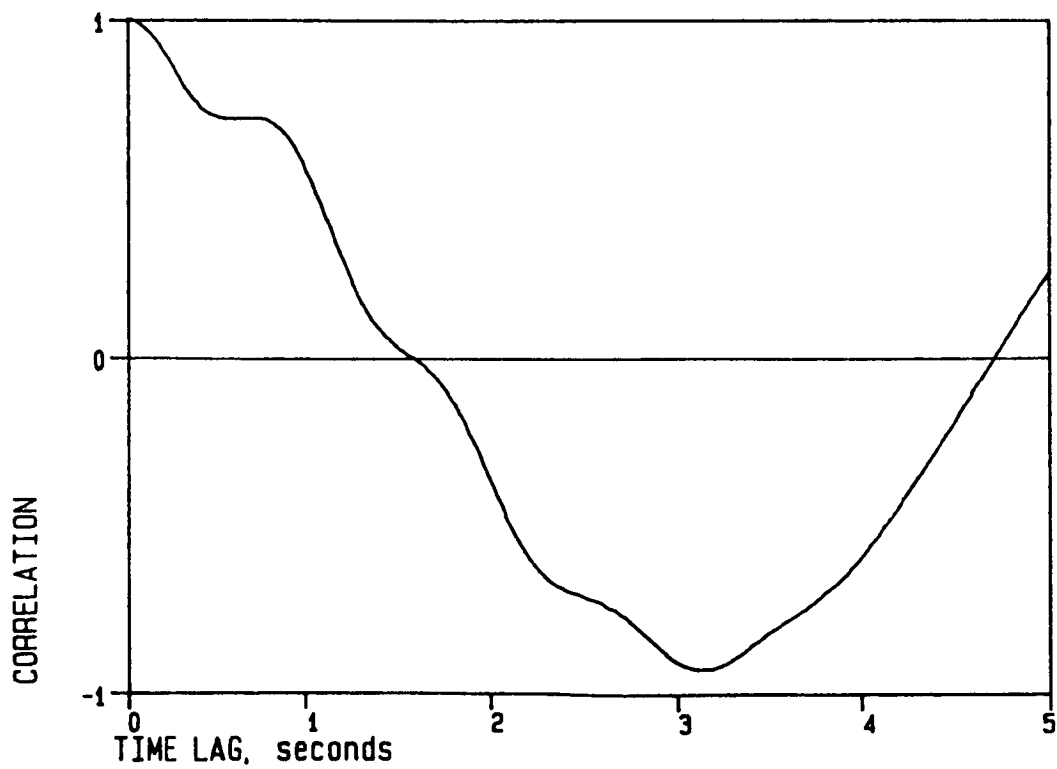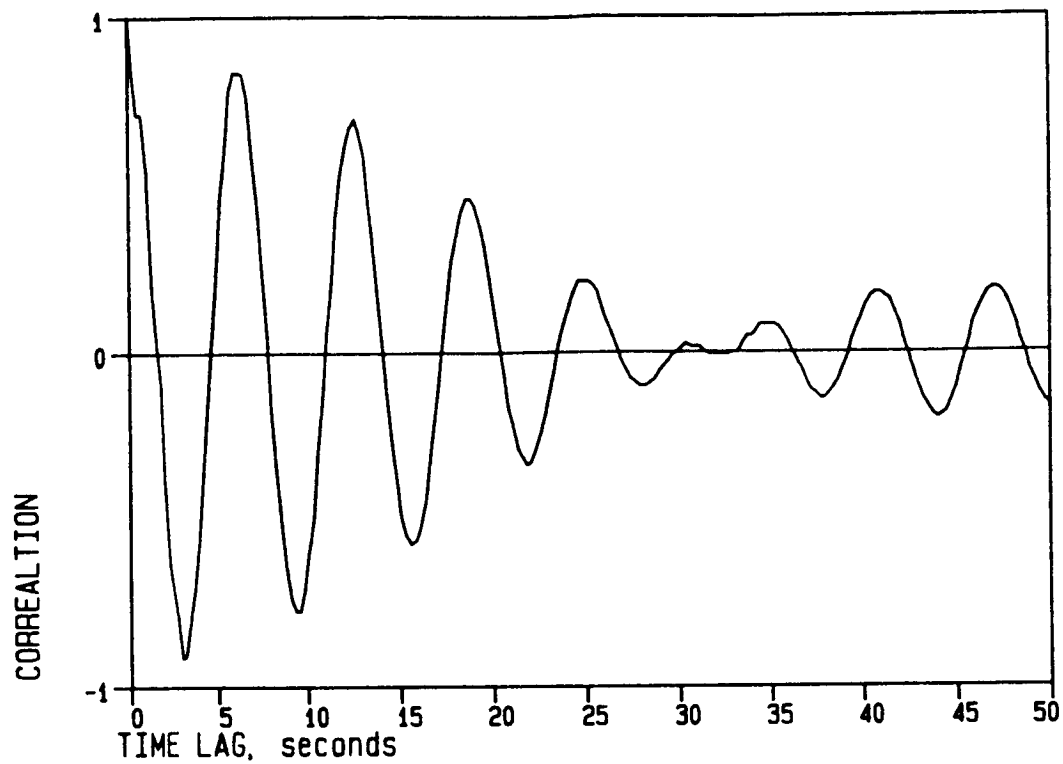
Figure 3.21 Autocorrelation Function: r = 7, b = 0.1
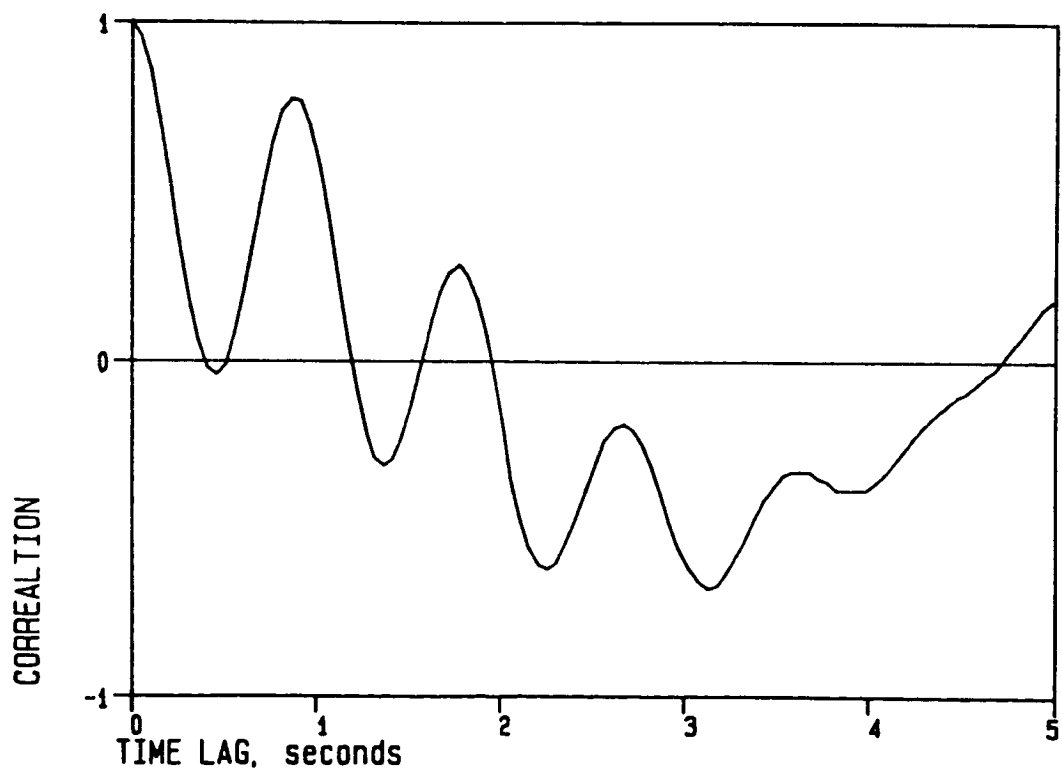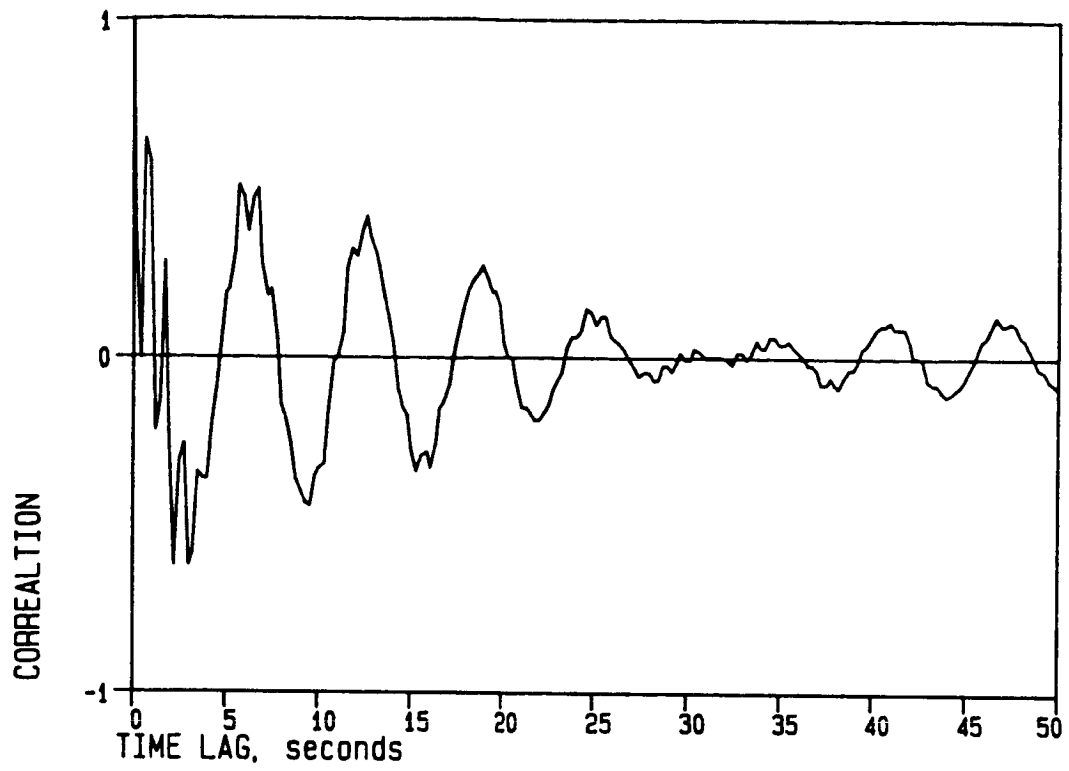
Figure 3.22   Autocorrelation Function: r = 7, b = 1.0
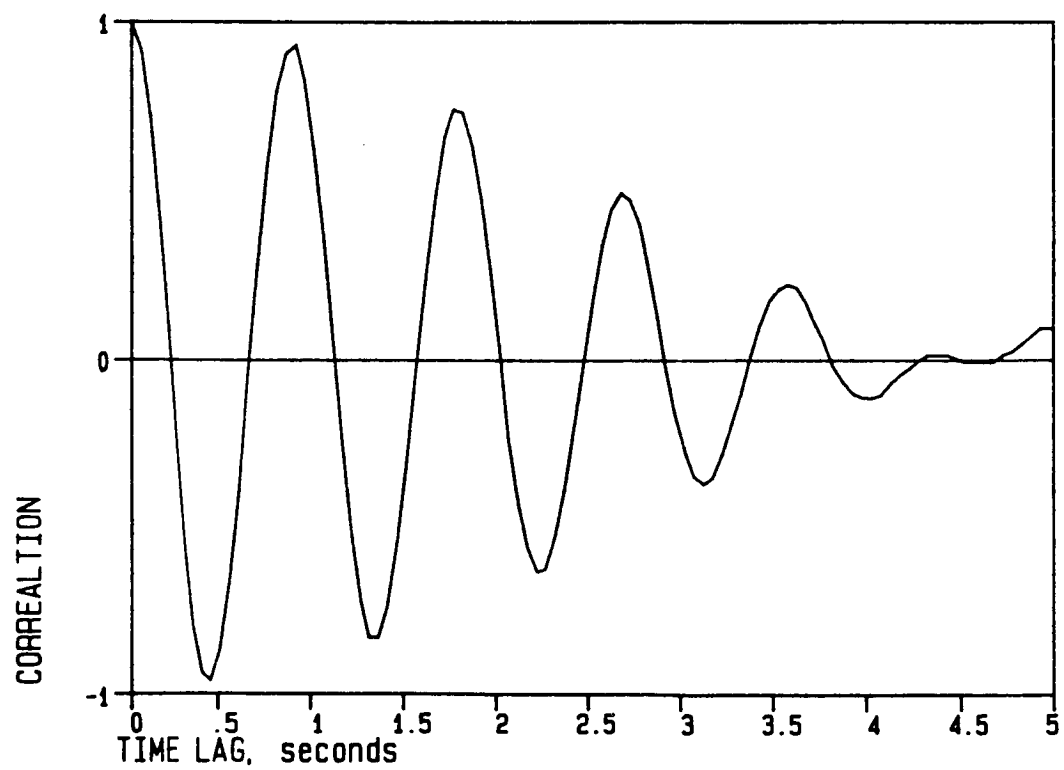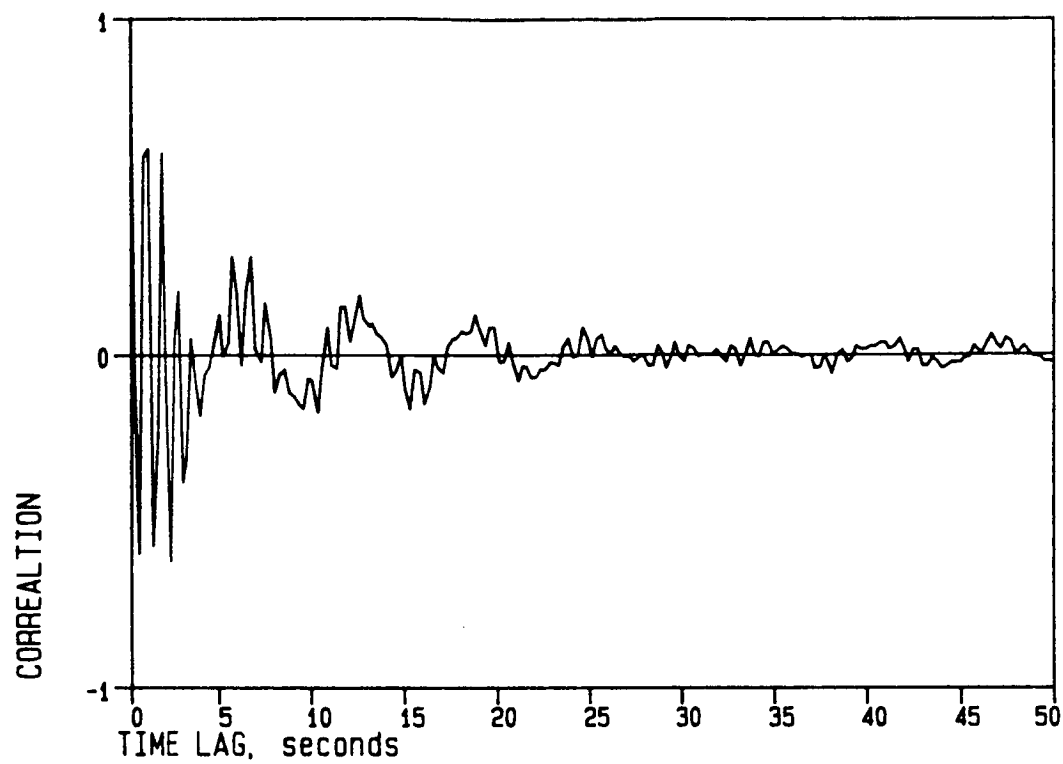
Figure 3.23   Autocorrelation Function: r = 7, b = 5.2
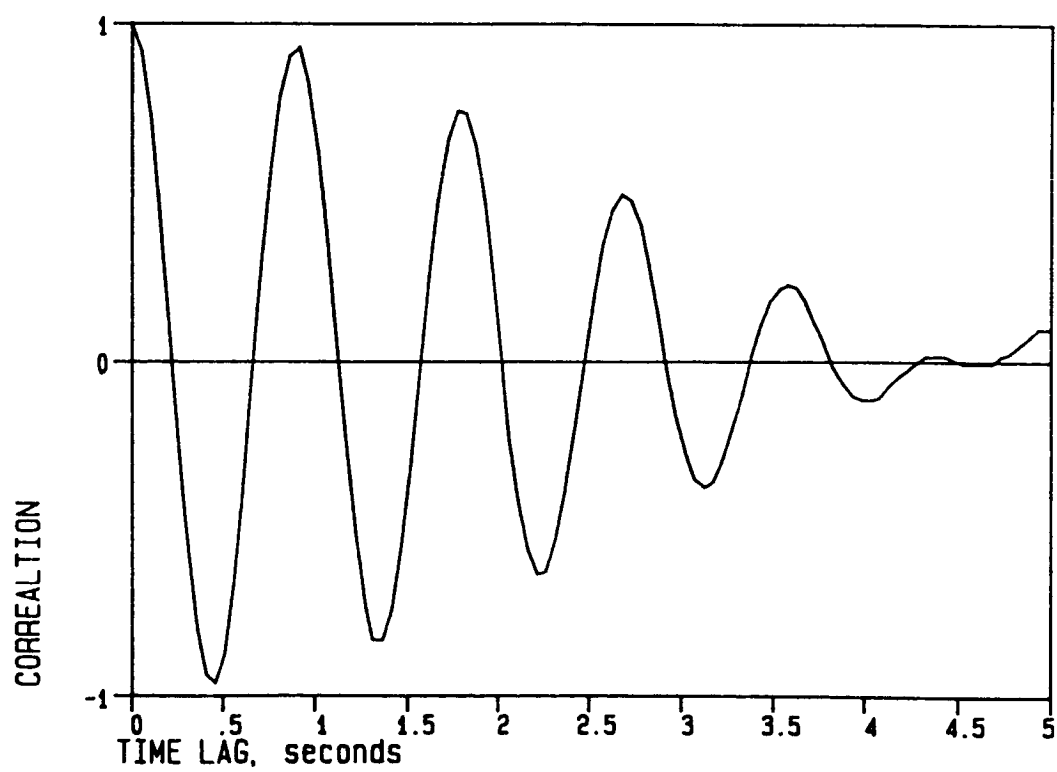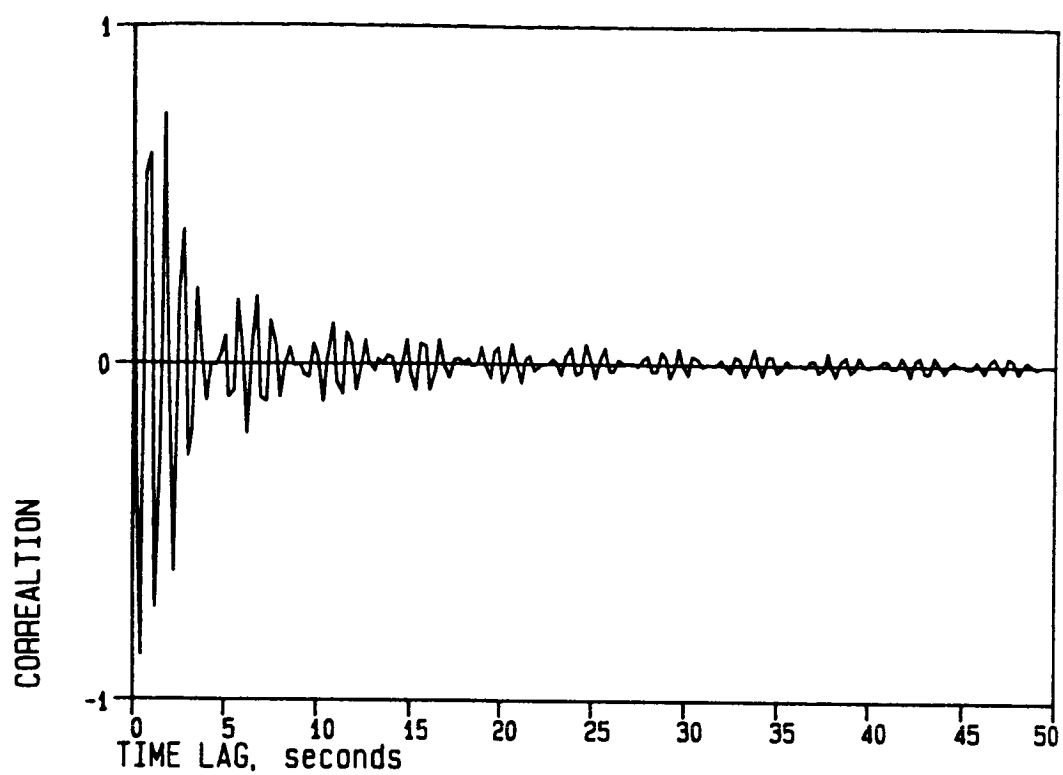
Figure 3.24   Autocorrelation Function: r = 7, b = 115

for purposes of comparison with Figures 3.13 through 3.15. The qualitative correspondence between the extrema of $R_{XX}(\tau)$ and the extrema correlations of $\{X(t)\}$ is very good in some cases, and the most significant extrema of $R_{XX}(\tau)$ can be an indicator of which P-V correlation will be most significant. Because of this qualitative correspondence between the extrema of $R_{XX}(\tau)$ and the extrema correlations of $\{X(t)\}$, it may be possible to develop an analytical method for obtaining the extrema correlations directly from $R_{XX}(\tau)$, but at this time the problem remains unsolved.

Appendix E presents the results of some efforts in this direction which, although they were not completely successful, have contributed to an improved understanding of the effects of random occurrence times and phase.

The complex behavior of the extrema correlations of processes having bimodal type psd's complicates the task of modeling the extrema as an AR process. Information is needed about both ρ_1 and ρ_{PV} as functions of bandwidth (or b and r). This introduces the difficulty of first predicting the lag at which ρ_{PV} will occur, and then of estimating its value. A technique for dealing with this problem is presented in Chapter 5 on the AR modeling of the extrema for bimodal psd's.

Chapter 4

AUTOREGRESSIVE SIMULATION: UNIMODAL PSD'S

This chapter describes the AR simulation technique as applied to random processes having a 1-block or unimodal type psd. Section 4.1 briefly reviews the characteristics of the AR(1) process previously presented in Section 2.4. Section 4.2 describes the specific application of AR(1) models to the simulation of extrema processes. The results of AR simulations are compared to those from Gaussian simulations in Section 4.3. Specifically, the rainflow range moments, $E[R^m]$, are compared as a measure of the accuracy of the simulation, and the relative computation times are compared as a measure of computational efficiency.

4.1 AR(1) Processes

The AR(1) process is a particular case of the general ARMA(p,q) family (see Section 2.4) and is determined by the equation:

$$Z_t = \phi_1 Z_{t-1} + a_t + \mu \tag{4-1}$$

in which: Z_t = current value of process

Z_{t-1} = previous value of process

ϕ_1 = autoregressive weighting parameter

a_t = current value of random variate

μ = constant

Recall that the parameter ϕ_1 is estimated by the autocorrelation observed at lag one:

$$\hat{\phi}_1 = r_1 \tag{2-40}$$

and that the random variates $\{a_k\}$ are usually i.i.d., mean-zero, normal variates, with variance estimated by:

$$\hat{\sigma}_a^2 = C_0(1 - r_1^2) \tag{2-44}$$

in which C_0 is the estimate for σ_Z^2. The autocorrelation function for an AR(1) process is given by:

$$\rho_k = \phi_1 \rho_{k-1} \quad k = 1,2,3,\dots \tag{4-2}$$

given that $\phi_1 = \rho_1$. Equation (4-2) implies that the correlations for an AR(1) process satisfy the relationship:

$$\rho_n = [\rho_1]^n \quad n = 2,3,4,\dots \tag{4-3}$$

4.2 AR(1) Application to Extrema Processes

Modeling the extrema of a random process by an AR(1) model required several innovations. First, because AR models define the present value, Z_t, as a sum of past values, the Central Limit Theorem may be invoked to conclude that the pdf of Z_t must approach a normal distribution. But the peaks (or valleys) of a Gaussian random process are known to have the S.O. Rice distribution, not a normal distribution. This difficulty was solved by mapping the extrema from the normal distribution, after the AR simulation, to the S.O. Rice distribution. The mapping of the extrema from the standard normal, N(0,1), distribution to an S.O. Rice distribution was performed using a two-stage table look-up procedure based on the inverse transform technique (1,28). Two tables or arrays were evaluated at the beginning of the simulation, the first giving the standard normal cdf from -2.75 to 2.75 at 512 points, the

58

other giving the S.O. Rice cdf from $-1.5\sigma_X$ to $5.5\sigma_X$ at 512 points. For the mapping, a table look-up or search was first performed on the normal cdf array, mapping each point Z_t to a point Y_t on the range [0,1]. A second table look-up on the S.O. Rice cdf array then mapped each point Y_t to a point X_t. This procedure is illustrated in Figure 4.1. The result at this point in the simulation was a sequence of S.O. Rice distributed, correlated peaks. The sequence of peaks and valleys required to perform a rainflow range identification was generated by simply changing the sign on alternating peak values. The simulation process is illustrated in Figure 4.2, showing the forms of the distributions at the various stages in the procedure. An outline of the simulation algorithm is given in Figure 4.3.

Two parameters are required for the simulation procedure: the AR(1) parameter, ϕ_1, and the irregularity factor, α. The parameter ϕ_1 determines the correlation between adjacent simulation values and may be estimated as the negative of the peak-to-valley correlation, ρ_1, given in Figure 3.11, or by Equation 3-20. The irregularity factor, α, which is needed to determine the S.O. Rice distribution used in the mapping is determined from the psd using Equation 2-17. Thus, the two spectral parameters q and α are the essential inputs required for the AR(1) simulation technique. The specific parameter values used for the AR(1) simulations are tabulated in Appendix C.

The mapping from the normal distribution to the S.O. Rice distribution is nonlinear. Because of this nonlinearity the correlations between simulated points would be expected to be changed by the mapping. This potential effect was studied during the Gaussian simulations described

59
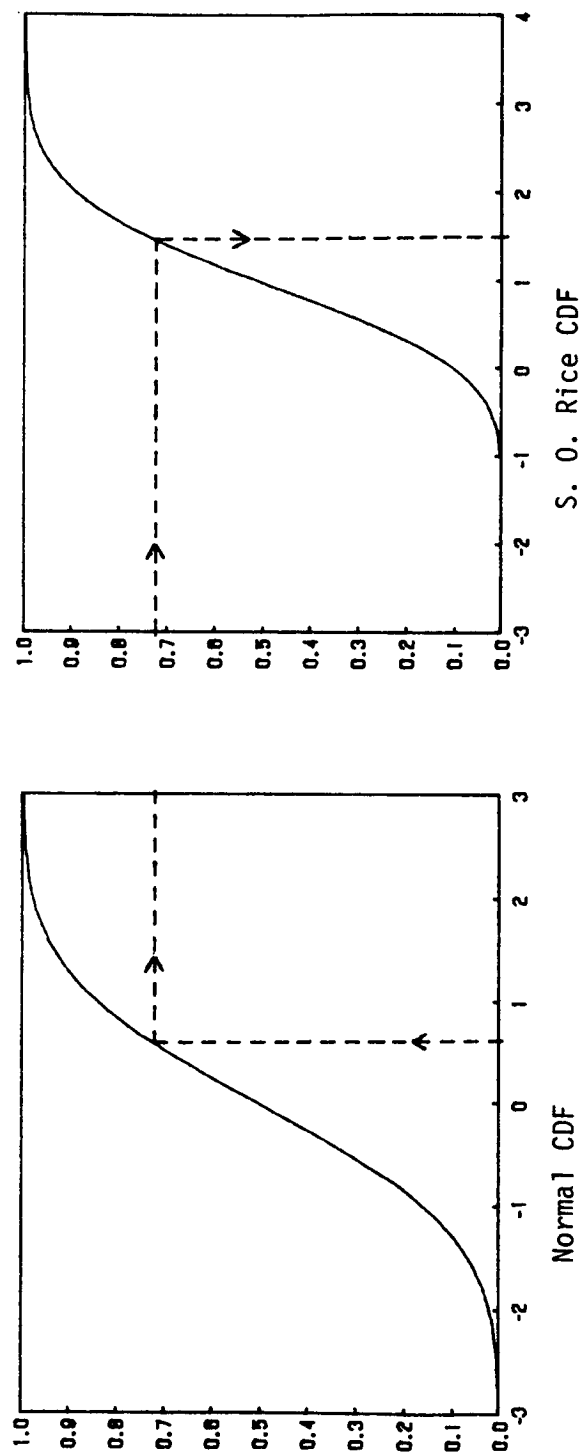
Figure 4.1 Mapping from Normal to S. O. Rice Distribution

60

AR(1) Model

$$Z_t = \phi_1 Z_{t-1} + a_t$$

Simulation

Sequence of
Correlated
Normal Random
Variables

Mapping

Sequence of
Correlated
S. O. Rice
Distributed
Random Variables

Alternate
Signs

Sequence of Correlated Extrema
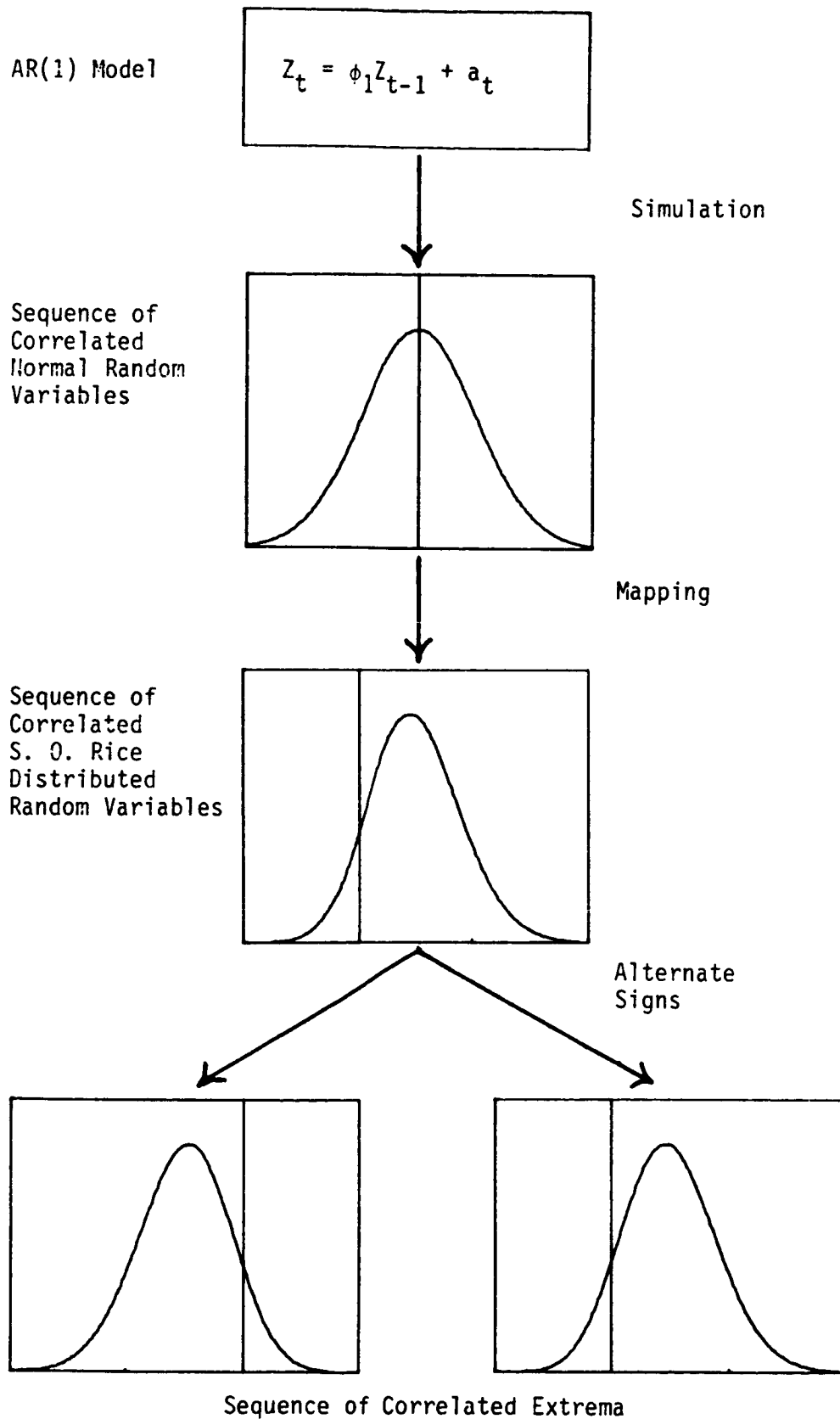
Figure 4.2 Autoregressive Simulation Technique

Figure 4.3

AR(1) SIMULATION ALGORITHM

1) Input Data: α, ϕ_1

2) Generate Arrays:

    FP - S.O. Rice CDF, Determined By α

    BG - Standard Normal CDF, N(0,1)

3) Compute Standard Deviation Of AR(1) Process:

$$SD = (1 - \phi_1^{2})^{-1/2}$$

4) AR Simulation:

    a) Generate N(0,1) Random Variate, U

    b) $W_n = \phi_1 * W_{n-1} + U$

    c) $Z_n = W_n/SD$

    d) Return To a) Until Required Number Of Points Simulated

5) Map From N(0,1) To S.O. Rice (α):

    a) Look-up Y_n Corresponding To Z_n From Array BG

    b) Look-up X_n Corresponding to Y_n From Array FP

6) Generate Peak-Valley Sequence

    $X_n = -X_n$ For n Odd

7) Perform Statistical And Rainflow Analysis On X_n Sequence As Required

in Chapter 3. By mapping the Gaussian simulation extrema from the S.O. Rice distribution to the normal distribution, and recomputing the extrema correlations, the actual change in the correlation due to the mapping was found. Note that this mapping procedure is simply the inverse of the mapping process used in the AR(1) simulation algorithm to go from the normal distribution to the S.O. Rice distribution. The effect of this mapping on the lag one correlation, ρ_1, is summarized in Table 4.1 for several unimodal and bimodal psd cases. It was found that if the mapping changed the correlation, it was always to make ρ_1 more positive. However, the magnitude of this change was very small and was no more than the change in ρ_1 observed between separate Gaussian simulation realizations for a particular psd. Therefore, the effect of the nonlinear mapping on the extrema correlations was neglected in the AR model.

4.3 Simulation Results

The results of the AR(1) simulations and rainflow range identification are compared to the results obtained using the Gaussian simulation procedure in Figures 4.4 through 4.6. The results are plotted in terms of the expected range moment, $E[R^m]$, as a function of Vanmarcke's bandwidth parameter, q, for m = 3,5,7, respectively. As shown, the AR(1) simulation technique closely reproduces the range moments obtained with the Gaussian method. Note that the value of $E[R^m]$ approaches the theoretical value of $E[S^m]$ for the limiting narrowband case, as given by Equation 2-32.

A comparison of the required computation time for the two methods showed that the AR(1) technique averaged 11.7 times faster than the

Gaussian technique. This comparison was made to Gaussian simulations which synthesized X(t) as a sum of 20 harmonics or psd components, (N = 20 in Equation 2-34) and which used relatively large time steps, such that approximately every fourth point in the time series is an extremum. These two conditions represent approximate limits on the efficiency of the Gaussian technique in that the use of fewer than 20 harmonics may bring into question the normality of the signal, while the use of larger time steps will decrease the accuracy of the extrema determination. Actual simulation time on an IBM AT Personal Computer (with a math coprocessor) for a sequence of 4,000 extrema averaged 7 minutes 24 seconds using the Gaussian technique. The AR(1) method required only 38 seconds for the simulation of 4,000 extrema.

Table 4-1   65

EFFECT OF MAPPING PROCEDURE ON CORRELATION ρ_1

PSD Type	q	ρ_1	
		S.O. Rice	Normal
Unimodal	.058	-.95	-.94
	.115	-.84	-.82
	.160	-.73	-.71
	.225	-.57	-.55
	.297	-.34	-.32
Bimodal			
r = 2.0	.097	-.90	-.88
	.247	-.52	-.49
	.321	-.30	-.29
	.336	-.32	-.30
r = 3.0	.098	-.90	-.89
	.332	-.27	-.26
	.450	.08	.09
	.503	.19	.20
r = 4.0	.098	-.91	-.89
	.384	-.17	-.16
	.517	.24	.24
	.600	.43	.43
r = 5.0	.098	-.91	-.90
	.427	-.05	-.04
	.557	.33	.33
	.668	.58	.58
r = 6.0	.098	-.91	-.90
	.429	-.09	-.08
	.583	.36	.36
	.713	.68	.68
r = 7.0	.098	-.92	-.90
	.441	-.09	-.07
	.602	.37	.38
	.745	.74	.74

Figure 4.4 Range Moment Comparison, AR(1) and Gaussian Techniques: m = 3
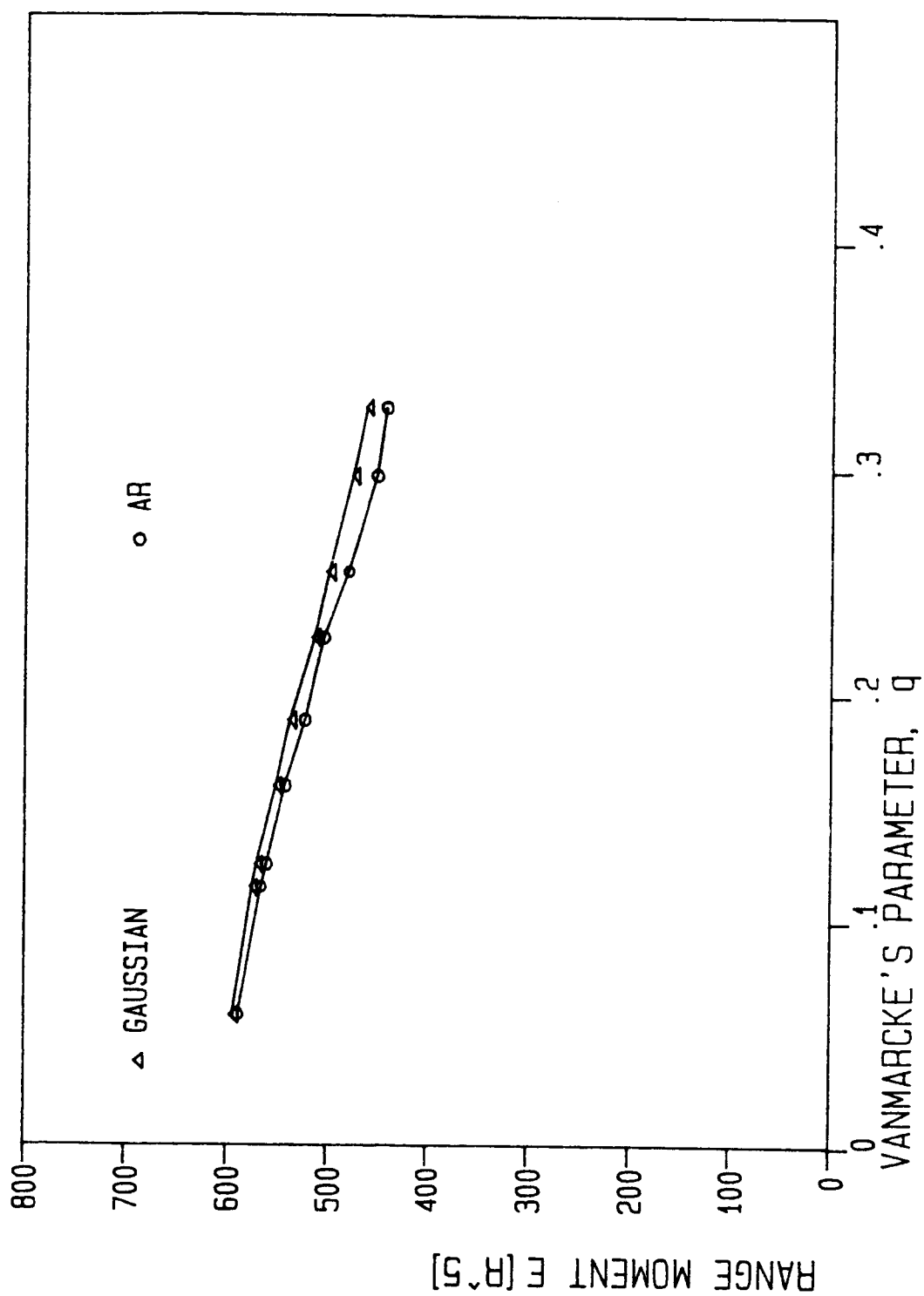
Figure 4.5 Range Moment Comparison, AR(1) and Gaussian Techniques: m = 5
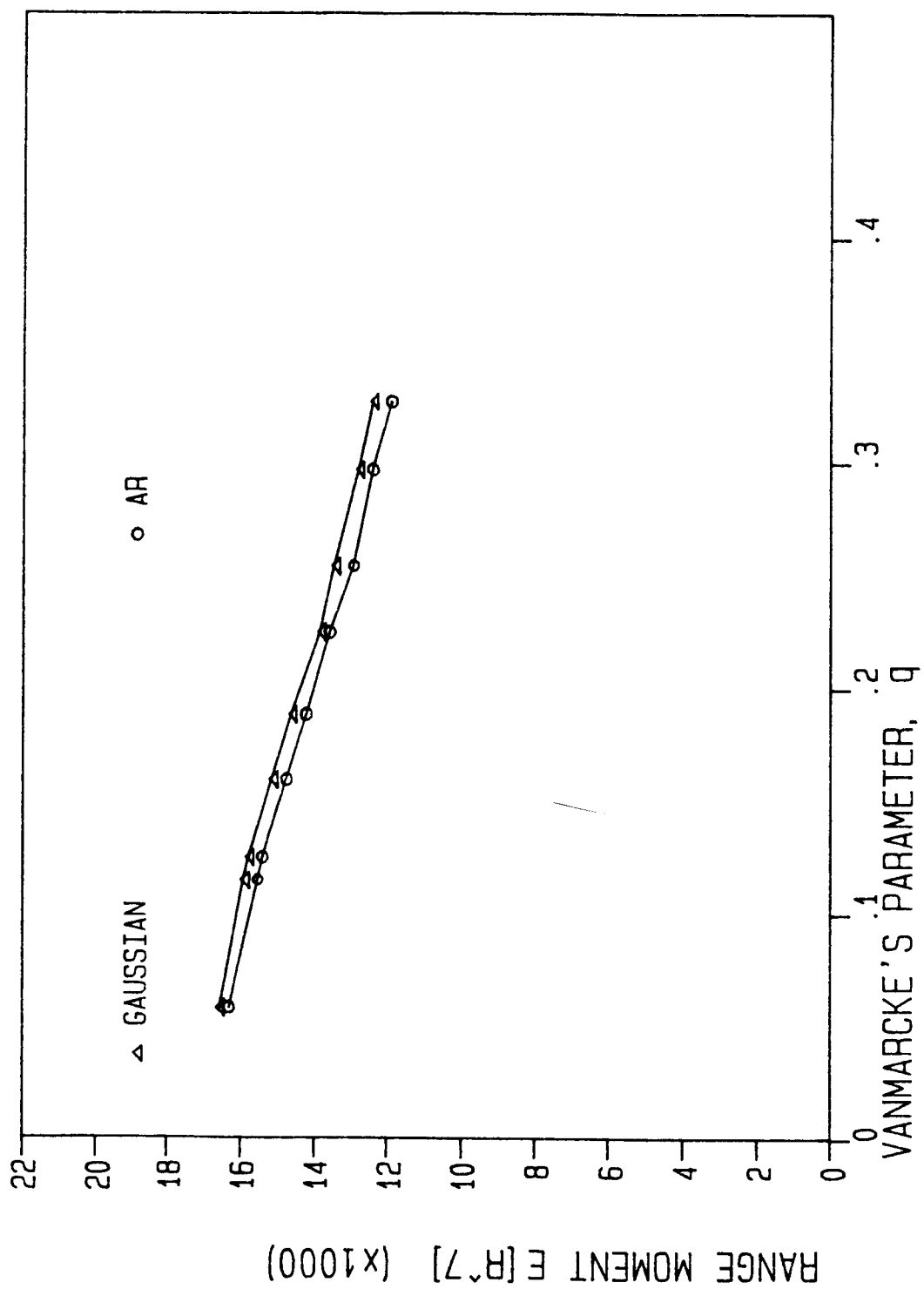
Figure 4.6 Range Moment Comparison, AR(1) and Gaussian Techniques: m = 7

Chapter 5

AUTOREGRESSIVE SIMULATION FOR BIMODAL PSD'S

This chapter discusses the adaptation of the AR(1) simulation technique for unimodal psd's to certain special cases of bimodal psd's. These special cases are the 2-block psd's described in Chapter 3.

Section 5.1 briefly discusses the difficulties encountered in modeling a bimodal psd extrema process with an AR(p) or ARMA(p,q) model. In Section 5.2 the details of the modifications to the AR(1) model are presented. Section 5.3 is a comparison of the results of the proposed technique to the Gaussian simulation method, in terms of predicted range moments and required computation time.

5.1 Bimodal PSD Process Modeling Difficulties

As discussed in Section 3.3, the extrema correlations for bimodal psd processes exhibit a complicated behavior which is a function of both b and r. (See Figures 3.13 through 3.15). Information about $\rho_1, \rho_2, \cdots \rho_{pv}$ as functions of bandwidth would be required for applying either an AR(p) or ARMA(p,q) type model. However, the usefulness of such a model is limited by the number of parameters required to define it.

An AR(p) or ARMA(p,q) model is determined by the ARMA parameters $\phi_1, \phi_2, \cdots \phi_p$, and $\theta_1, \theta_2, \cdots \theta_q$, which may be estimated as functions of the extrema correlations, which in turn must be described in some form as functions of bandwidth (or b and r). A high order ARMA(p,q) model would be needed to reproduce the complex behavior of the extrema correlations $\rho_1, \rho_2, \cdots \rho_{pv}$. Thus, using an AR(p) or ARMA(p,q) model to directly simulate the extrema of a bimodal psd random process would require

considerable effort in estimating a large number of parameters. However, a much simpler adaptation of the AR(1) model which seems promising is discussed below.

5.2 Adaptation of the AR(1) Model

Rather than modeling the extrema of a bimodal psd process as an ARMA(p,q) process with many parameters, the technique proposed herein is to model the extrema process as the superposition of two AR(1) models. The 2-block psd's described in Chapter 3 were all composed of two narrow-band single blocks, and for such a single block psd the AR(1) model has been shown to produce damage predictions comparable to those obtained using the Gaussian technique. The following development attempts to simulate the extrema for a 2-block psd by superposition of two AR(1) models (one for each block), with the superposition depending directly on the frequency ratio, r, and the area ratio, b.

The superposition technique is most easily implemented for psd's which have odd integer values of r, so that every r^{th} extrema of the high-frequency AR(1) component matches an extremum in the low-frequency AR(1) component. An interpolation of the low-frequency component at r-1 points between its extrema is also necessary in order to augment this component with intermediate points corresponding to the "unmatched" extrema in the high frequency component. The superposition of the two components can then be performed. The relative contribution of the two components to the variance of the random process {X(t)} is determined by the psd area ratio, b, and is provided for by scaling each component prior to the superposition.

The superposition introduces an approximation by assuming that the two components have extrema which exactly coincide in time, whereas this is not true for the actual random process. The effect of this approximation should be to overestimate the stress ranges when r is an odd integer, because each peak in the low frequency component matches a peak in the high frequency component and each valley matches a valley. See Figure 5.1a.

When r is an even integer, however, the effect of the superposition is to underestimate the stress ranges, because now a peak in one of the components may match with a valley in the other. See Figure 5.1b. This effect can be expected to grossly distort the simulated time history and stress ranges. As r becomes large, though, this error is reduced because for each peak (or valley) in the low-frequency component there is a peak (or valley) very close to it in the high-frequency component. See Figure 5.1c. An approximate value for r beyond which this effect may be neglected without significant loss of accuracy is discussed in Section 5.3.

The extension of the superposition to the general case of non-integer values of r requires interpolation of both the high and low frequency components because in general the extrema in the components no longer correspond in time. Thus each component must be augmented by intermediate points which correspond in time to the extrema in the other component.

The key to performing the required interpolation is to note that the psd frequency ratio r gives the number of high frequency component extrema which occur for each low frequency component extremum. For
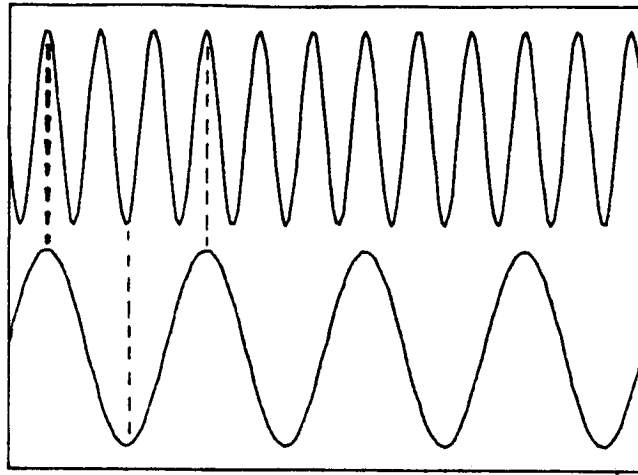
a) r = 3
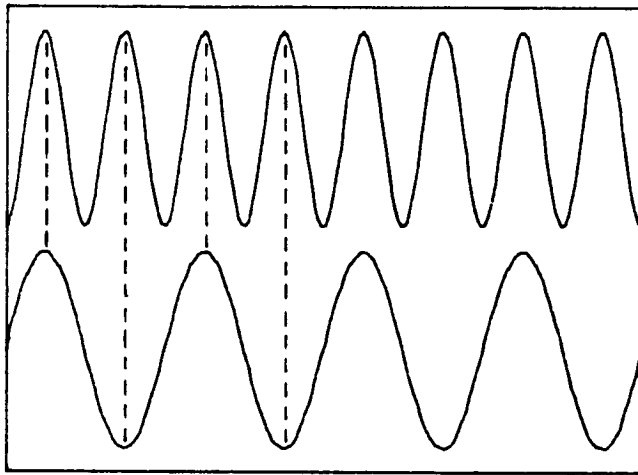
b) r = 2
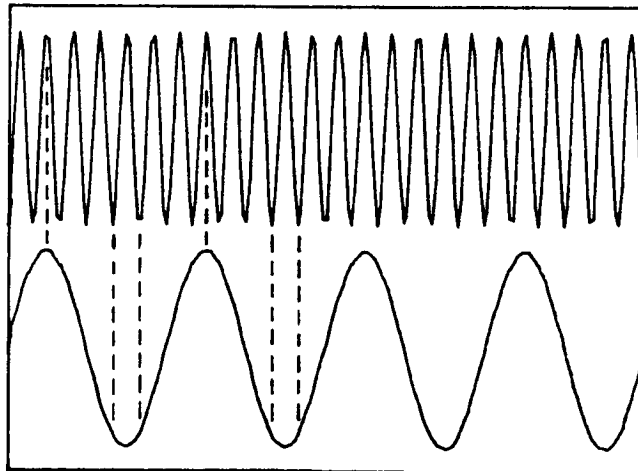
c) r = 6

Figure 5.1 Superposition of Time History Components

example, a value of r = 3.5 means that "3 and 1/2" extrema   occur in the high frequency component for each low frequency extremum. Of course, the extrema are actually integer numbered. Thus, to superimpose the two components the high frequency component must be interpolated after every 3rd extremum to find a value to match with a low frequency extremum.

In general, the largest integer less than r, INT(r), gives the extremum multiple after which an interpolation must be made, and the fractional (or non-integer) part of r, r-INT(r), gives the "time" after this extrema at which the high frequency component must be interpolated.

Similarly, the inverse of the psd frequency ratio, 1/r, determines the points at which the low frequency component must be interpolated to provide values matching the high frequency component extrema. See Figure 5.2.

The general interpolation equation used in the simulation algorithm is:

$$Y = \frac{X(i) - X(i+1)}{2} \cos(\varepsilon\pi) + \frac{X(i) + X(i+1)}{2} \qquad (5-1)$$

in which:

Y = interpolated value

X = extrema sequence being interpolated

X(i) = X(mn), m = 1,2,3,...

n = INT(r)

X(i + 1) = X(mn + 1)

ε = r - INT(r)

73
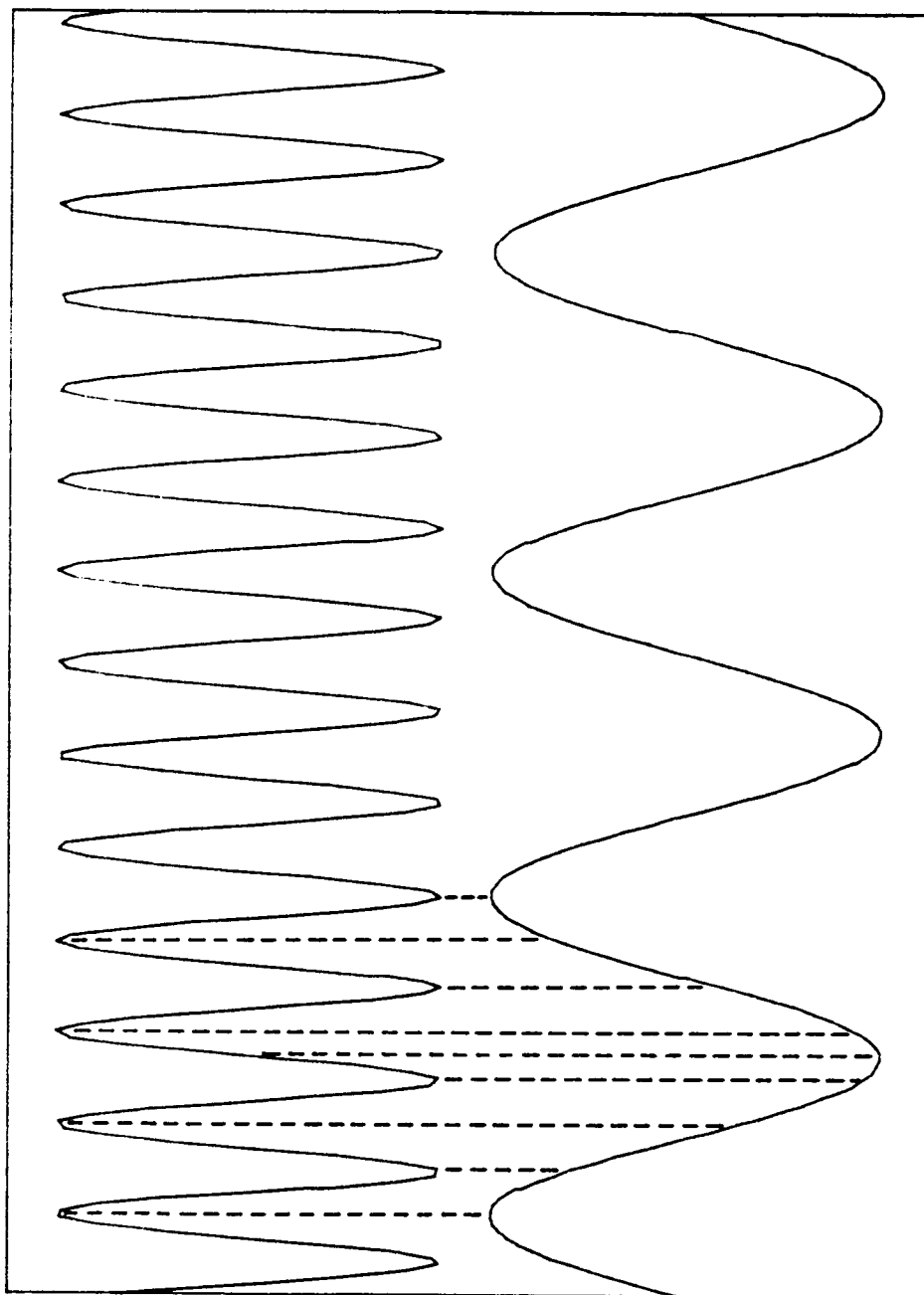
Figure 5.2 General Component Superposition

74

The outline of the algorithm to perform the general AR(1) superposition technique, for any $r > 1$, is given in Figure 5.3.

5.3 Simulation Results

The expected rainflow range moments computed using the proposed AR(1)-superposition technique are compared to the results obtained by the Gaussian simulation procedure in Figures 5.4 through 5.6. The expected range moment, $E[R^m]$, ($m = 3,5,7$) is plotted as a function of Vanmarcke's bandwidth parameter, q, for several values of the 2-block psd frequency ratio, r, from $r = 1.5$ to $r = 10.0$. (See Appendix E for parameters of the cases simulated.)

Note that for values of $r = 2.5$ and higher the proposed technique closely reproduces the range moments obtained by the Gaussian simulation method. For values of $r = 1.5$ and $r = 2.0$, the proposed technique underestimates the stress ranges, as expected for small values of r. Thus, the proposed technique should be an accurate alternative to the Gaussian simulation method for 2-block psd's with $r = 2.5$ or greater.

It was found by comparison of the computation times required by the two techniques that the AR(1) superposition method was 9 to 13 times faster than the Gaussian technique. The Gaussian simulations used 40 harmonic components (N=40) and required approximately 15 minutes and 20 seconds (on an IBM PC AT) to synthesize 4000 extrema. The AR(1) superposition technique required only 70 to 100 seconds, to simulate the same number of extrema.

FIGURE 5.3

AR(1) SUPERPOSITION ALGORITHM

1) Use AR(1) unimodal technique to generate an extrema sequence from the 1-block psd component (see Figure 4.3)

2) Divide this sequence into two arrays of component sequences, each scaled by that component's relative contribution to the process variance: XL(N1), XH(N2)

3) Check that XL(1) and XH(1) are of same sign. If not, drop first point of XH array.

4) Using the following, step through the high frequency component array, doing interpolation and superposition to form the peak/valley sequence for the 2-block psd:

    k = low frequency component interpolation counter
    n = high frequency component interpolation counter
    i = index for high frequency array, XH(N2)
    l = index for low frequency array, XL(N1)
    m = index for resultant time history array, Z
    s = flag for low frequency interpolation
    q = flag for high frequency interpolation

    a) Initialize: k=1, l=1, m=1, n=1, q=r, s=1/r

    b) Do direct superposition if i = q

        1. increment low frequency index:

            l=l+1

        2. do superposition:

        Z(m)=xh(i)+xl(l)

        3. increment Z array index and flags q and s:

            m=m+1
            n=n+1
            q=n*r
            k=k+1
            s=k/r

        4. return to b)

    c) Do low frequency interpolation

        1. compute fraction

            ε=s-INT(s)

        2. do interpolation using equation 5-1

3. do superposition

   $Z(m)=xh(i)+y$

4. increment Z array index and flag s

   $m=m+1$
   $k=k+1$
   $x=k/r$

d) Do high frequency interpolation if (i+1) is greater than q

   1. increment low frequency index:

      $l=l+1$

   2. compute fraction

      $\varepsilon=q-INT(q)$

   3. do interpolation using equation 5-1

   4. do superposition $Z(m)=xl(l)+y$

   5. increment Z array index and flag q

      $m=m+1$
      $n=n+1$
      $q=n*r$

e) Repeat until out of data

5) Sort the resulting array Z(m) to remove any intermediate points which are not peaks or valleys

6) Perform rainflow or statistical analysis on Z(m) as required
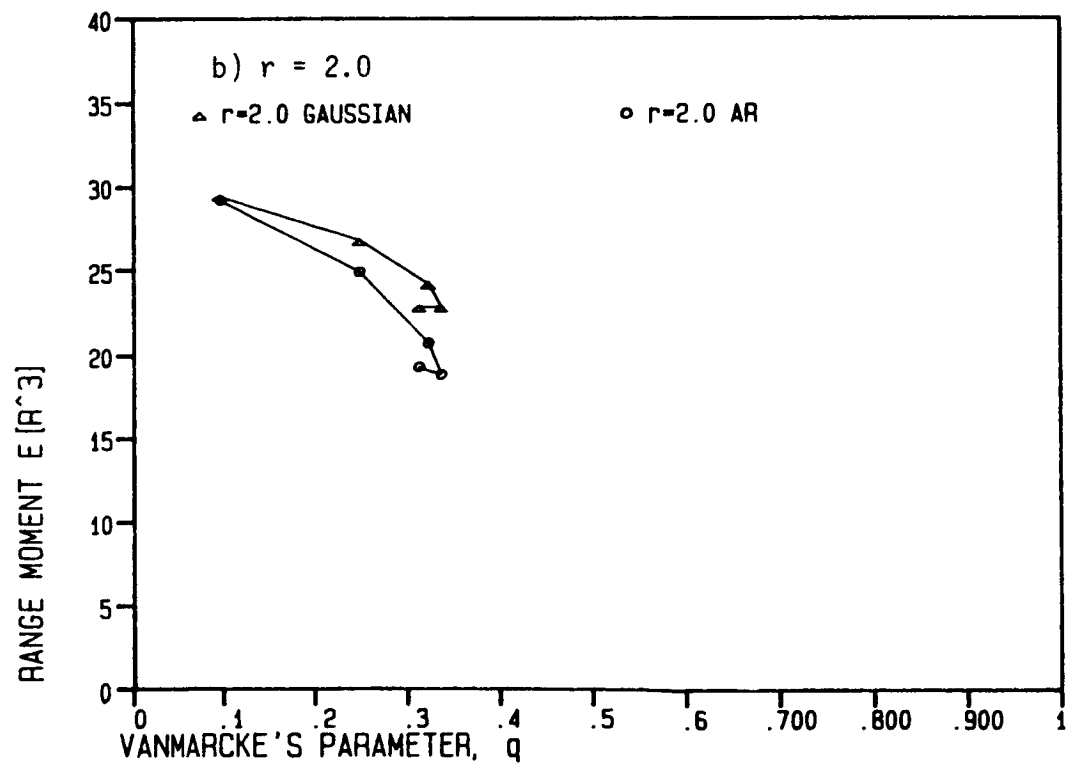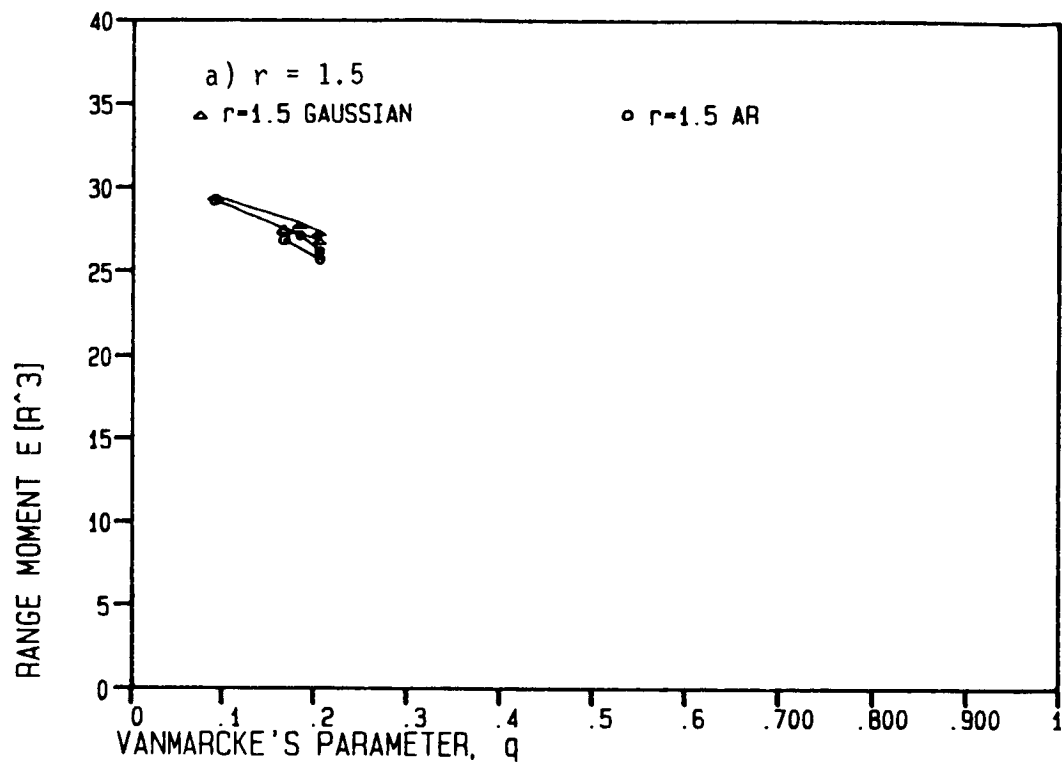
Figure 5.4 Range Moment Comparison AR(1)
Superposition and Gaussian Techniques: m = 3
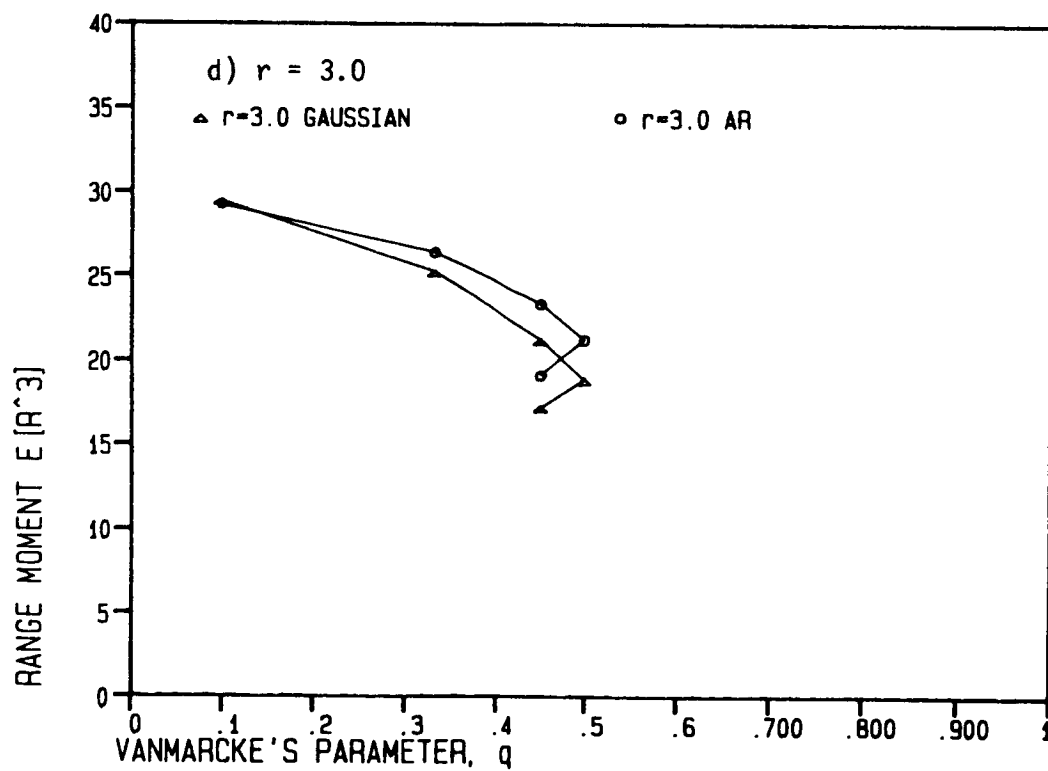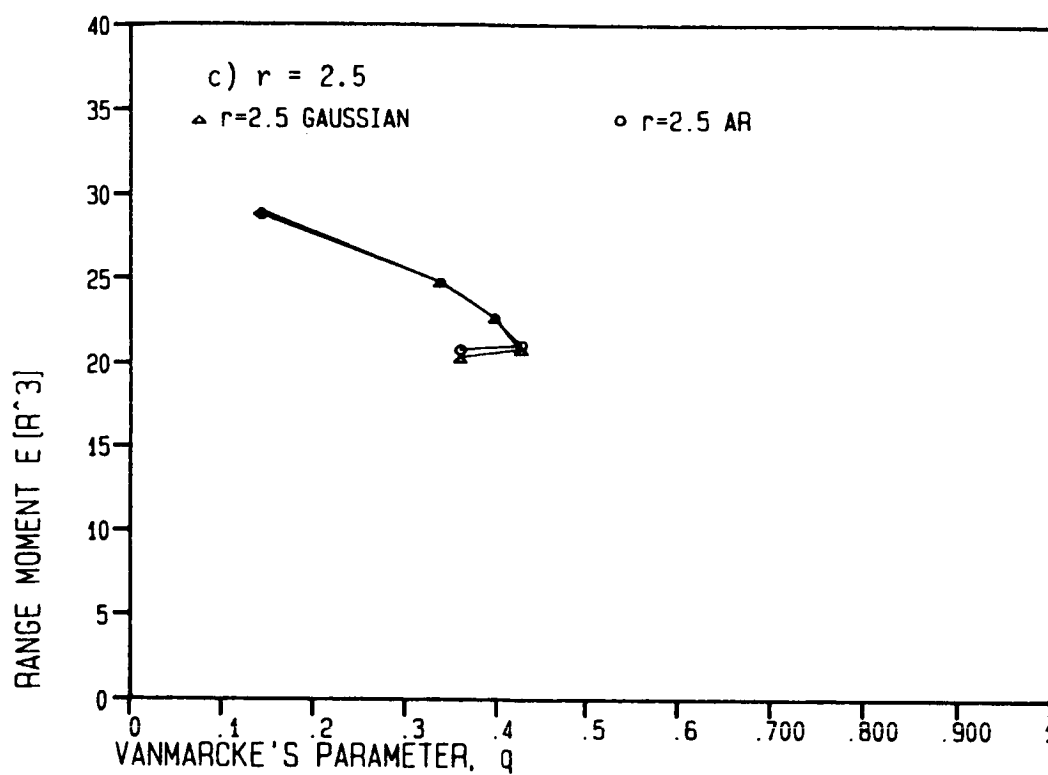
c) r = 2.5

△ r=2.5 GAUSSIAN   ○ r=2.5 AR

d) r = 3.0

△ r=3.0 GAUSSIAN   ○ r=3.0 AR

Figure 5.4   (Continued)

79

e) r = 3.5

RANGE MOMENT E [R^3]

VANMARCKE'S PARAMETER, q

△ r=3.5 GAUSSIAN   o r=3.5 AR

f) r = 4.5

RANGE MOMENT E [R^3]

VANMARCKE'S PARAMETER, q

△ r=4.0 GAUSSIAN   o r=4.0 AR

Figure 5.4   (Continued)

g) r = 4.5

▲ r=4.5 GUASSIAN   o r=4.5 AR

h) r = 5.0

▲ r=5.0 GAUSSIAN   o r=5.0 AR

Figure 5.4 (Continued)

81

i) r = 7.5

△ r=7.5 GAUSSIAN   ○ r=7.5 AR

RANGE MOMENT E [R^3]

VANMARCKE'S PARAMETER, q

j) r = 10.0

△ r=10.0 GAUSSIAN   ○ r=10.0 AR

RANGE MOMENT E [R^3]

VANMARCKE'S PARAMETER, q

Figure 5.4   (Continued)

a) r = 1.5

△ r=1.5 GAUSSIAN   o r=1.5 AR

b) r = 2.0

▲ r=2.0 GAUSSIAN   o r=2.0 AR
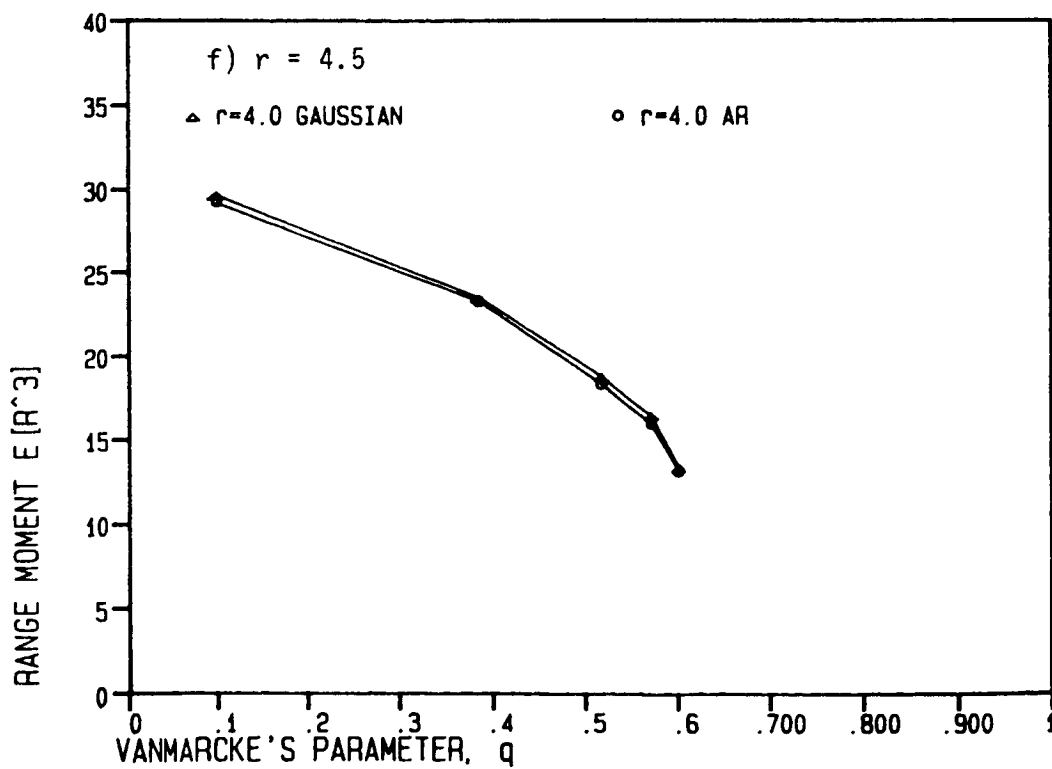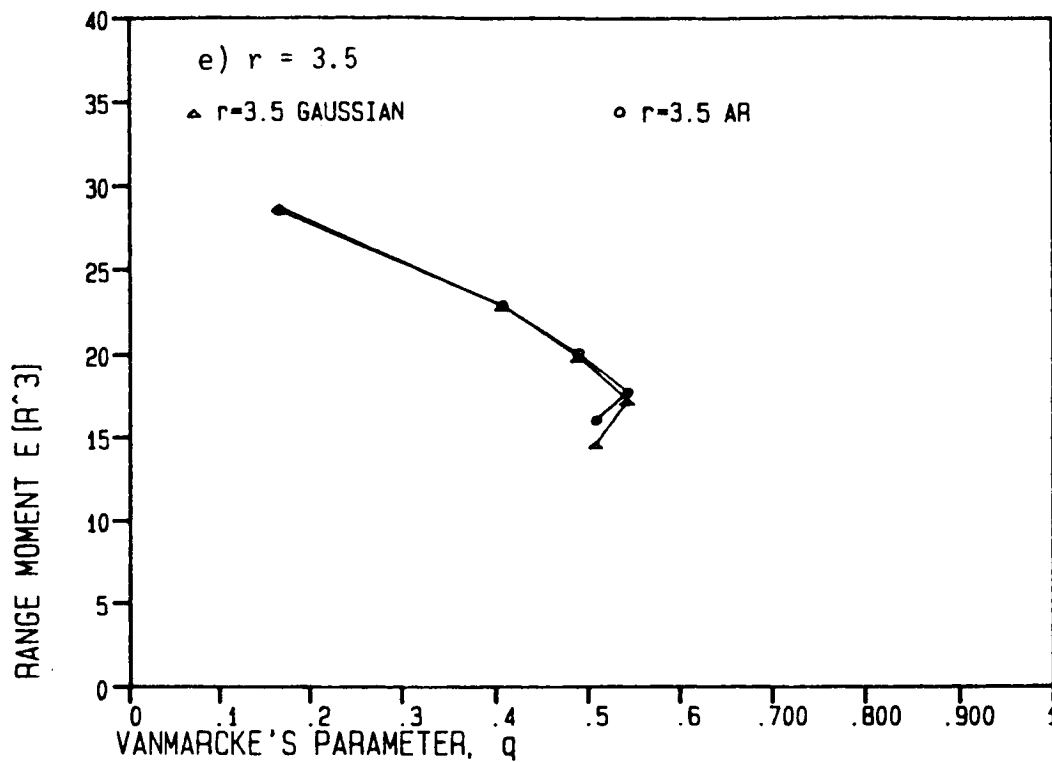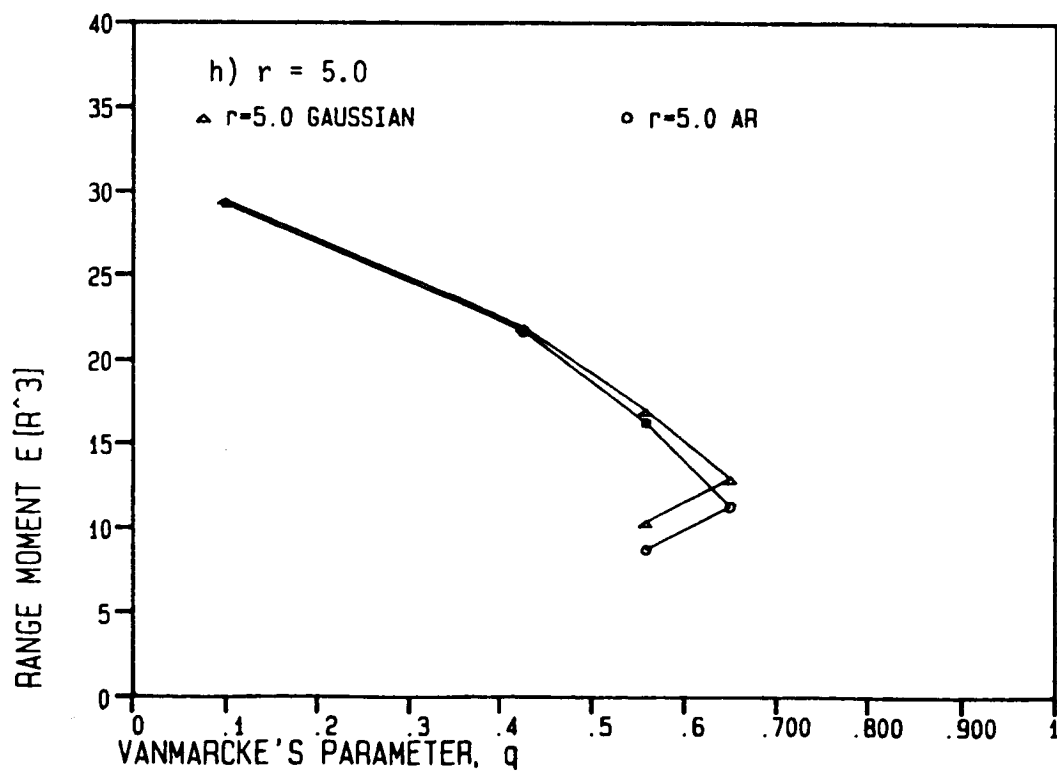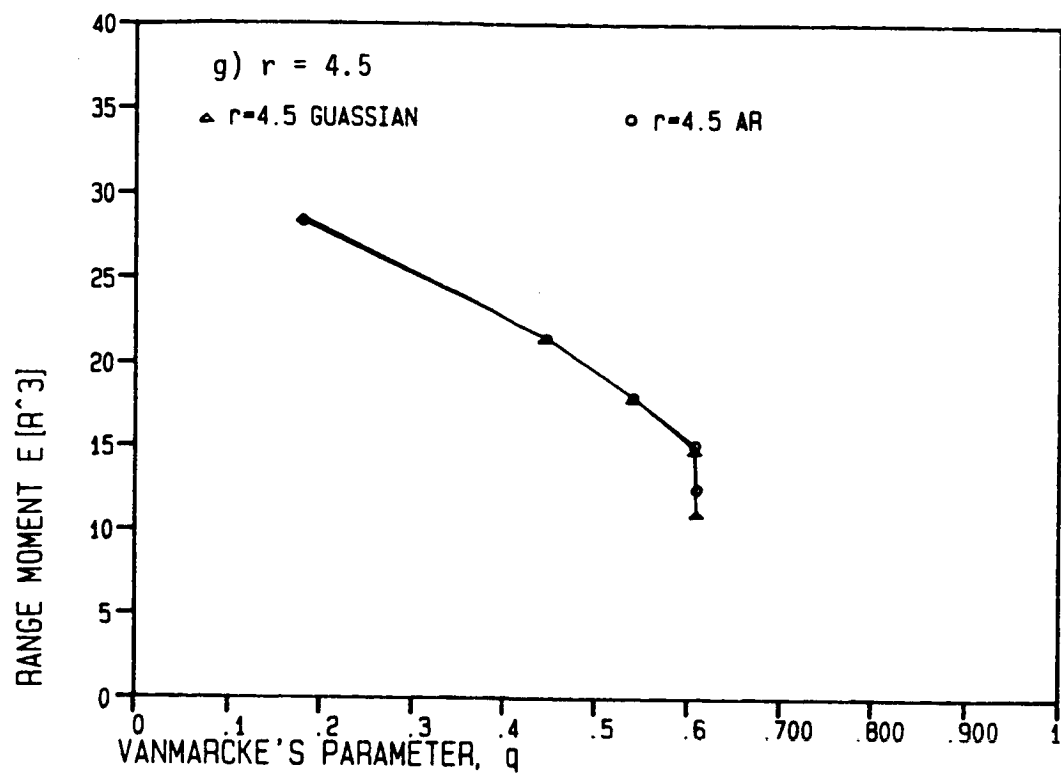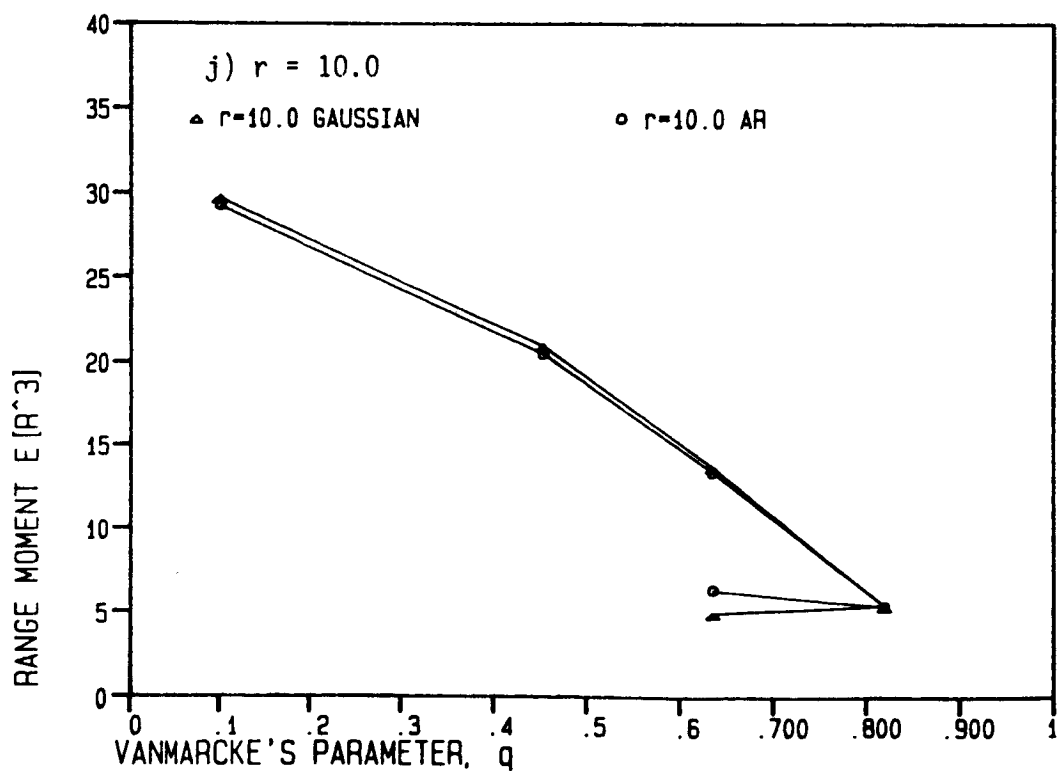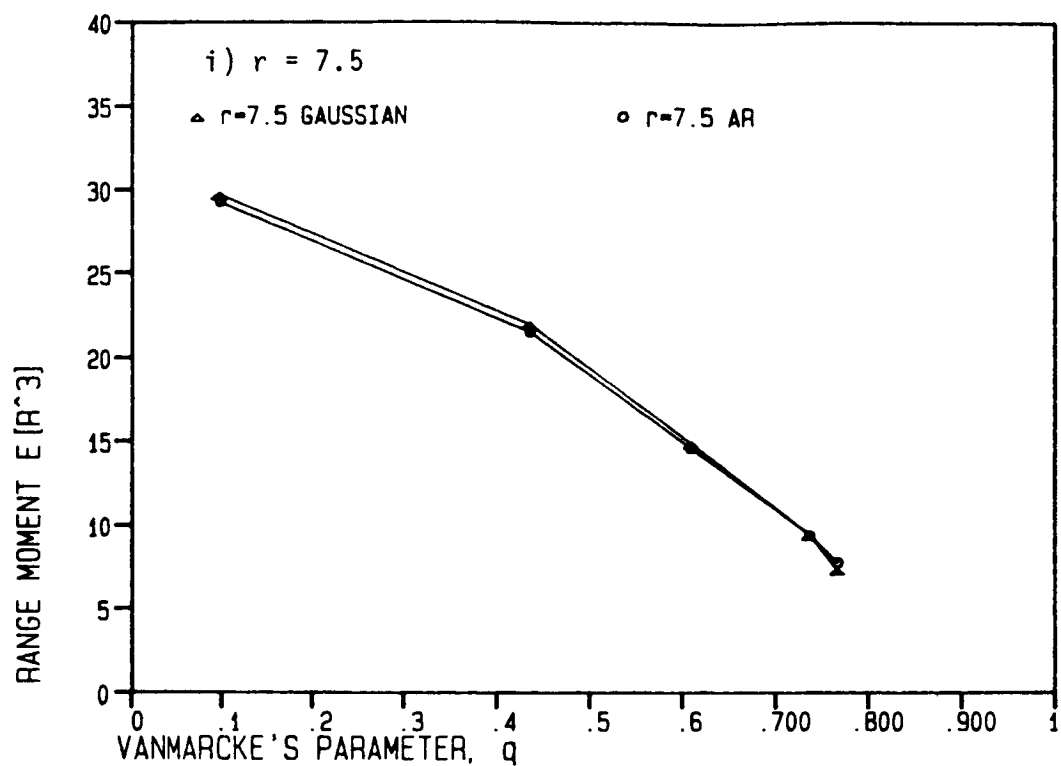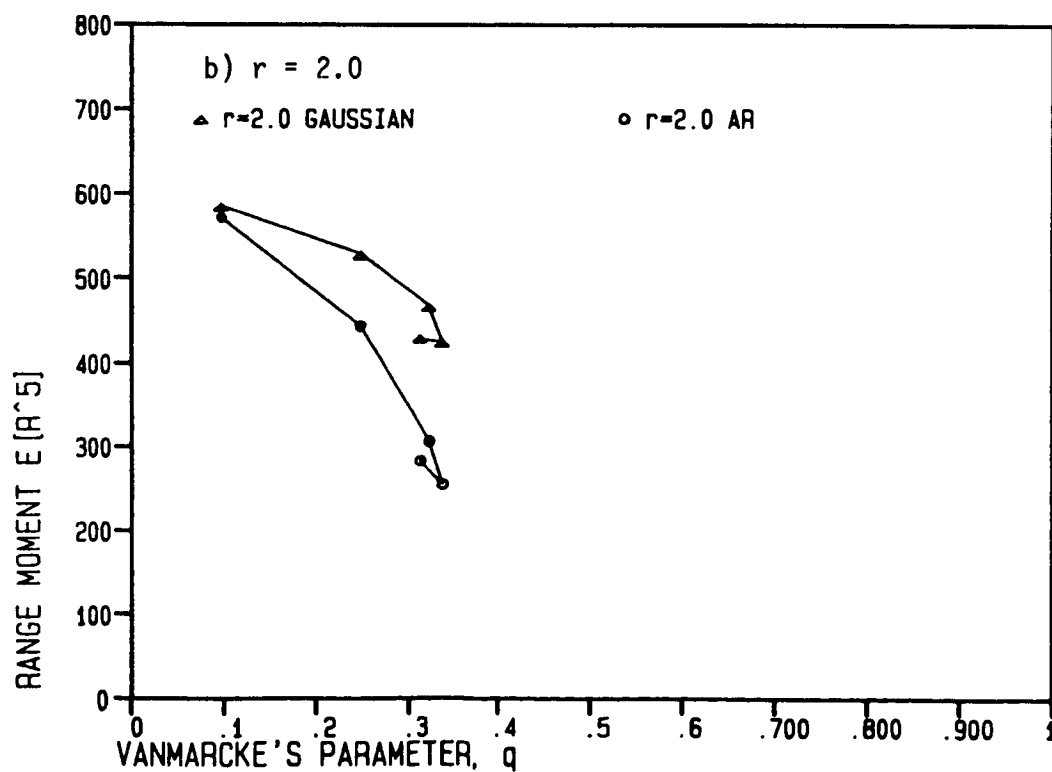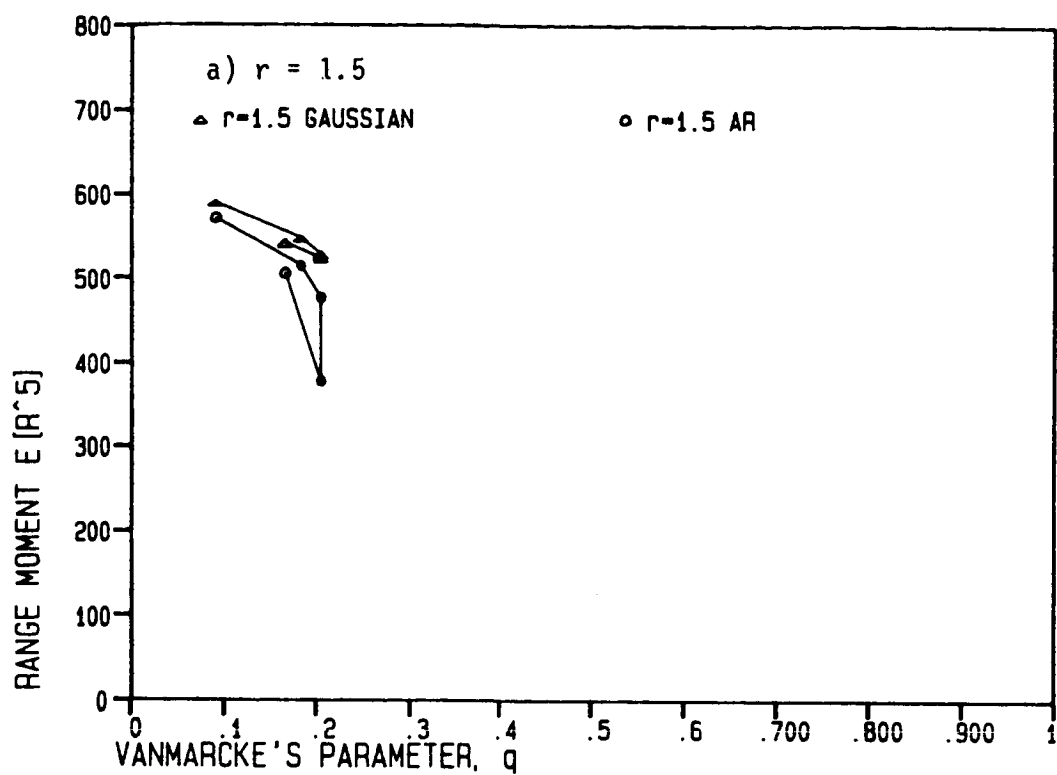
Figure 5.5   Range Moment Comparison AR(1)
Superposition and Gaussian Techniques: m = 5
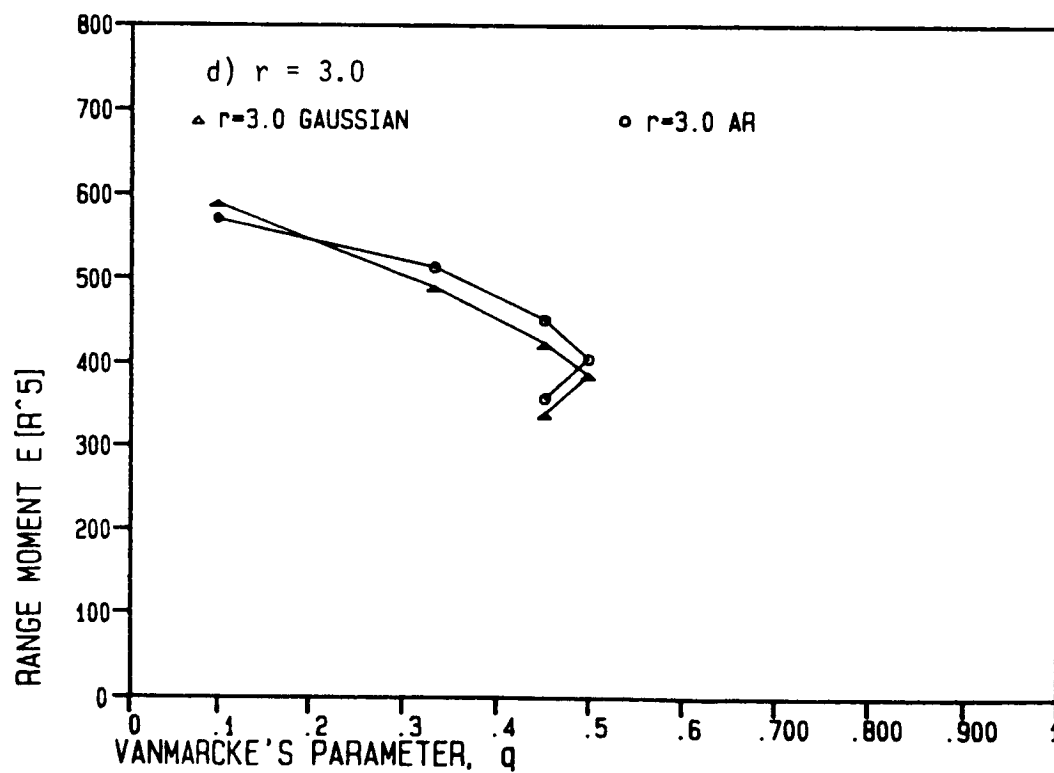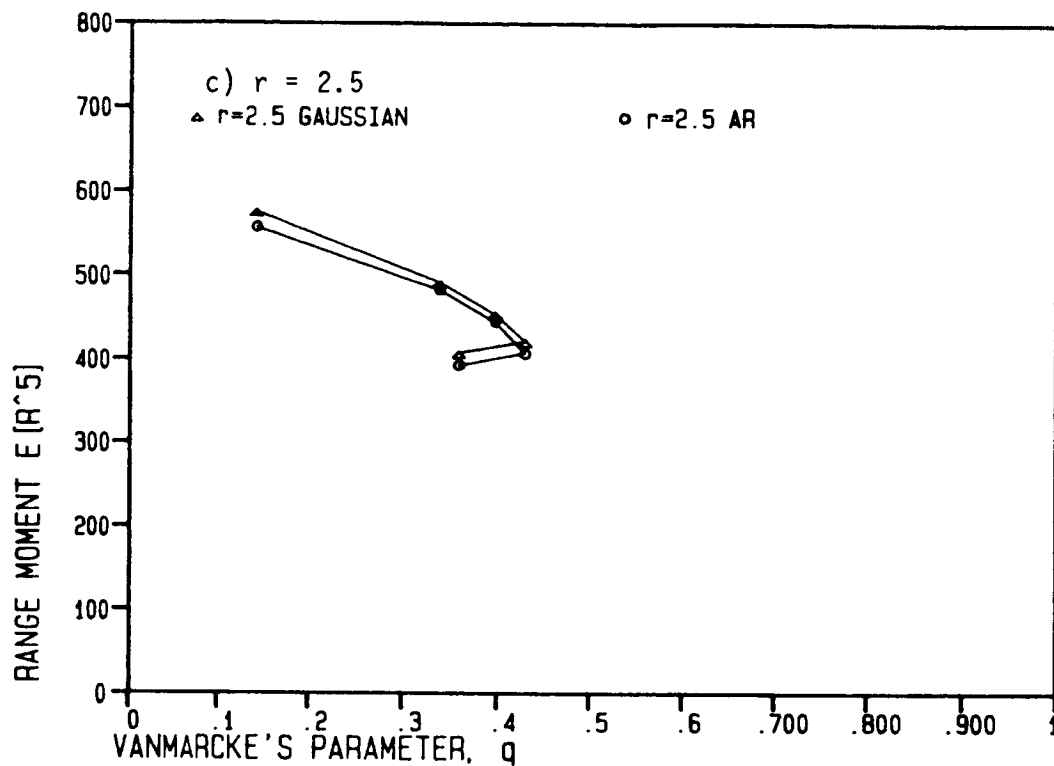
Figure 5.5 (Continued)

Figure 5.5   (Continued)

Figure 5.5   (Continued)

i) r = 7.5

△ r=7.5 GAUSSIAN   o r=7.5 AR

j) r = 10.0

△ r=10.0 GAUSSIAN   o r=10.0 AR
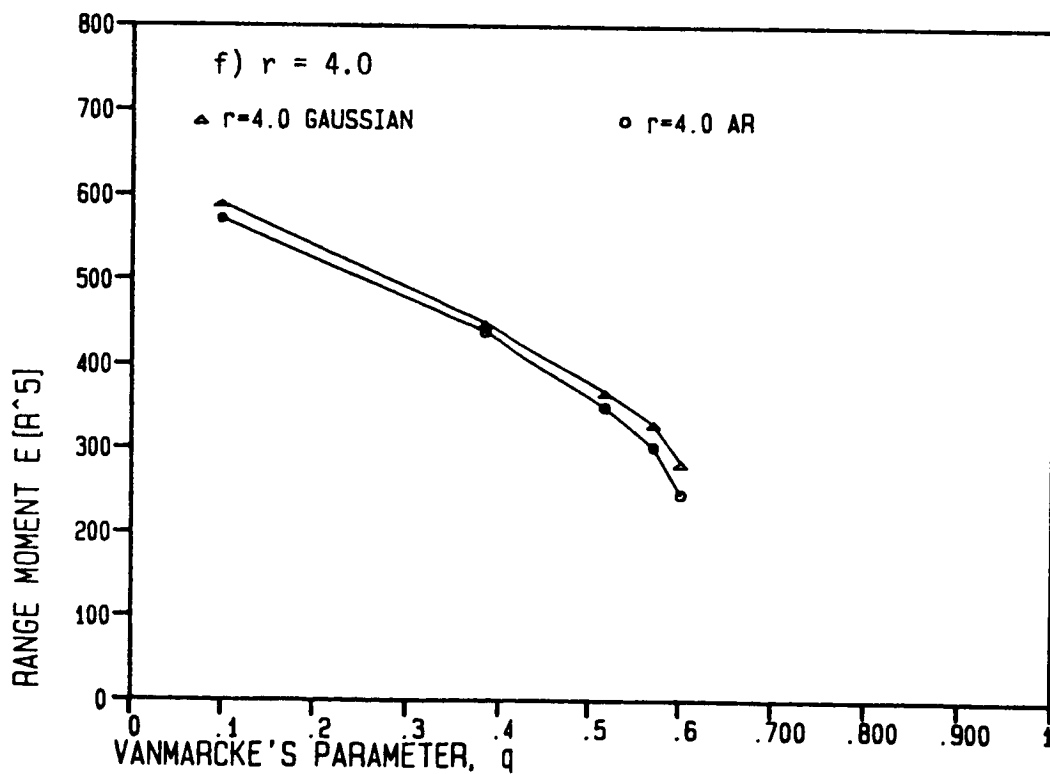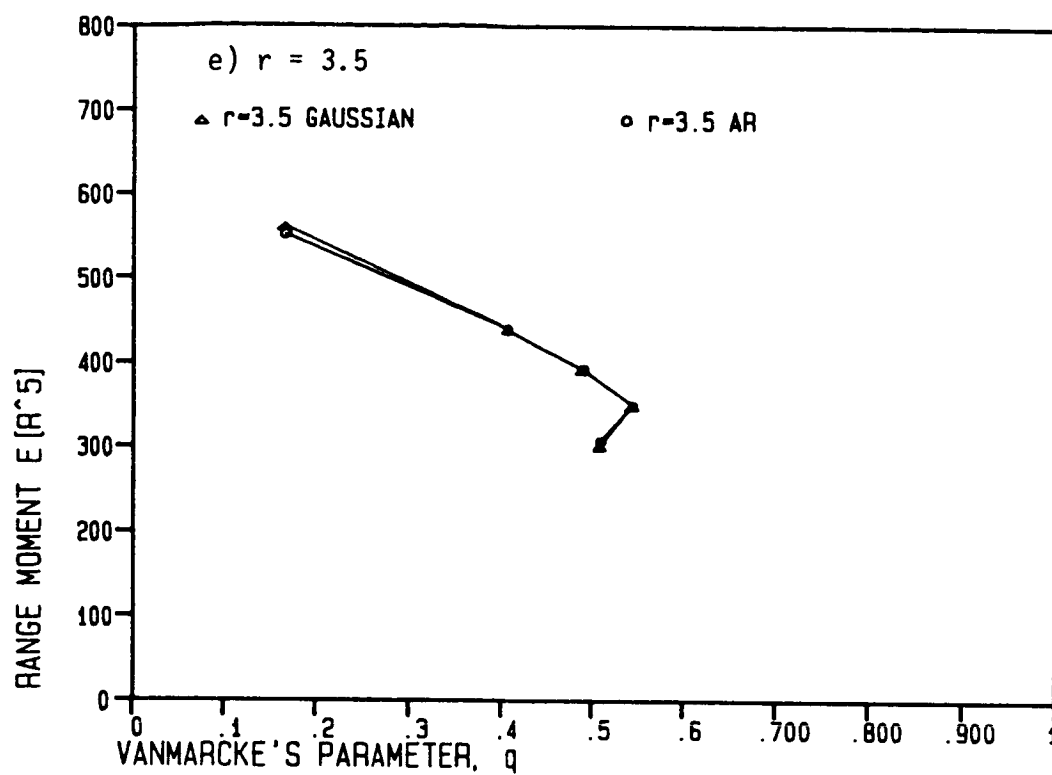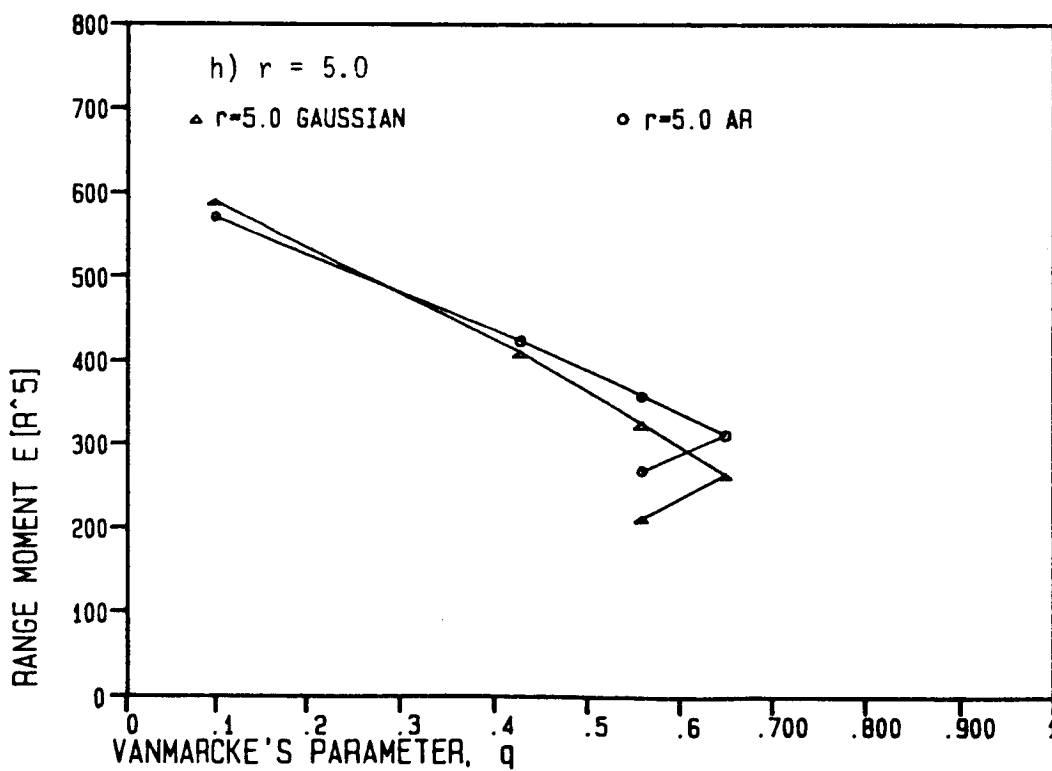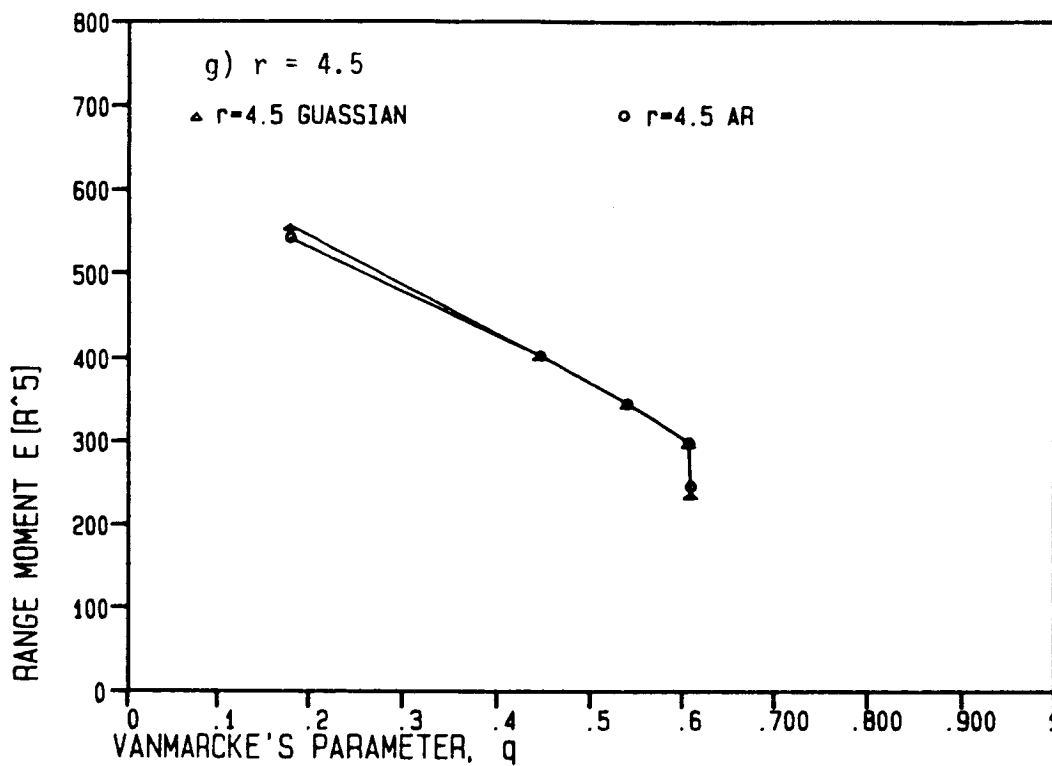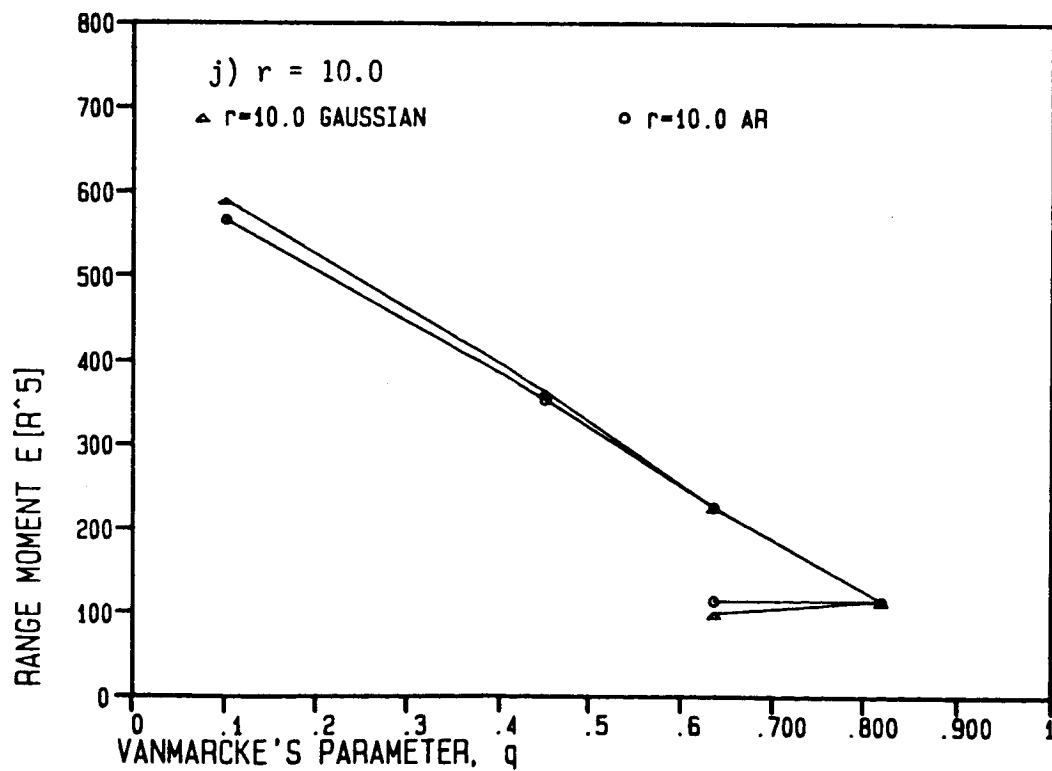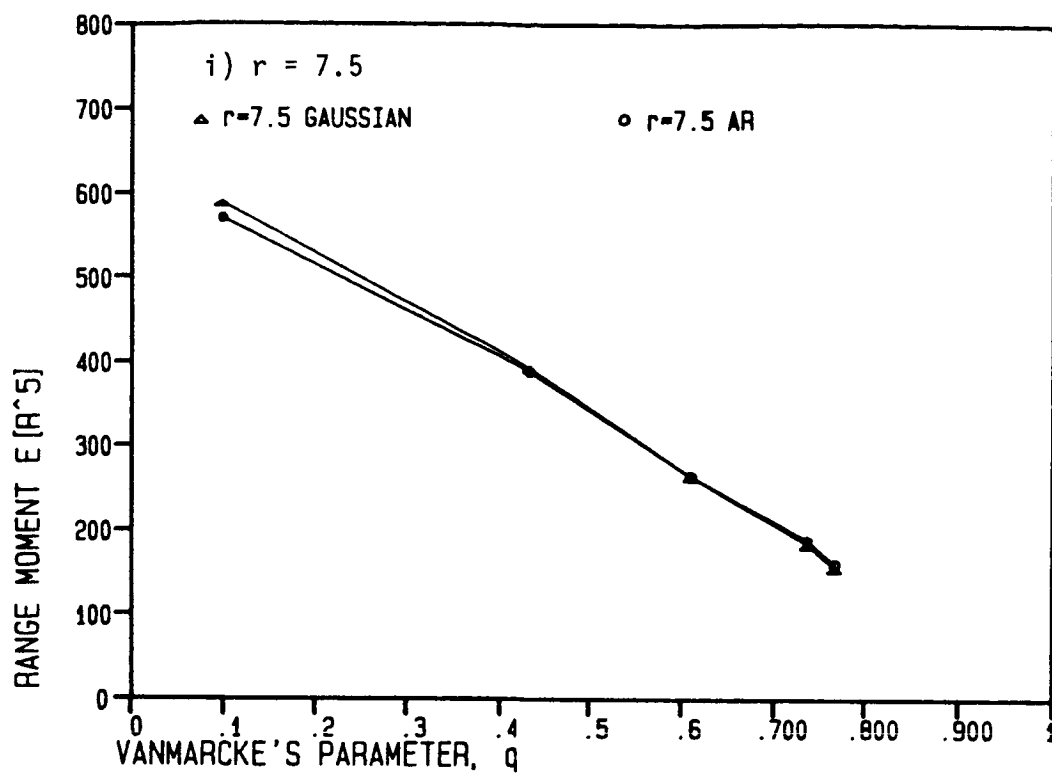
Figure 5.5   (Continued)
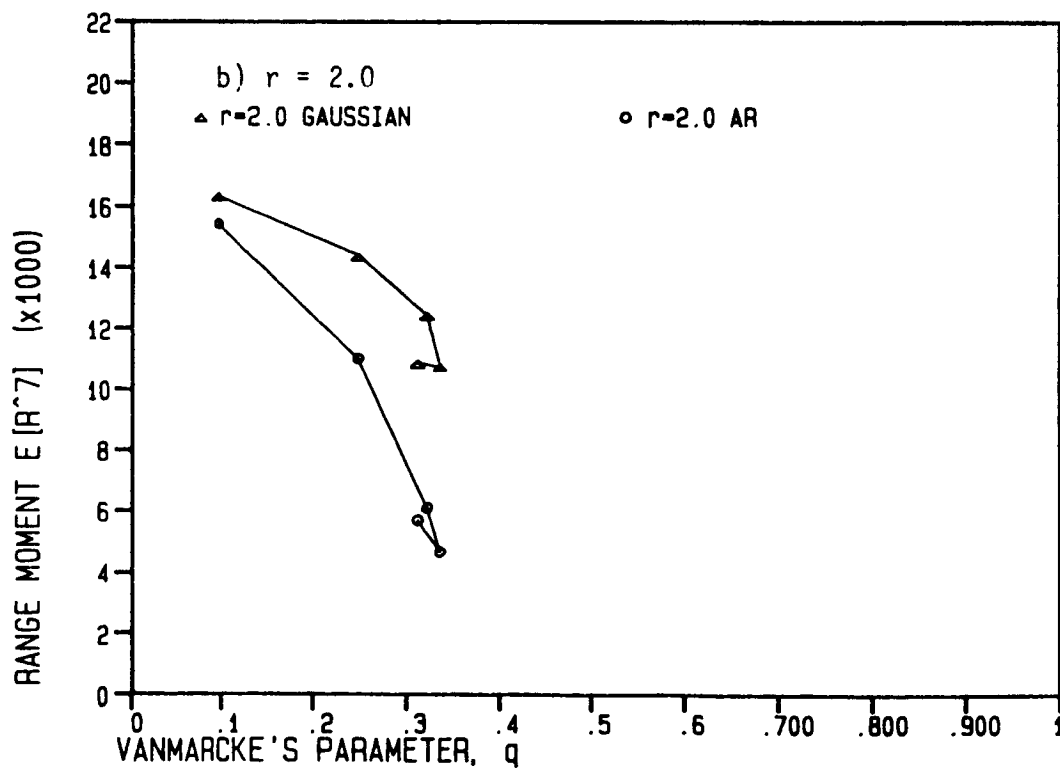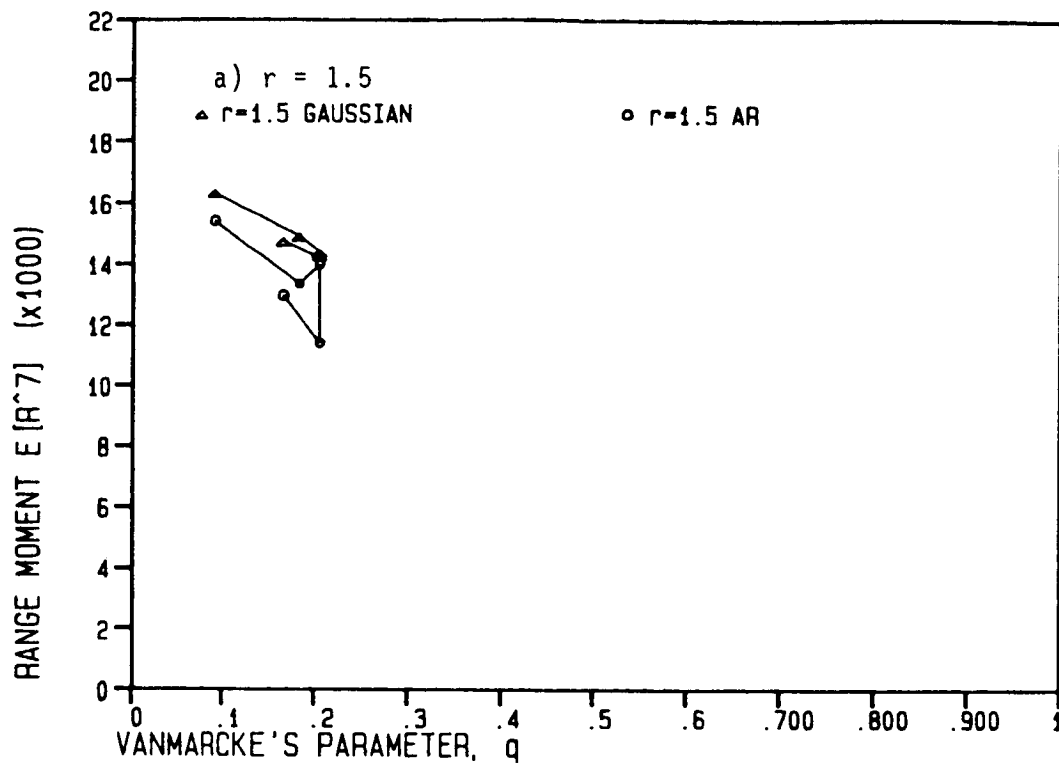
Figure 5.6   Range Moment Comparison AR(1)
Superposition and Gaussian Techniques: m = 7

C-2
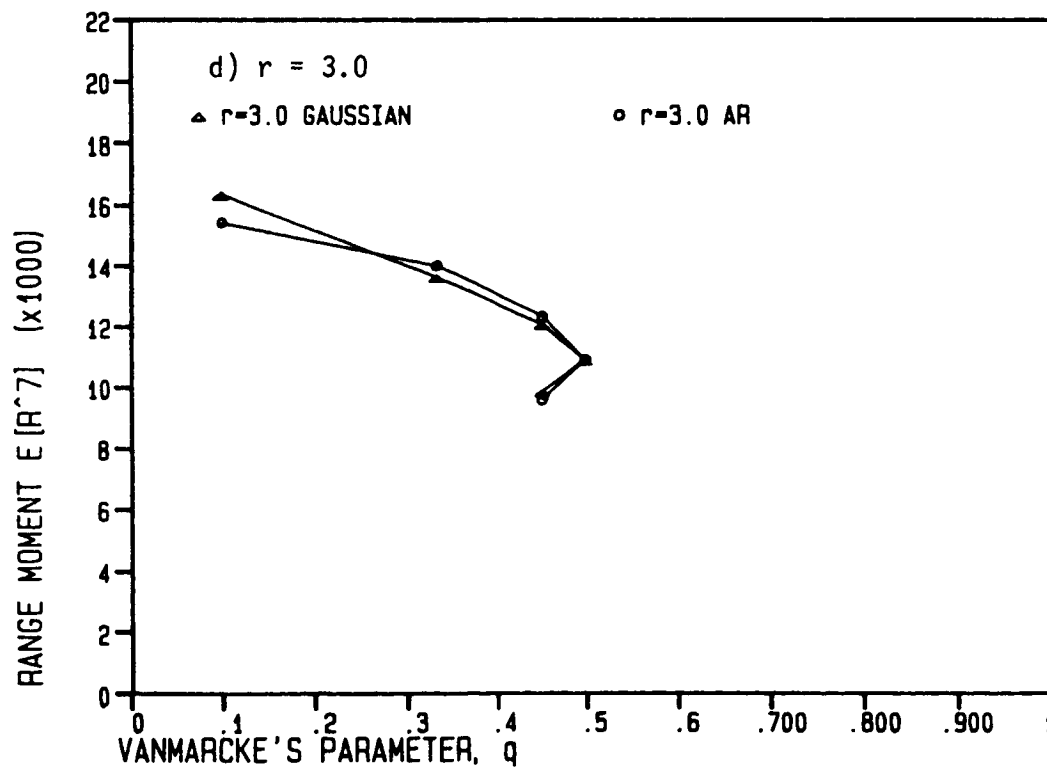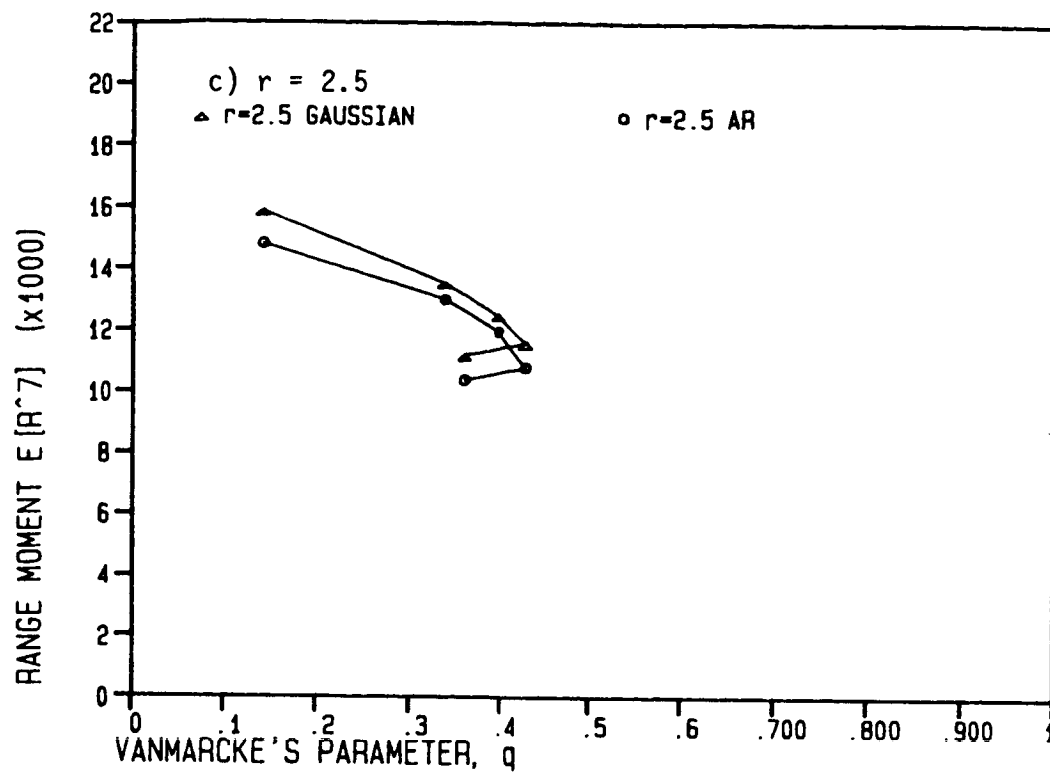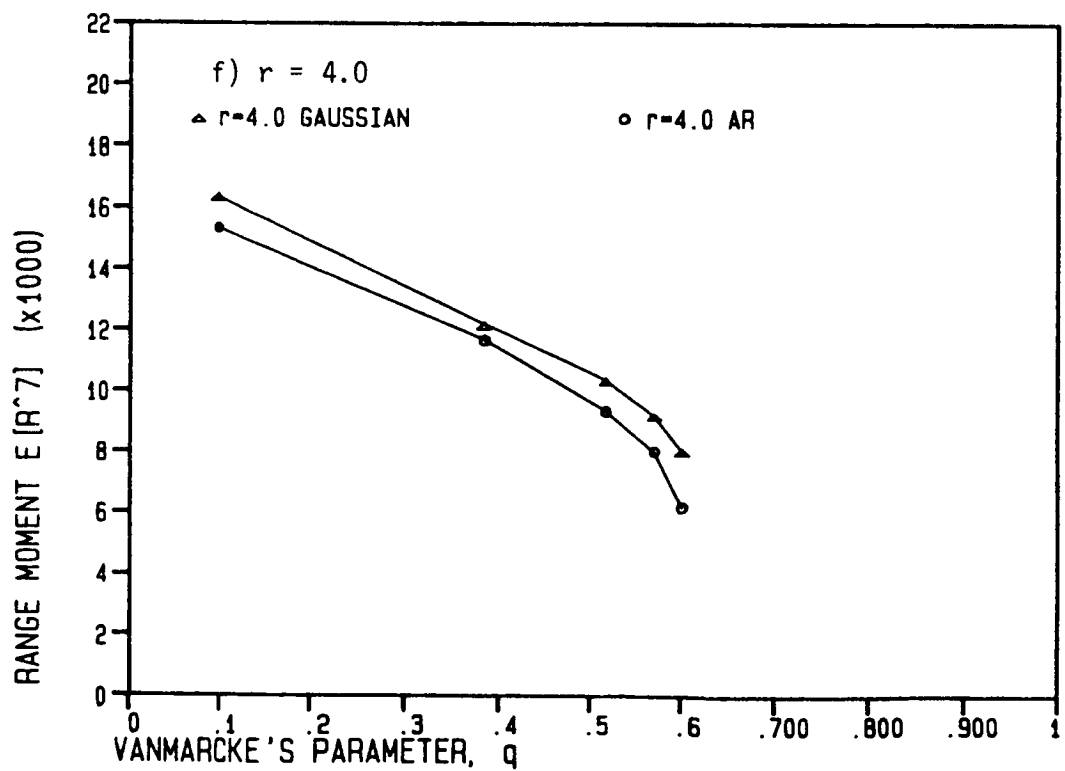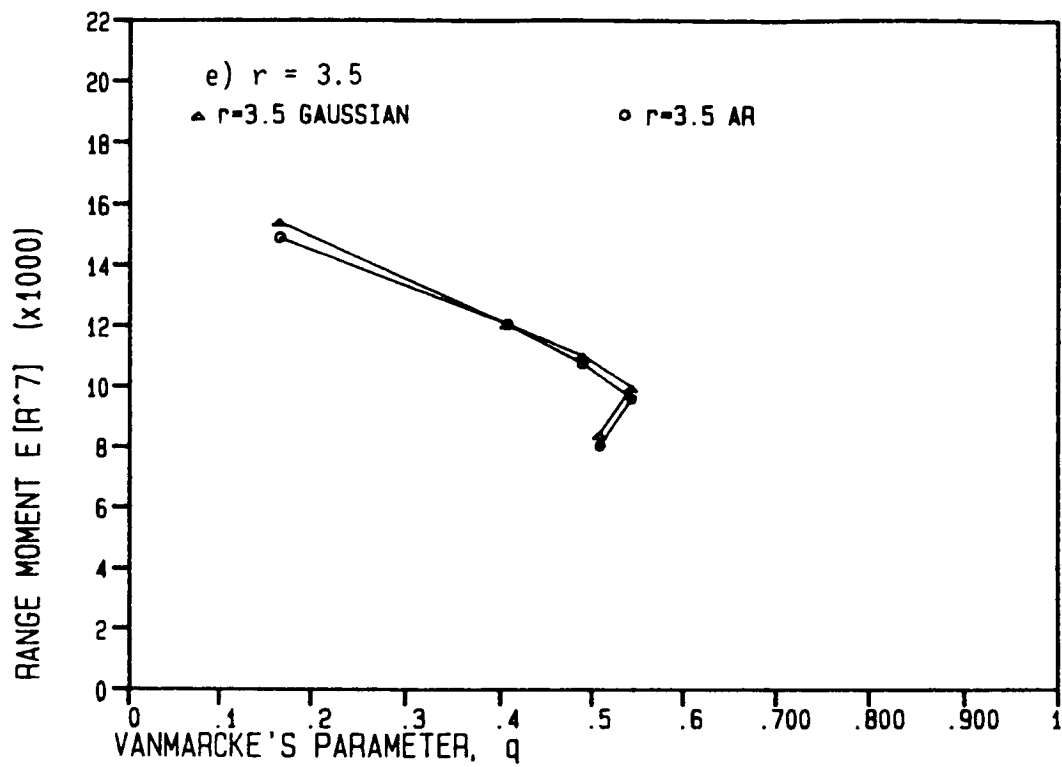
Figure 5.6 (Continued)

Figure 5.6 (Continued)

90

g) r = 4.5
▲ r=4.5 GUASSIAN   ○ r=4.5 AR

h) r = 5.0
▲ r=5.0 GAUSSIAN   ○ r=5.0 AR

Figure 5.6 (Continued)

i) r = 7.5

△ r=7.5 GAUSSIAN   ○ r=7.5 AR

RANGE MOMENT E [R^7] (x1000)

VANMARCKE'S PARAMETER, q

j) r = 10.0

△ r=10.0 GAUSSIAN   ○ r=10.0 AR

RANGE MOMENT E [R^7] (x1000)

VANMARCKE'S PARAMETER, q
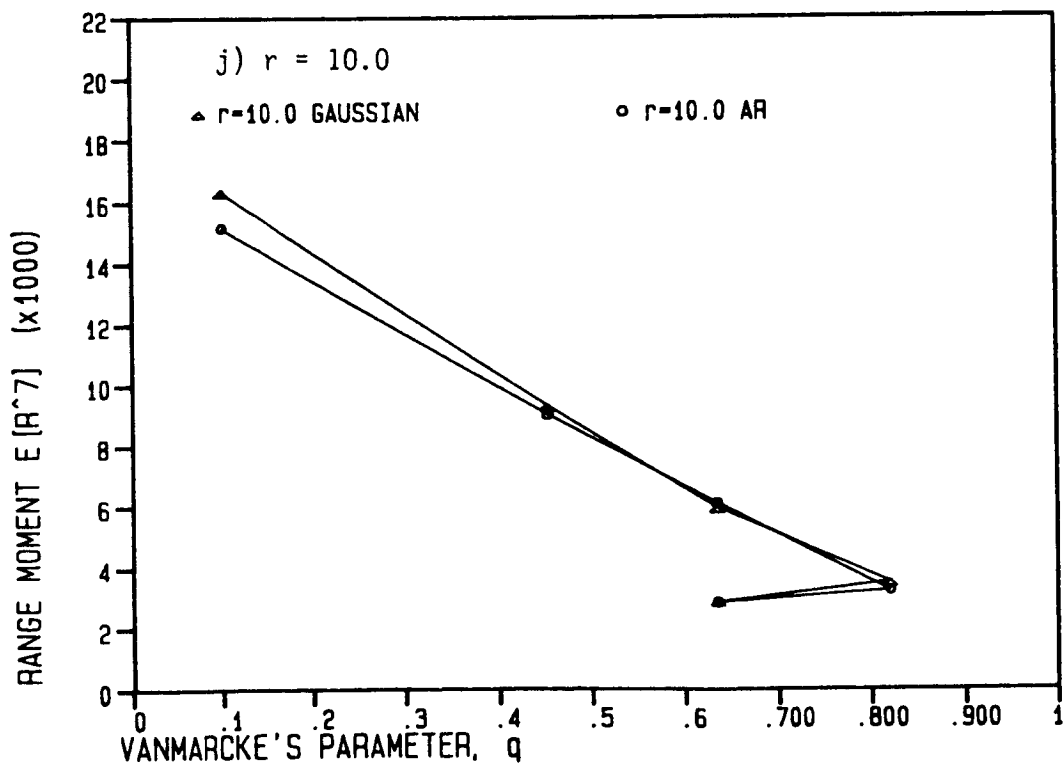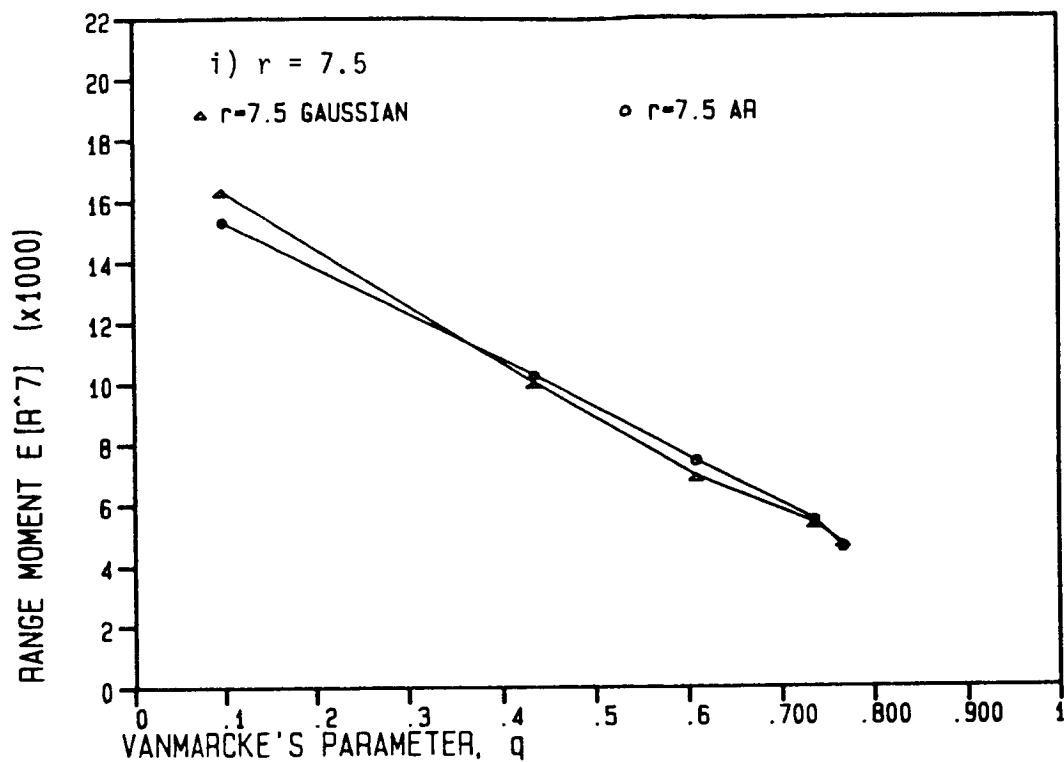
Figure 5.6 (Continued)

CHAPTER 6

CONCLUSION

The objective of this investigation was to develop a simulation technique which synthesized the extrema of a random process more efficiently than the Gaussian simulation technique. The incentive for such a technique exists because the statistic required from a stress time history for stochastic fatigue analysis is a statistic of the extrema - the expected range moment, $E[R^m]$. Considerable computational effort is wasted in the Gaussian technique because the entire time history is simulated, while only the resulting extrema are necessary for estimating $E[R^m]$. An extrema-synthesizing technique should be expected to greatly reduce the required computation time because nearly all of the values generated are extrema.

A general description of ARMA(p,q) stochastic models was presented and an AR(1) model was proposed for simulating the extrema of processes having unimodal psd's. The proposed AR(1) technique was found to produce expected rainflow stress range moments, $E[R^m]$, which compared very well with those computed using the Gaussian technique. A considerable savings in computation time was realized, with the AR(1) technique averaging 11.7 times faster than the Gaussian technique.

An adaptation of the AR(1) technique was proposed for processes having bimodal psd's. The adaptation involves using two AR(1) processes in order to simulate the extrema due to each mode, and then superimposing the two sequences of extrema, taking into account the frequency separation between the modes of the psd. An intermediate step necessary prior to the superposition is an interpolation between the extrema

of one component to provide points in that component time series corresponding to those in the other component.

The generation of these intermediate values was not found to be detrimental to the overall efficiency of the technique as it was found to be 9 to 13 times faster than the Gaussian technique. A comparison of the results for $E[R^m]$ from the two techniques showed that the AR(1) superposition technique produced comparable values for frequency ratios of r = 2.5 and greater. As expected for small values of r, the proposed technique was found to underestimate $E[R^m]$ for r = 1.5 and r = 2.0.

The effects of a random stress process's psd shape characteristics were also studied as a part of this investigation. For bimodal psd's, the contribution of the two components to the expected fatigue damage rate was determined. The range of area ratios for which both components must be considered was determined to be from b = 0.01 to b = 10 for frequency ratios from r = 1.5 to r = 15 (and material S-N curves with m = 3,5, or 7). For bimodal psd's outside this range, the expected damage rate may be determined with sufficient accuracy for practical fatigue analysis by considering the psd to be unimodal.

The effect of high frequency truncation on the expected damage rate was also studied for two unimodal psd's. A shape or truncation parameter defined as the ratio of the Vanmarcke bandwidth parameter for the truncated psd to that for the "infinite-tail" psd, denoted q/q_0, was found useful to describe the truncation frequency required for a desired analysis accuracy. This parameter appeared to account for the different decay rates of the tails of the two psd's studied, such that the expected damage rate vs. q/q_0 could be described as

94

a unique curve. From this data, a value of $q/q_0 = 0.6$ was proposed as a truncation point for unimodal psd's for use in practical fatigue analysis.

The effect of psd bandwidth and shape on the correlation of the extrema of the process was also studied. A linear regression of ρ_1, the correlation between adjacent extrema or lag one correlation, on Vanmarcke's bandwidth parameter, q, was proposed as a practical description of the change in ρ_1 with psd bandwidth for unimodal psd's and bimodal psd's within the region of significance (b = 0.01 to b = 10).

The behavior of higher lag extrema correlations and a possible relationship to the autocorrelation function of the random process were also discussed. No analytical relationship is known at this time, however. This is an area requiring further research if a direct ARMA(p,q) model of the extrema of bimodal psd processes is desired as an alternative to the AR(1) superposition technique presented herein.

APPENDIX A

PSD CASES STUDIED USING GAUSSIAN TECHNIQUE

Note: ω has units of radians/second

Unimodal psd's

1-Block

ω_1	ω_2	G	q	α_2	$E[R^3]$	$E[R^5]$	$E[R^7]$
1.0	1.2	5.0	.052	.995	30.11	600.6	16750
0.9	1.1	5.0	.058	.993	29.79	593.9	16550
1.0	1.4	2.5	.096	.982	29.55	587.4	16310
6.0	9.0	.333	.115	.975	29.06	574.3	15860
4.5	7.0	.400	.125	.971	28.85	570.6	15790
4.5	8.0	.286	.160	.954	28.12	551.7	15100
4.5	9.0	.222	.189	.937	27.43	535.6	14620
3.0	7.0	.250	.225	.915	26.60	513.9	13880
3.0	8.0	.200	.254	.896	25.90	498.4	13410
3.0	10.0	.143	.297	.868	24.77	476.2	12790
3.0	12.0	.111	.327	.848	23.96	460.4	12380
1.0	7.0	.167	.397	.803	22.34	429.4	11580

Eq'n 3-3, $\beta = 0.01$

ω_c	q	α_2	$E[R^3]$	$E[R^5]$	$E[R^7]$
.392	.262	.879	25.27	484.8	12980
.587	.343	.785	22.31	427.7	11500
.783	.391	.712	20.26	390.2	10470
.979	.422	.654	18.61	357.7	9514
1.958	.489	.488	14.00	270.2	7190
3.916	.525	.354	10.84	206.1	6383
9.787	.539	.228	8.32	154.3	3993

Eq'n 3-4, c = 1.0, u = 4.0

ω_c	q	α_2	$E[R^3]$	$E[R^5]$	$E[R^7]$
6.0	.166	.954	28.10	467.7	15110
7.0	.187	.940	27.59	524.5	14730
7.5	.193	.936	27.43	538.4	14650
8.0	.195	.933	27.30	533.2	14550
9.0	.196	.932	27.27	532.1	14480

Bimodal (2-Block) psd's

Note: For 2-block psd;

$$\omega_1 = 0.9 \qquad \omega_3 = 0.9r$$

$$\omega_2 = 1.1 \qquad \omega_4 = 1.1r$$

$$G_1 = \frac{5}{1+b} \qquad G_2 = \frac{5b}{(1+b)r}$$

r	b	q	α_2	$E[R^3]$	$E[R^5]$	$E[R^7]$
1.5	21.	.091	.987	29.50	586.4	16290
	4.0	.153	.964	28.52	561.4	15430
	2.0	.183	.946	27.81	544.2	14920
	1.5	.194	.938	27.58	538.1	14720
	1.0	.204	.927	27.21	529.3	14420
	.67	.208	.920	27.53	525.1	14360
	.44	.204	.917	26.90	522.1	14216
	.30	.194	.920	26.98	528.7	14570
	.15	.166	.934	27.52	539.4	14760
	.02	.089	.980	29.29	582.7	16200
2.0	41.	.097	.987	29.49	585.8	16280
	6.2	.191	.954	28.14	554.0	15230
	3.0	.247	.922	26.89	525.4	14357
	2.0	.278	.899	26.03	504.6	13620
	1.0	.321	.852	24.35	465.6	12363
	.59	.337	.819	23.25	437.7	11341

r	b	q	α_2	$E[R^3]$	$E[R^5]$	$E[R^7]$
2.0 con't.	.39	.336	.802	22.74	423.7	10800
	.21	.312	.796	22.75	425.9	10880
	.006	.096	.969	28.93	576.1	16035
3.0	70.	.098	.988	29.51	585.9	16260
	7.0	.240	.943	27.29	534.3	14690
	3.0	.332	.390	25.10	489.6	13590
	1.5	.410	.823	22.81	452.6	12700
	1.0	.450	.776	21.11	423.5	12090
	.63	.484	.720	19.60	400.0	11360
	.47	.497	.686	18.87	385.4	10900
	.33	.503	.650	17.83	365.8	10800
	.25	.499	.626	17.26	355.3	10090
	.11	.450	.596	17.10	339.7	9783
	.01	.199	.801	23.97	478.3	13350
	.0016	.098	.947	28.32	563.9	15700
4.0	88.	.098	.989	29.54	586.7	16300
	5.5	.298	.924	26.02	497.1	13420
	2.8	.384	.871	23.54	447.2	12140
	1.87	.439	.828	21.74	414.8	11370
	1.0	.517	.745	18.78	367.2	10370
	.575	.570	.663	16.37	331.0	9147
	.39	.592	.608	15.04	309.3	8919
	.21	.600	.532	13.50	280.7	8025
	.00075	.100	.920	27.56	549.5	15310
5.0	101.	.098	.989	29.52	585.9	16260
	5.0	.329	.914	25.66	476.0	12670
	2.5	.427	.853	21.92	407.1	11000
	1.85	.472	.817	20.32	374.1	10060
	1.0	.557	.730	16.97	322.7	9039
	.58	.617	.643	14.52	290.4	8473
	.39	.648	.579	12.91	262.6	7663
	.20	.668	.485	11.06	230.9	6734

r	b	q	α_2	$E[R^3]$	$E[R^5]$	$E[R^7]$
5.0 con't.	.10	.646	.416	10.15	209.5	6006
	.04	.557	.382	10.37	209.5	5915
	.01	.360	.459	14.25	281.6	7760
	.0004	.098	.897	26.81	534.2	14890
6.0	108.	.098	.989	29.53	586.2	16280
	5.3	.336	.916	24.86	464.2	12370
	2.8	.429	.861	21.86	394.0	10286
	1.85	.493	.812	19.57	348.9	9166
	1.0	.583	.722	16.00	293.7	8034
	.575	.650	.629	13.15	252.9	7217
	.39	.684	.563	10.62	231.0	6781
	.21	.713	.468	9.70	202.5	5968
	.00026	.099	.867	25.97	517.7	14440
7.0	115.	.098	.989	29.55	586.8	16294
	5.2	.348	.913	24.58	448.2	11500
	2.8	.441	.859	21.59	380.5	9658
	1.84	.508	.808	19.06	331.5	8549
	1.0	.602	.717	15.38	272.4	7389
	.575	.673	.621	12.26	226.0	6311
	.39	.710	.553	10.54	205.3	6000
	.21	.745	.454	8.57	175.2	5144
	.10	.746	.360	7.30	153.4	4492
	.01	.492	.295	8.40	169.6	4731
	.001	.194	.565	17.32	335.8	9252
	.000185	.100	.834	24.88	496.1	13849
7.5	116.	.099	.989	29.55	586.6	16260
	7.5	.302	.935	25.80	478.1	12410
	3.0	.435	.865	21.87	390.4	9971
	2.3	.478	.836	20.10	352.4	9112
	1.7	.527	.796	18.25	321.3	8443
	1.0	.609	.715	14.94	263.5	6888
	.62	.673	.632	12.25	226.9	6476

r	b	q	α_2	$E[R^3]$	$E[R^5]$	$E[R^7]$
7.5 con't.	.46	.705	.579	10.79	204.6	5883
	.32	.735	.516	9.35	183.3	5294
	.18	.762	.426	7.79	162.1	4813
	.133	.766	.386	7.31	156.2	4702
	.018	.609	.260	6.72	137.9	3946
8.0	120.	.098	.989	29.55	587.0	16290
	5.2	.355	.913	24.84	460.5	12091
	2.7	.456	.854	21.48	378.5	9466
	1.83	.520	.806	19.06	326.5	8215
	1.0	.616	.713	15.16	258.8	6758
	.577	.689	.617	11.91	210.1	5805
	.39	.729	.547	10.07	185.2	5243
	.21	.768	.444	7.95	158.9	4717
	.10	.777	.346	6.54	138.5	4112
	.01	.546	.250	6.64	133.9	3764
	.001	.222	.468	13.41	265.7	7392
	.00018	.109	.763	22.75	454.9	12720
9.0	122.	.099	.989	29.54	585.8	16210
	5.2	.361	.912	24.36	447.3	11680
	2.7	.464	.852	20.86	362.4	9159
	1.83	.529	.804	18.35	308.9	7817
	1.0	.626	.711	14.28	238.6	6323
	.576	.702	.613	11.05	194.6	5466
	.39	.743	.543	9.32	171.7	4956
	.21	.786	.438	7.22	145.5	4338
	.10	.800	.336	5.85	124.9	3772
	.01	.593	.219	5.64	114.3	3228
	.001	.250	.390	11.27	222.2	6194
	.00009	.095	.793	23.73	472.5	13160
10.0	125.	.099	.990	29.56	586.7	16247
	10.	.277	.948	26.52	496.4	12910
	3.0	.452	.863	20.94	363.3	9259

r	b	q	α_2	$E[R^3]$	$E[R^5]$	$E[R^7]$
10.0 con't.	2.3	.497	.833	19.27	333.2	7884
	1.7	.548	.793	17.26	290.6	7463
	1.0	.635	.710	13.70	227.3	5921
	.62	.703	.624	10.83	186.2	5119
	.46	.738	.570	9.26	166.3	4721
	.32	.772	.504	7.87	150.0	4425
	.17	.809	.401	6.07	124.4	3726
	.10	.819	.329	5.30	114.4	3482
	.05	.803	.260	4.70	100.9	3001
	.01	.635	.197	4.99	101.1	2867
11.0	127.	.099	.990	29.59	587.7	16268
	5.2	.369	.911	24.46	445.8	11500
	2.7	.475	.851	21.04	361.0	8763
	1.83	.541	.802	18.33	302.4	7374
	1.0	.642	.708	14.26	232.4	5899
	.575	.720	.609	10.72	176.7	4762
	.39	.764	.537	8.75	150.5	4237
	.21	.811	.430	6.50	123.1	3647
	.10	.834	.324	5.02	103.8	3123
	.01	.671	.180	4.02	82.92	2392
	.001	.304	.281	7.67	146.0	3928
	.000075	.104	.692	20.69	409.1	11410
15.0	132.	.099	.990	29.55	586.5	16280
	5.2	.378	.911	24.03	430.6	10920
	2.7	.487	.850	20.76	353.1	8581
	1.83	.556	.801	18.17	297.9	7287
	1.0	.660	.706	13.87	216.3	5292
	.574	.742	.605	10.12	155.1	4037
	.39	.788	.532	8.14	128.0	3525
	.21	.840	.423	5.79	99.25	2865
	.10	.871	.313	4.08	80.51	2412
	.01	.774	.143	2.71	57.37	1698
	.001	.403	.169	4.29	80.21	2159
	.0001	.150	.413	11.38	214.3	5816
	.00004	.105	.576	17.35	336.9	9308

APPENDIX B

A NOTE ON THE CORRECTION OF RANGE MOMENTS FROM SIMULATED

STRESS TIME HISTORIES

The range moments computed from a simulated time history may exhibit a considerable amount of scatter or statistical inaccuracy for a number of reasons. First, the random number generation algorithm used in the simulation will produce pseudo-random numbers which do not exactly fit the desired theoretical distribution. Second, any time history must also be of finite length, and is not the desired infinite sample of an ergodic process. Third, in the Gaussian simulation technique, the number of terms in the summation must be very large for the Central Limit Theorem to hold and an "exact" simulation result. In practice only 20 to 40 terms are used. Finally, the simulated time history is often sampled at a relatively small number of discrete time-points per cycle which may not exactly correspond to the times of occurrence of the extrema.

Lutes and Zimmerman (21,42) used an approximate procedure, which has also been applied to the results of this study, to correct for the "imperfections" in the simulated sequence of peaks and valleys. For example, before applying the correction Zimmerman found that the range moment (for $m = 7$) from 10 different simulations of the same process could vary as much as ±14% from the mean value. The corresponding corrected moments varied only ±1% from the mean.

The correction is based on the fact that the theoretical distribution of the peaks and valleys is known, Equation 2-20, and it corrects

for deviations of the simulated sequence from that distribution. The corrected range moment is defined by:

$$E[R^m]_C = \frac{E[Z^m]_T}{E[Z^m]_E} E[R^m]_E \tag{B-1}$$

in which:

$E[R^m]_C$ = corrected range moment

$E[R^m]_E$ = empirical range moment (from simulation)

$E[Z^m]_T$ = theoretical moment related to peak distribution

$E[Z^m]_E$ = empirical moment related to peak distribution (from simulation)

The justification for this correction is that the stress ranges are computed from the peak values, so that errors in the peak distribution moments should introduce comparable errors in the stress range moments. Two slightly different definitions of Z have been used to apply the correction. In the first definition Z was the absolute value of any peak or valley, so it is distributed as the absolute value of a peak. The alternative definition was to take Z as a peak value or the negative of a valley value, so it has simply the peak distribution.

The two definitions give essentially the same correction, so that the choice between them is a matter of convenience. For example, if m is an odd integer and {X(t)} is normal, defining Z as a peak value or negative of a valley value allows one to analytically evaluate the term $E[Z^m]_T$ in Equation B-1 (see Reference 21, Appendix II). For other cases this term must be evaluated numerically.

APPENDIX C

AR(1) Technique Simulation Cases

q	α_2	$r_1 = \hat{\phi}_1$
.058	.993	.95
.115	.975	.83
.125	.971	.82
.160	.954	.73
.189	.937	.65
.225	.915	.56
.254	.896	.48
.297	.868	.36
.327	.848	.29

APPENDIX D

AR(1) Superposition Technique Simulation Cases

	b	q	α_2
r = 1.5	21.	.091	.987
	2.0	.183	.946
	1.0	.204	.927
	.44	.204	.917
	.15	.166	.934
r = 2.0	41.	.097	.987
	3.0	.247	.923
	1.0	.321	.852
	.39	.336	.802
	.21	.312	.796
r = 2.5	20.	.142	.977
	2.0	.338	.871
	1.0	.398	.805
	.5	.430	.738
	.1	.359	.695
r = 3.0	70.	.098	.988
	3.0	.332	.890
	1.0	.450	.776
	.47	.497	.686
	.11	.450	.596
r = 3.5	20.	.166	.973
	2.0	.408	.843
	1.0	.488	.757
	.5	.543	.663
	.1	.508	.527
r = 4.0	88.	.098	.989
	2.8	.384	.871
	1.0	.517	.745
	.575	.570	.663
	.21	.600	.532
r = 4.5	20.	.179	.972
	2.0	.447	.831
	1.0	.539	.736
	.5	.608	.629
	.1	.690	.442

	b	q	α_2
r = 5.0	101.	.098	.989
	2.5	.427	.853
	1.0	.557	.730
	.39	.648	.579
	.04	.557	.382
r = 7.5	116.	.099	.989
	3.0	.435	.865
	1.0	.609	.715
	.32	.735	.516
	.133	.766	.386
r = 10.0	125.	.099	.990
	3.0	.452	.863
	1.0	.635	.710
	.10	.819	.329
	.01	.635	.197

APPENDIX E

Relating Extrema Correlations to the

Autocorrelation Function

The simulation of the extrema of a random process by means of an ARMA(p,q) model requires knowledge of the correlation of the extrema to estimate the parameters in the model. This appendix describes an effort that was made to formulate an analytical relationship between the correlation of extrema of a random process and its autocorrelation function. Although the problem remains unsolved, it is hoped that the work described herein may provide an indication of the direction future efforts should take. In approaching this problem it seemed more promising to attempt first to approximate the autocorrelation function, $R_{XX}(\tau)$, given that the extrema correlations were known. This information was then to be applied to the inverse problem of computing the extrema correlations from a known autocorrelation function.

E.1 The Step-Type Model

This section focuses on the way in which $R_{XX}(t)$ will be affected by the randomness of the occurrence time of the extrema of $X(t)$ when the correlation values for the magnitudes of the extrema are presumed to be known. Much of the effort is devoted to an attempt to find a reasonable model for a set of occurrence times $(t_1, t_2, t_3, \cdots)$. Let:

$$X(t) = \frac{P_j}{(m_p^2 + \sigma_p^2)^{\frac{1}{2}}} \text{ for } \tau_j \leq t \leq \tau_{j+1}$$

in which P_j is an extremum (either a peak or a valley) and the τ_j values are like the times midway between a peak and a valley. The normalization

used for $X(t)$ makes $E[X^2(t)] = 1$. This is arbitrary, but convenient in that it makes $\rho_{XX}(\tau) = R_{XX}(\tau)$. Assume that the τ_j's form a random sequence. Then a given interval τ, $(t, t + \tau)$, may include any number of τ_j arrivals. Let:

$N(s)$ = Number of arrivals in $(0,s)$

$N(t)$ = Number of arrivals in $(0,t)$

$N^* = N(S) - N(t)$ = Number of arrivals in (t,S)

Then: N^* = Even integer if $X(t)$ and $X(s)$ are both peak values or both valley values

N^* = Odd integer if one of $X(t)$ and $X(S)$ is a peak and the other is a valley

Let $\rho(j) = \rho_{P_k P_{k+j}}$ be the correlation coefficient for extrema. Then:

$$E[P_k P_{k+j}] = m_p^2 (-1)^j + \sigma_p^2 \rho(j) \qquad \text{(E-1)}$$

and:

$$E[X(t)X(S) | N^*] = \frac{1}{m_p^2 + \sigma_p^2} [m_p^2 (-1)^{N^*} + \sigma_p^2 \rho(N^*) \qquad \text{(E-2)}$$

Thus:

$$R_{XX}(\tau) = E[X(t)X(S)]$$

$$= \frac{1}{m_p^2 + \sigma_p^2} \sum_{j=0}^{\infty} P[N^* = j][m_p^2 (-1)^j + \sigma_p^2(j)] \qquad \text{(E-3)}$$

To evaluate $P[N^* = j]$, let $\Delta_j = \tau_{j+1} - \tau_j$ denote the interval length, also a random variable. Let A be the event that t and $t + \tau$ are in

the same interval, or the event that $t + \tau < \tau_{j+1}$ when $\tau_j \leq t \leq \tau_{j+1}$. Presuming that t is randomly located within Δ_j gives:

$$P[t < \tau + 1 - \tau | t \in \Delta_j, \Delta_j = u = \begin{cases} 1 - \frac{\tau}{u} & \text{for } u > \tau \\ 0 & \text{for } u < \tau \end{cases} \qquad (E-4)$$

Thus:

$$P(A) = \int p_{\Delta j}(u) P(A | \Delta_j = u, t \in \Delta_j) du \qquad (E-5)$$

Assuming that the Δ_j's are identically distributed, then:

$$P(A) = P(N^* = 0) = P(N^* < 1) = \int_{\tau}^{\infty} p_{\Delta}(u)(1 - \frac{\tau}{u}) du$$

$$= P(\Delta > \tau) - \int_{\tau}^{\infty} \frac{\tau}{u} p_{\Delta}(u) du \qquad (E-6)$$

The Poisson process is most commonly used for counting arrivals. It gives an exponential distribution for interarrival times, but that is not sufficiently flexible for the present problem. Rather, assume that the Δ_j's are gamma distributed and that there exists another related Poisson process with mean rate λ and exponentially distributed inter-arrival or wait times. Let $M(t)$ = the number of arrivals in $(0,t)$ for this new process, and let every k^{th} arrival of the new process be an arrival in the original $(\tau_1, \tau_2, \tau_3, \cdots)$ process. (The parameter k can be chosen later to give a reasonable approximation.) Thus:

$$N(t) = i \text{ if and only if } \quad ik \leq M(t) < (i + 1)K$$

and:

$$P(\Delta > \tau) = P[N(\tau) = 0] = P[M(\tau) < k]$$

$$= \sum_{i=0}^{k-1} \frac{(\lambda\tau)^i e^{-\lambda\tau}}{i!}$$

$$= P[T_K > \tau] \qquad\qquad (E-7)$$

in which T_k denotes the time of the kth arrival in the new process. Then:

$$p_{T_K}(\tau) = -\frac{d}{dt}\left[\sum_{i=0}^{k-1} \frac{(\lambda\tau)^i e^{-\lambda\tau}}{i!}\right]$$

$$= \lambda \sum_{i=0}^{k-1} \frac{(\lambda\tau)^i e^{-\lambda\tau}}{i!} - \sum_{i=1}^{k-1} \lambda \frac{(\lambda\tau)^{i-1} e^{-\lambda\tau}}{(i-1)!}$$

$$= \lambda \frac{(\lambda\tau)^{k-1}}{(k-1)!} e^{-\lambda\tau} \qquad\qquad (E-8)$$

Now for $k = 1$:

$$p_{T_1}(\tau) = \lambda e^{-\lambda\tau} \qquad\qquad (E-9)$$

So: $m_{T_1} = \frac{1}{\lambda}$ and $\sigma^2_{T_1} = \frac{1}{\lambda^2}$

Thus: $m_{T_k} = \frac{k}{\lambda}$ and $\sigma^2_{T_k} = \frac{k}{\lambda^2}$

Now for large k, a normal approximation to $P[T_k > \tau]$ gives:

$$P[T_k > \tau] \simeq \Phi\left(\frac{m_{T_k} - \tau}{\sigma_{T_k}}\right)$$

$$= \Phi\left(\frac{k/\lambda - \tau}{\sqrt{k}/\lambda}\right)$$

$$= \Phi\left(\frac{k - \lambda\tau}{\sqrt{k}}\right) \qquad\qquad (E-10)$$

Thus: $P(\Delta > \tau) = \Phi\left(\frac{k - \lambda\tau}{\sqrt{k}}\right)$ $\qquad\qquad (E-11)$

110

Also: $\int_\tau^\infty \frac{\tau}{u} p_\Delta(u)du = \frac{\lambda\tau}{k-1} P[M(\tau) < k-1]$

$$= \frac{\lambda\tau}{k-1} P[T_{k-1} > \tau]$$

$$\simeq \frac{\lambda\tau}{k-1} \Phi\left(\frac{k-1-\lambda\tau}{\sqrt{k-1}}\right) \qquad \text{(E-12)}$$

An expression for $P(N^* = 0)$ can then be written as:

$$P(N^* = 0) = P(N^* < 1) \simeq \Phi\left(\frac{k-1-\lambda\tau}{\sqrt{k}}\right) - \frac{\lambda\tau}{k-1} \Phi\left(\frac{k-1-\lambda\tau}{\sqrt{k-1}}\right) \qquad \text{(E-13)}$$

Assuming that t is in the interval Δ_i, there are two cases which, if they occur, will cause the event $[N^* > 1]$. Either there are 2 or more short intervals, $\Delta_i + \Delta_{i+1} < \tau$, or $\Delta_i + \Delta_{i+1} > \tau$, with $\Delta_{i+1} < \tau$ and $(\tau_{i+1} - t) > \tau - \Delta_{i+1}$. Thus:

$$P[N^* > 1] = P[\Delta_i + \Delta_{i+1} < \tau]$$

$$+ P[\Delta_i + \Delta_{i+1} > \tau, \Delta_{i+1} < \tau, \tau_{i+1} - t > \tau - \Delta_{i+1}]$$

and presuming $\tau_{i+1} - t$ to be uniform on $(0, \Delta_i)$ gives:

$$P[N^* > 1] = P[\Delta_i + \Delta_{i+1} < \tau] + P[\Delta_i + \Delta_{i+1} > \tau, t > \tau - \Delta_{i+1}]$$

$$= P[\Delta_i + \Delta_{i+1} < \tau] + \int_0^\tau \int_{\tau-v}^\infty p_{\Delta_i}(u) p_{\Delta_{i+1}}(v) \left(\frac{\tau - v}{u}\right) du\, dv \qquad \text{(E-14)}$$

Similarly, in general, for $[N^* > j]$:

$$P[N^* > j] = P[\Delta_i + \Delta_{i+1} + \dots + \Delta_{i+j} < \tau]$$

$$+ \int_0^\tau \int_{\tau-v}^\infty p_{\Delta_i}(u) p_{\Delta_{i+1}+\Delta_{i+2}+\dots+\Delta_{i+j}}(v) \left(\frac{\tau - v}{u}\right) du\, dv \qquad \text{(E-15)}$$

Assuming that the Δ_i's are i.i.d. with the gamma distribution, $G(k,\lambda)$, then $\Delta_i + \Delta_{i+1}$ is $G(2k,\lambda)$ distributed. Thus:

$$P[\Delta < \tau] = 1 - \sum_{j=0}^{k-1} \frac{(\lambda\tau)^j e^{-\lambda\tau}}{j!} \qquad (E\text{-}16)$$

$$P[\Delta_i + \Delta_{i+1} < \tau] = 1 - \sum_{j=0}^{2k-1} \frac{(\lambda\tau)^j e^{-\lambda\tau}}{j!} \qquad (E\text{-}17)$$

and the pdf's are:

$$p_{\Delta_i}(u) = \frac{\lambda(\lambda u)^{k-1} e^{-\lambda u}}{(k-1)!} \qquad (E\text{-}18)$$

$$p_{\Delta_{i+1} + \Delta_{i+2} + \ldots + \Delta_{i+j}}(v) = \frac{\lambda(\lambda v)^{jk-1} e^{-\lambda u}}{(jk-1)!} \qquad (E\text{-}19)$$

Next the assumed $G(k,\lambda)$ distribution of Δ can be approximated by $N(\frac{k}{\lambda},\frac{k}{\lambda^2})$ to give:

$$P[\Delta < \tau] \simeq \Phi\left(\frac{\tau - k/\lambda}{\sqrt{k}/\lambda}\right) = \Phi\left(\frac{\lambda\tau - k}{\sqrt{k}}\right) \qquad (E\text{-}20)$$

and similarly for $P[\Delta_i + \Delta_{i+1} + \ldots + \Delta_{i+j} < \tau]$:

$$P[\Delta_i + \Delta_{i+1} + \ldots + \Delta_{i+j} < \tau] \simeq \Phi\left(\frac{\lambda\tau - jk}{\sqrt{jk}}\right) \qquad (E\text{-}21)$$

These expressions then give the first terms in $P[N^* > 1]$ or $P[N^* > j]$.

Working with the inside integral of equation E-15 next, substituting equation E-18 for $p_{\Delta_i}(u)$ gives:

$$\int_{\tau-v}^{\infty} p_{\Delta_i}(u)\left(\frac{\tau - v}{u}\right)du = \tau - v \int_{\tau-v}^{\tau} \frac{1}{u} \frac{\lambda(\lambda u)^{k-1} e^{-\lambda u}}{(K-1)!} du$$

$$= \frac{\lambda(\tau - v)}{k-1} \int_{\tau-v}^{\infty} \frac{\lambda(\lambda u)^{k-2} e^{-\lambda u}}{(K-2)!} du \qquad (E\text{-}22)$$

112

Now the integral in this expression can be recognized as $P[Z > \tau - v]$ for a random variable Z which is $G(k - 1, \lambda)$ distributed. Approximating this with a $N\left(\dfrac{k - 1}{\lambda}, \dfrac{k - 1}{\lambda^2}\right)$ distribution gives:

$$\int_{\tau-v}^{\infty} p_{\Delta_i}(u)\left(\frac{\tau - v}{u}\right)du \simeq \frac{\lambda(\tau - v)}{k - 1} \, \Phi\left(\frac{v - \tau - \frac{k - 1}{\lambda}}{\sqrt{k - 1}/\lambda}\right)$$

$$\simeq \frac{\lambda(\tau - v)}{k - 1} \, \Phi\left(\frac{\lambda(v - \tau) - k + 1}{\sqrt{k - 1}}\right) \tag{E-23}$$

Approximating $p_{\Delta_{i+1}+\Delta_{i+2}+\ldots+\Delta_{i+j}}(v)$ as $N\left(\dfrac{jk}{\lambda}, \dfrac{jk}{\lambda^2}\right)$ gives:

$$p_{\Delta_{i+1}+\Delta_{i+2}+\ldots+\Delta_{i+j}}(v) \simeq \frac{1}{\sqrt{2\pi\frac{jk}{\lambda^2}}} \, \exp\left[-\frac{1}{2}\left(\frac{v - jk/\lambda}{\sqrt{jk/\lambda^2}}\right)^2\right]$$

$$\simeq \frac{\lambda}{\sqrt{2\pi jk}} \, \exp\left[-\frac{(\lambda v - jk)^2}{2jk}\right] \tag{E-24}$$

Now the double integral of equation E-15 can be written as:

$$\frac{\lambda^2}{(k - 1)\sqrt{2\pi jk}}\int_0^{\tau} (\tau - v)\exp\left[-\frac{(\lambda v - jk)^2}{2jk}\right]\Phi\left[\frac{\lambda(v - \tau) - k + 1}{\sqrt{k - 1}}\right]dv \tag{E-25}$$

This can be written in dimensionless form by letting $\lambda v = u$, $v = u/\lambda$, and $dv = du/\lambda$:

$$\frac{1}{(k - 1)\sqrt{2\pi jk}}\int_0^{\tau} (\lambda\tau - u)\exp\left[-\frac{(u - jk)^2}{2jk}\right]\Phi\left[\frac{u - \lambda\tau - k + 1}{\sqrt{k - 1}}\right]du \tag{E-26}$$

The equations necessary to compute $P[N^* = j]$ can be summarized as:

$$P[N^* = 0] = \Phi\left(\frac{k - \lambda\tau}{\sqrt{k}}\right) - \frac{\lambda\tau}{k - 1} \, \Phi\left(\frac{k - 1 - \lambda\tau}{\sqrt{k - 1}}\right) \tag{E-27}$$

113

$$P[N^* > j] = \Phi(\frac{\lambda\tau - jk}{\sqrt{jk}})$$

$$+ \frac{1}{(k-1)\sqrt{2\pi jk}}\int_0^\tau (\lambda\tau - u)\exp[-\frac{(u-jk)^2}{2jk}]\Phi[\frac{u - \lambda\tau - k + 1}{\sqrt{k-1}}]du \quad (E-28)$$

$$P[N^* = 1] = 1 - P[N^* > 1] - P[N^* = 0] \quad (E-29)$$

$$P[N^* = j] = P[N^* > j-1] - P[N^* > j], \ j = 2,3,... \quad (E-30)$$

To evaluate the usefulness of this model, an example case was evaluated for a 1-block psd with ω_1 = 6.0, ω_2 = 9.0, for which α_2 = 0.975 and q = 0.115. Rice's peak distribution was evaluated for this psd to determine m_p^2 = 1.4932 and σ_p^2 = 0.4576, and from simulations the extrema correlations were estimated as ρ_1 = -0.8334, ρ_2 = 0.5095, ρ_3 = -0.1888, ρ_4 = -0.0248 and ρ_j = 0 for j $\geq$ 5.

A value of k = 1000 was found to give a reasonable estimate for the first two extrema of $R_{XX}(\tau)$, as shown in Table E-1. A larger value of k could be used to better fit to the first extrema of $R_{XX}(\tau)$, but at the cost of worsening the agreement for the later extrema. In addition, k = 1000 corresponds to a coefficient of variation for Δ of $V_\Delta = \frac{1}{\sqrt{k}}$ = 0.0316, while the estimate from simulation was found to be V_Δ = 0.20, which corresponds to k = 25. This indicates that the distribution for Δ required for the model to fit $R_{XX}(\tau)$ is much narrower than the distribution actually observed. It was also found that this model failed to produce a decay in the estimated autocorrelation extrema which was as fast as that of the actual autocorrelation function, as shown in Table E-1. Neither could the beat effect, which is evident

114

TABLE E-1

Comparison of $R_{XX}(\tau)$ Extrema Values to Values
Predicted by Step-Type Model

$R_{XX}(\tau)$ Extrema	Step-Type Estimate
-.94	-.91
.76	.82
-.51	-.74
.25	.68

1-block psd: $\omega_1 = 6.0$, $\omega_2 = 9.0$
$\alpha_2 = 0.975$, $q = 0.115$
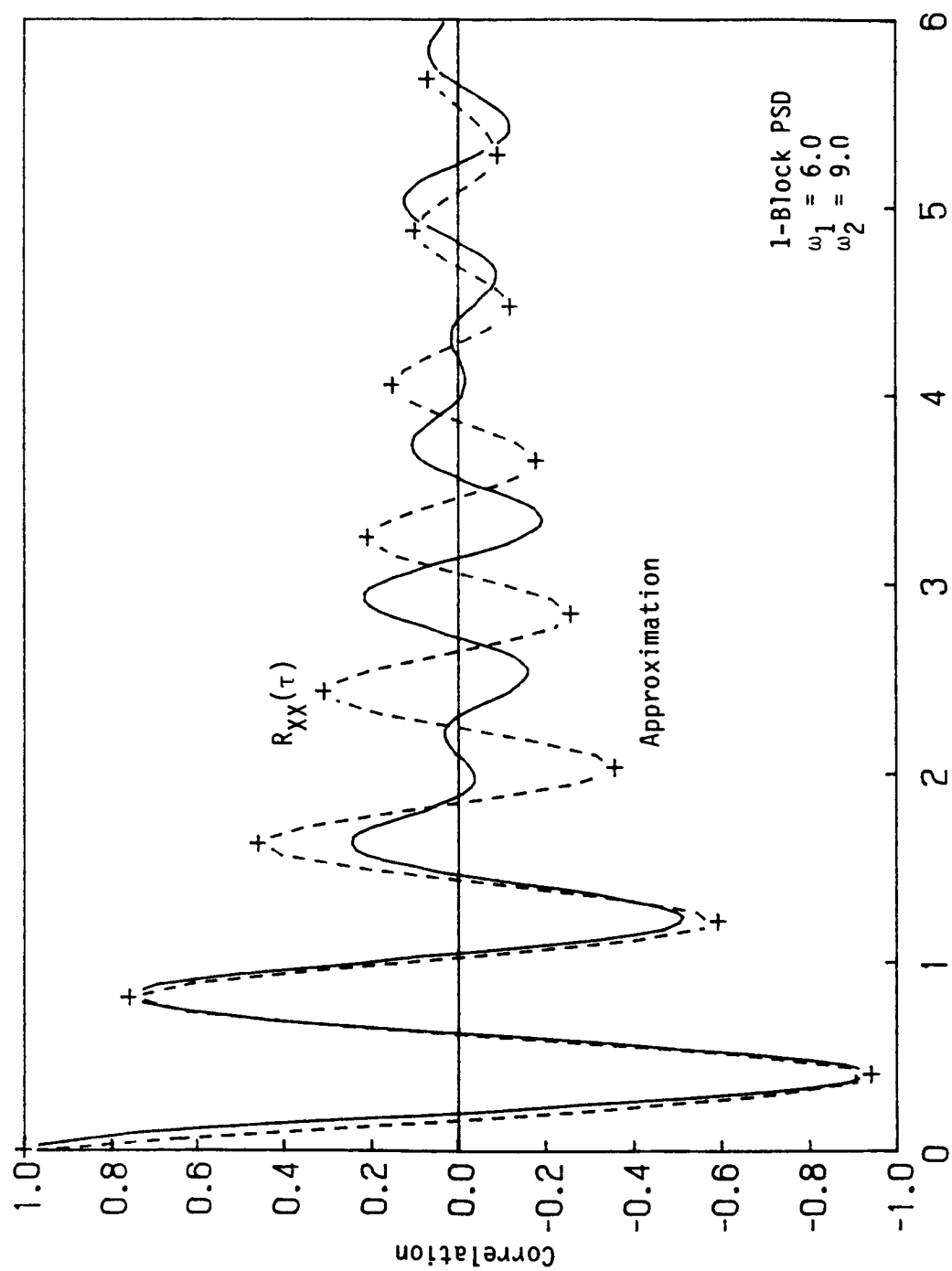
Figure E-1 Comparison of $R_{XX}(\tau)$ to Approximation

116
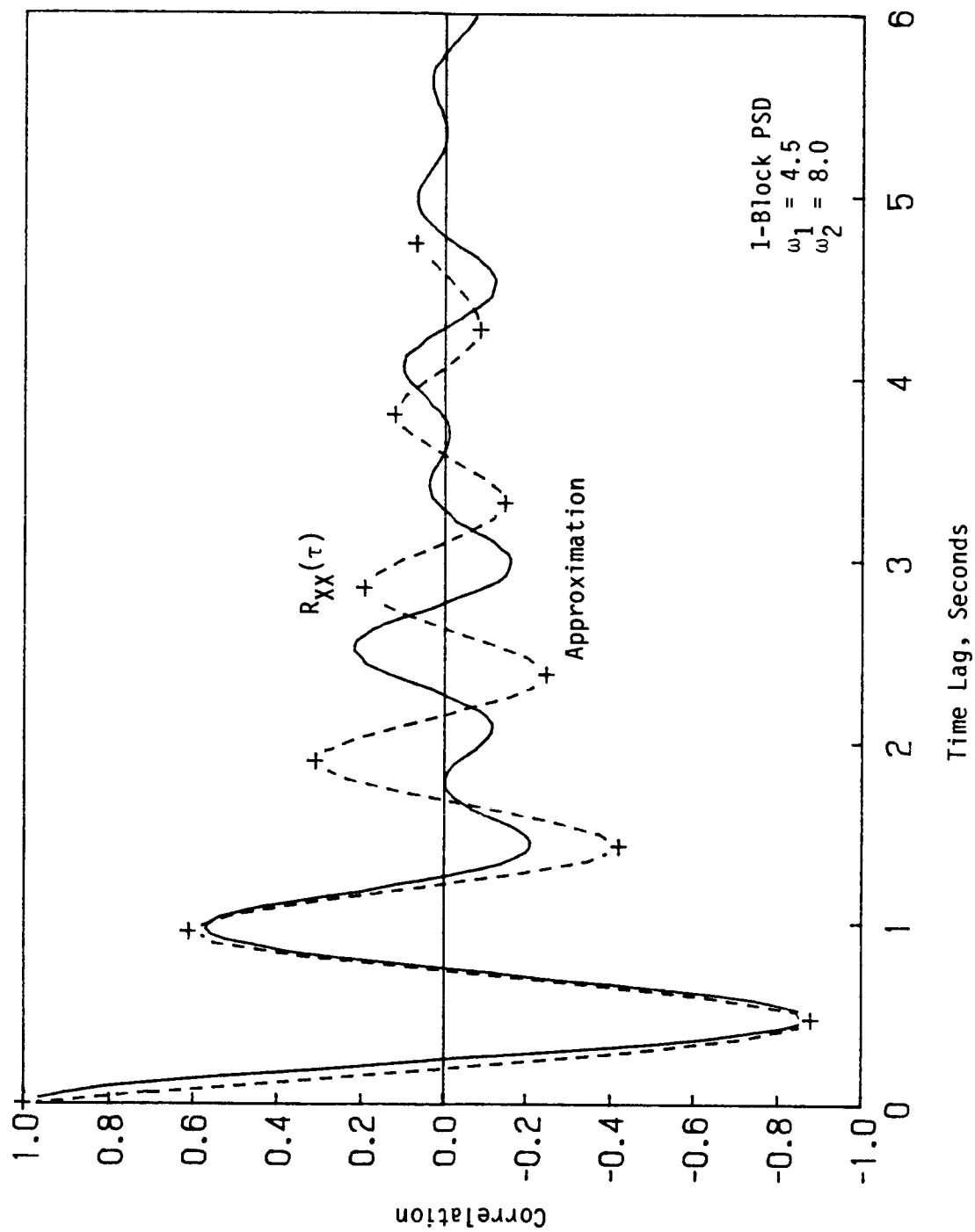
Figure E-2 Comparison of $R_{XX}(\tau)$ to Approximation

117
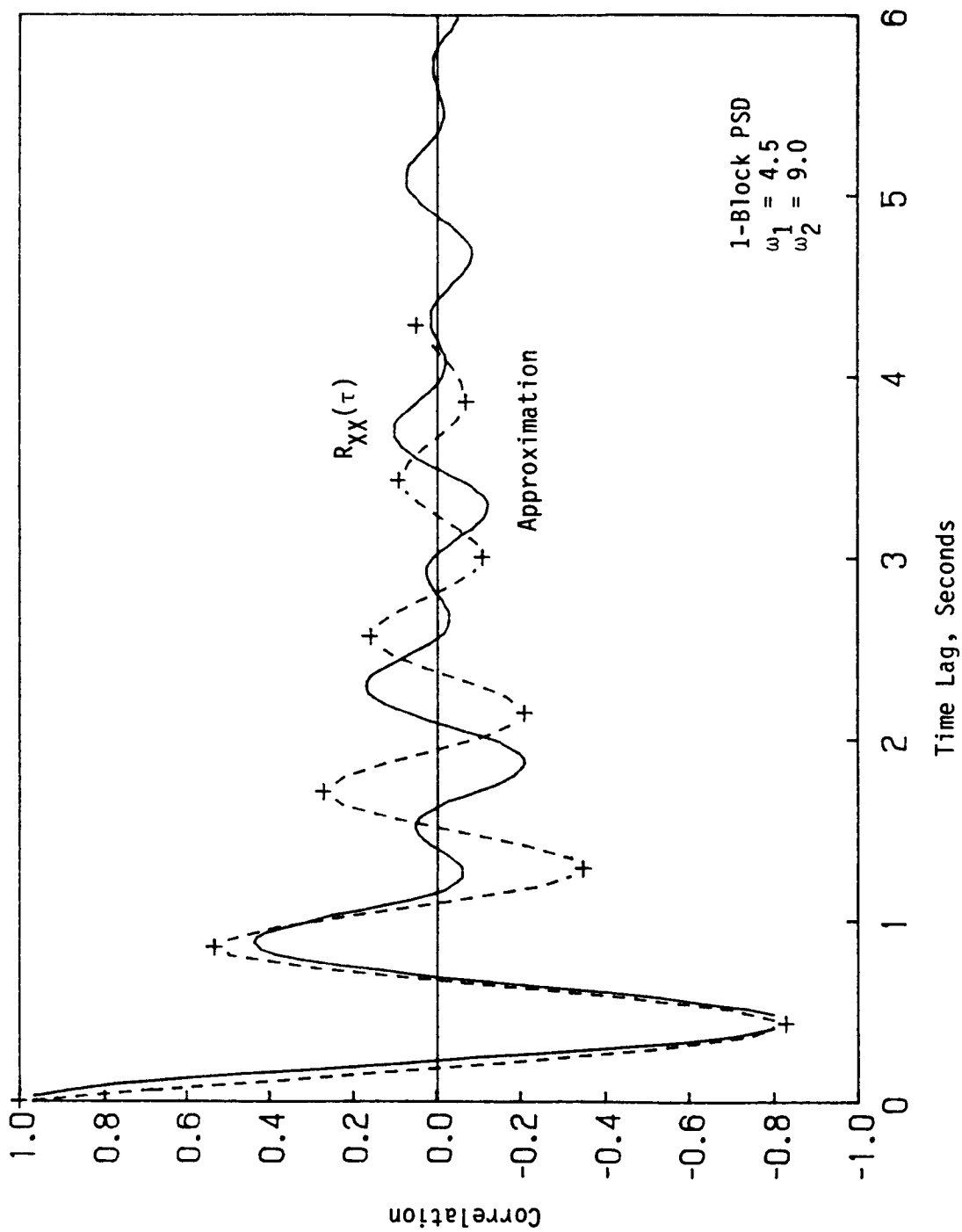
Figure E-3 Comparison of $R_{XX}(\tau)$ to Approximation

118
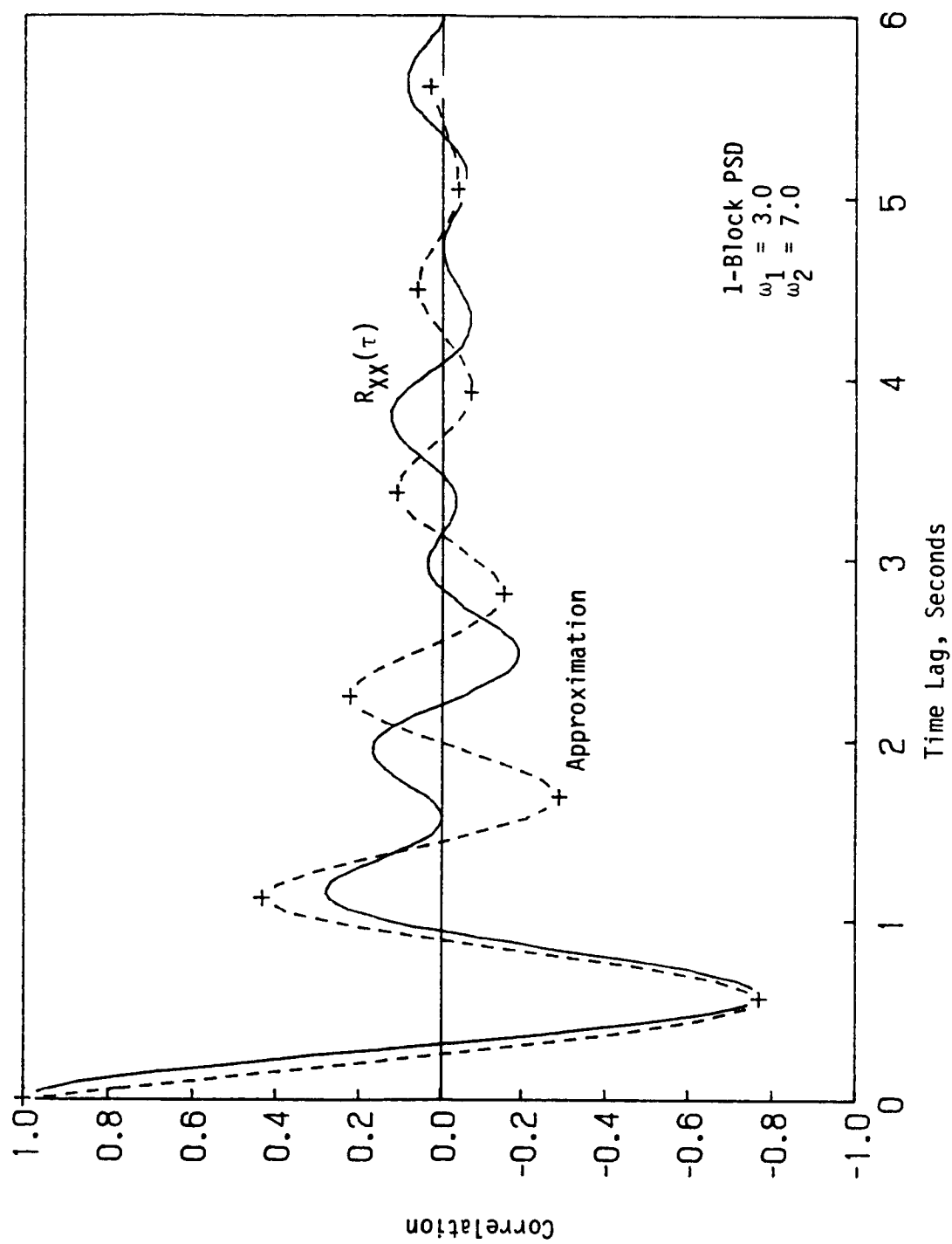
Figure E-4 Comparison of $R_{XX}(\tau)$ to Approximation

119
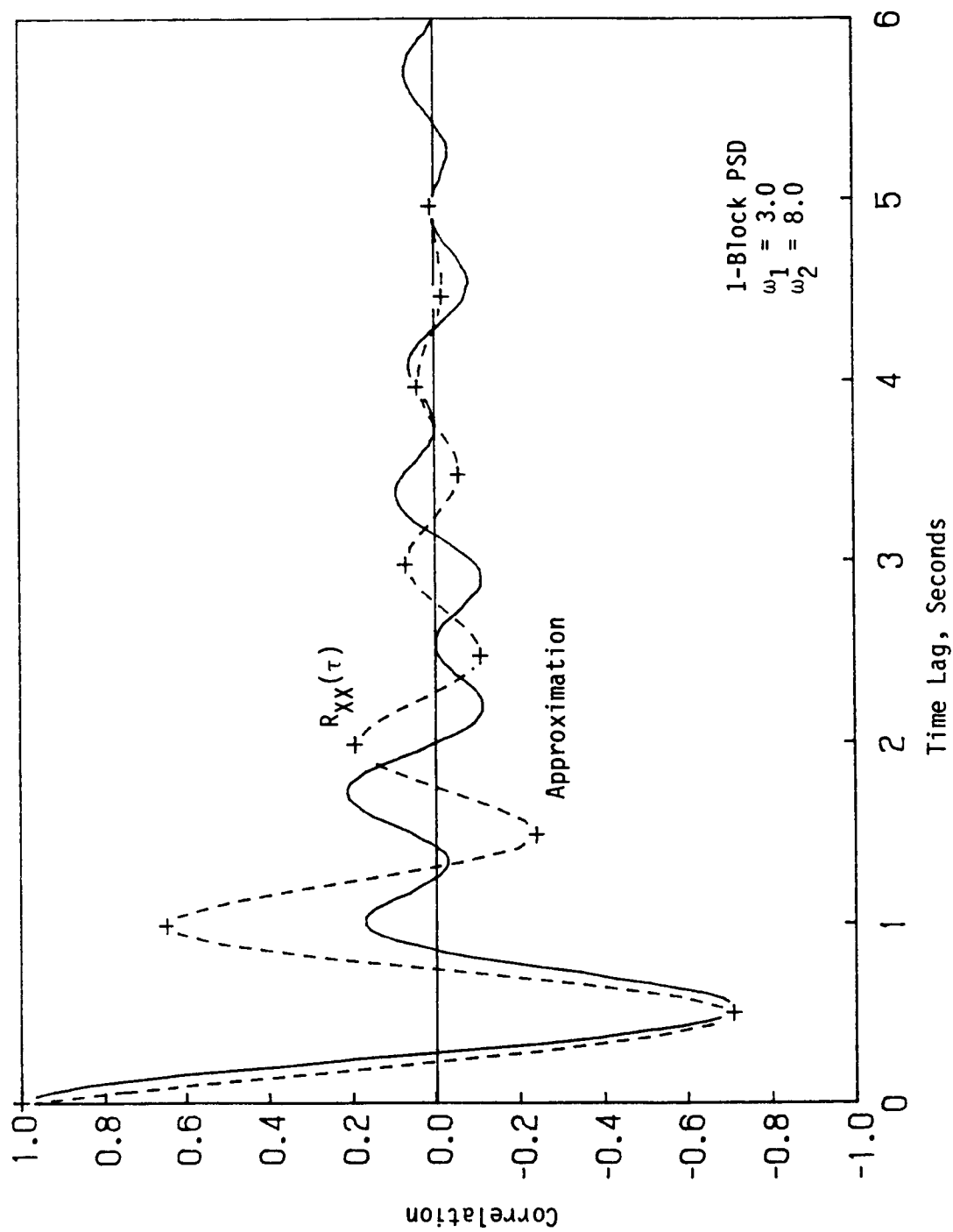
Figure E-5 Comparison of $R_{XX}(\tau)$ to Approximation

120
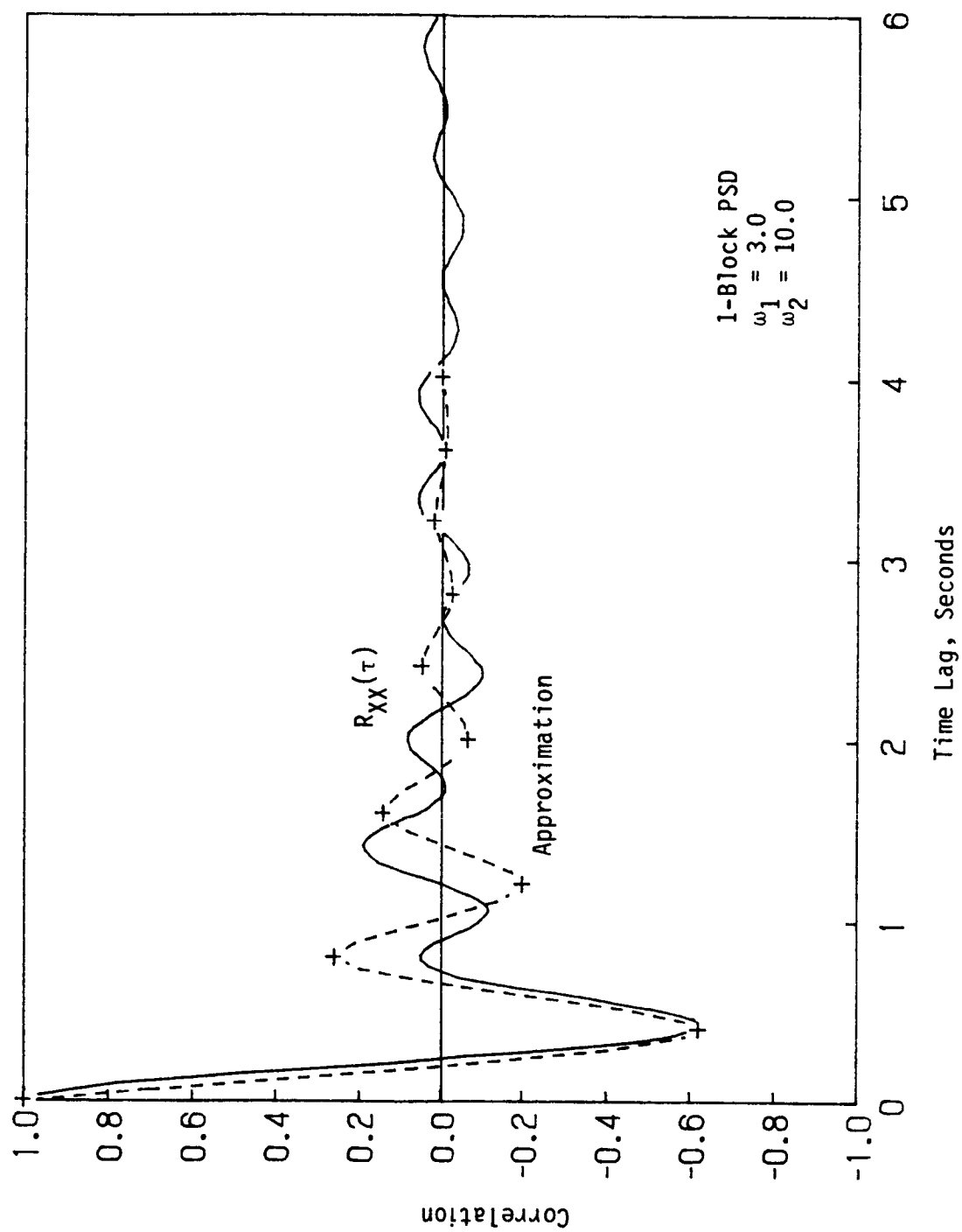
Figure E-6 Comparison of $R_{XX}(\tau)$ to Approximation

121
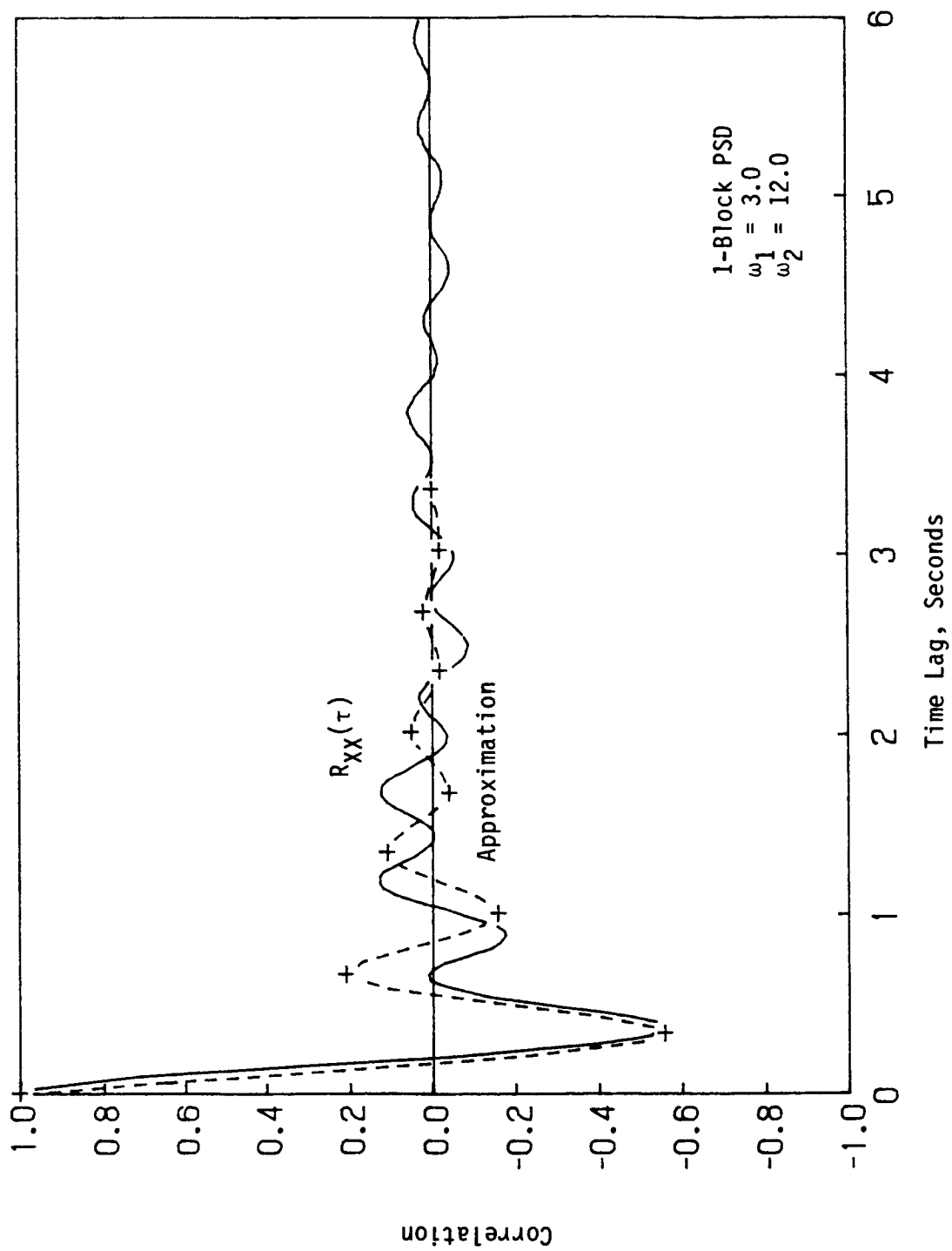
Figure E-7 Comparison of $R_{XX}(\tau)$ to Approximation

122

in $R_{XX}(\tau)$ (see Figures 3.19-3.24 for example), be reproduced by this model.

E.2 A Normal Approximation for the Distribution of N^*

Rather than using equations E-27 to E-30 to find $P[N^* = j]$ it is convenient to use a normal approximation for the distribution of N^*. Using the usual half-integer approximation for application of the normal distribution to a discrete random variable gives:

$$P[N^* > j] = 1 - \Phi \left(\frac{j + 0.5 - m_{N^*}}{\sigma_{N^*}} \right)$$

$$P[N^* < j] = \Phi \left(\frac{j + 0.5 - m_{N^*}}{\sigma_{N^*}} \right)$$

This can be written as:

$$P[N^* = j] = \beta \tag{E-31}$$

$$P[N^* < j] = P[N^* > j] = \frac{1 - \beta}{2} \tag{E-32}$$

with:

$$\Phi(u) = 1 - \frac{1 - \beta}{2} = \frac{1 + \beta}{2} \tag{E-33}$$

if

$$m_{N^*} = j$$

and

$$u = \frac{0.5}{\sigma_{N^*}}$$

Obviously $m_{N^*} = j$ only at the time $\tau = \frac{jk}{\lambda}$, where λ is the arrival

rate in the Poisson process (for which every k^{th} arrival counts as one N^* arrival). If one neglects the probability that $|N^* - m_{N^*}| \geq 2$, then this gives:

$$P[N^* = j \,|\, \lambda\tau = jk] = \beta \qquad\qquad (E\text{-}34)$$

$$P[N^* = j + 1 \,|\, \lambda\tau = jk] = P[N^* = j - 1 \,|\, \lambda\tau = jk] = \frac{1 - \beta}{2} \qquad (E\text{-}35)$$

Substituting into equation E-3 gives:

$$R_{XX}(\tau) = \frac{1}{m_p^2 + \sigma_p^2} \left\{ (2\beta - 1)m_p^2(-1)^{\frac{\lambda\tau}{k}} \right.$$

$$\left. + \sigma_p^2 \left[\beta\rho\left(\frac{\lambda\tau}{k}\right) + \frac{1 - \beta}{2}\left[\rho\left(\frac{\lambda\tau}{k} - 1\right) + \rho\left(\frac{\lambda\tau}{k} + 1\right)\right]\right]\right\} \qquad (E\text{-}36)$$

Let $R_{XX}(\tau_1)$ denote the value of the first valley of $R_{XX}(\tau)$. Using an observed value of $R_{XX}(\tau)$ along with $\rho_0 = 1$ and observed values of ρ_1 and ρ_2, one can solve equation E-36 for β. The value of u corresponding to this first valley is then found from equation E-33 as:

$$u = \Phi^{-1}\left(\frac{1 + \beta}{2}\right) \qquad\qquad (E\text{-}37)$$

Based on the results for Poisson arrivals it is reasonable to presume that σ_{N^*} grows like $\sqrt{m_{N^*}}$. This gives $u_j = \frac{u}{\sqrt{j}}$ for $j > 1$. From equation E-33 one then finds the β for use in equation E-34 for $P[N^* = j]$. In general one must consider $\frac{1 - \beta}{2}$ to give $P[N^* > j]$ and $P[N^* < j]$; $1 - \Phi(3u)$ to give $P[N^* > j + 1]$ and $P[N^* < j - 1]$, etc. As j becomes large, the values for $P[N^* = j + 2] = P[N^* = j - 2]$ become significant and must be incorporated into the model. In this study they were included when they exceeded a value of 0.001. A reasonably good estimate

of the overall decay of $R_{XX}(\tau)$ as τ grows results from this model, as shown in Figures E-1 through E-7. However, the beat effect in $R_{XX}(\tau)$ is still not accounted for. In addition, the value of u or β used to fit the model to a particular $R_{XX}(\tau)$ must still be related, if only empirically, to some parameter of either $R_{XX}(\tau)$ or the psd.

E.3 A Phase-Angle Approximation

An improvement to the step-type model was sought by considering $X(t)$ to behave harmonically in the neighborhood of an extremum. Particularly for a narrowband process and with the time lag τ equal to a small number of half-periods there is little uncertainty about how many extrema have occurred, but there is uncertainty about the precise location of the anticipated extremum. To illustrate, let the initial time be at a peak and the second time be near the following valley:

$$X(t) = P_1$$

$$X(t + \tau) \simeq V_1 \cos\theta$$

$$\tau = \frac{1}{n_p} \tag{E-38}$$

with θ a random variable, $|\theta|$ small and $m_\theta = 0$. Then:

$$E[X(t)X(t + \tau)|X(t) = P_1] = E[P_1 V_1 \cos\theta] \tag{E-39}$$

Assuming P_1 and V_1 are independent of θ gives:

$$E[P_1 V_1 \cos\theta] = E[P_1 V_1]E[\cos\theta]$$

$$= [-m_p^2 + \sigma_p^2 \rho_1]E[\cos\theta] \tag{E-40}$$

125

Assuming that $R_{XX}(\tau)$ for $E[X^2] = 1$ is approximately equal to $E[X(t)X(t + \tau)|X(t) = P_1]$ normalized by $E[P^2]$ gives:

$$R_{XX}(\tau) \simeq \frac{-m_p^2 + \sigma_p^2 \rho_1}{m_p^2 + \sigma_p^2} \, E[\cos\theta] \qquad \text{(E-41)}$$

The small θ assumption gives:

$$E[\cos\theta] \simeq 1 - \frac{E[\theta^2]}{2} + \frac{E[\theta^4]}{4!} \qquad \text{(E-42)}$$

and assuming θ is normally distributed gives:

$$E[\cos\theta] \simeq 1 - \frac{\sigma_\theta^2}{2} + \frac{\sigma_\theta^4}{8} \qquad \text{(E-43)}$$

An attempt to quantify θ was made by relating it to T, the "time" between extrema. For n half-cycles:

$$T = n\pi + \theta \qquad \text{(E-44)}$$

so that:

$$m_T = n\pi$$

$$\sigma_T^2 = \sigma_\theta^2$$

$$V_T = \frac{\sigma_\theta}{n\pi} \qquad \text{(E-45)}$$

Thus, knowledge of V_T would suffice to give a value for σ_θ. Based on the results for Poisson arrivals it seems reasonable to expect V_T to be approximately the same as V_{N^*} for the number of extrema in an interval of length m_T. An equation is available for $E[N^2]$ (6,39), in which N is the number of zero crossings of $\{X(t)\}$ in $(0,T)$:

$$E[N^2] = E[N] + \frac{2}{\pi^2} \int_0^T (T - \tau) \frac{(M_{33}^2 - M_{34}^2)^{1/2}}{[1 - r^2(\tau)]^{3/2}}$$

$$\times \left[1 + \frac{M_{34}}{(M_{33}^2 - M_{34}^2)^{1/2}} \tan^{-1}\left(\frac{M_{34}}{(M_{33}^2 - M_{34}^2)^{1/2}}\right) \right] d\tau \qquad \text{(E-46)}$$

in which:

$$r(\tau) = R_{XX}(\tau)$$

M_{ij} = cofactor of (ij)th element of the covariance matrix of the random variables $X(t_1), X(t_2), \dot{X}(t_1), \dot{X}(t_2)$, with $\tau = t_2 - t_1$

Letting N^* denote the number of extrema occurrences, the above equation can be used to compute V_{N^*} because $E[N^2]$ for $\{\dot{X}(t)\}$ gives $E[N^{*2}]$ for $\{X(t)\}$. Empirical simulation results were also used to compute V_T for comparison with V_{N^*} computed using equation E-46. As shown in Table E-2, the assumption that $V_{N^*} = V_T$ is not supported by these results, although the trends of increasing V with increasing bandwidth are quite similar. V_{N^*} was also computed from equation E-46 for $E[N^*]$ = 1, 2, 3 and 4 for psd 1 of Table E-2. Table E-3 compares these results to V_T observed from simulations and also to the V_T values which would be required in order that equations E-41 and E-43 would match empirical values of $R_{XX}(\tau)$. Again, the empirical V_T values are up to 32% smaller than the calculated V_N values. Even more serious, though, is the discrepancy in computing $R_{XX}(\tau)$. The V_N values are as much as five times larger than what one would need for V_T to make equation E-41 be correct. The serious discrepancy between empirical V_T values and the values required for equation E-41 indicates that

127

some assumptions made in deriving equation E-41 must be in error. In particular, empirical data from simulations indicate that the terms [PV] and [cosθ] in the model are not independent, so the following has been proposed to account for the correlation:

$$E[PV \cos\theta] = E[PV]E[\cos\theta] + \rho_{PV,\cos\theta}\sigma_{PV}\sigma_{\cos\theta} \qquad (E-47)$$

For practical use, further simulation data were used to compute an empirical correction factor, K, to account for the correlation:

$$R_{XX}(\tau) \simeq \frac{-m_p^2 + \sigma_p^2\rho_1}{m_p^2 + \sigma_p^2} K \left[1 - \frac{\sigma_\theta^2}{2} + \frac{\sigma_\theta^4}{8} \right] \qquad (E-48)$$

Figures E-8 and E-9 show K vs q and σ_θ^2 vs q, respectively, for 1-block unimodal and smooth unimodal psd's; that is, psd types a) and c) of Figure 3.1. Note that these data indicate that K and σ_θ^2 for the smooth unimodal psd's are significantly different from the values observed for the 1-block psd, for q > 0.3. That is, bandwidth seems to have a much more significant effect on K and σ_θ^2 for the smooth unimodal psd than for the 1-block psd.

Table E-2

Comparison of V_N* to V_T for 5 Unimodal PSD's

__1-Block PSD__

	$\underline{\omega}_1$	$\underline{\omega}_2$	$\underline{V_N*}\left(\begin{matrix}\text{Equation}\\ \text{E - 46}\end{matrix}\right)$	$\underline{V_T}$ (Empirical)
1	6.0	9.0	.3325	.2260
2	4.5	8.0	.3838	.2667
3	4.5	9.0	.4100	.2997
4	3.0	7.0	.4355	.3159
5	3.0	10.0	.4687	.3508

Table E-3

V_N* Compared to V_T for $E[N^*] = 1,2,3,4$
(1-Block PSD, $\omega_1 = 6.0$, $\omega_2 = 9.0$)

$\underline{E[N^*]}$	$\underline{V_N*}\left(\begin{matrix}\text{Equation}\\ \text{E - 46}\end{matrix}\right)$	$\underline{V_T}$ (Empirical)	$\underline{V_T}$ (Required)
1	.3325	.2260	.0651
2	.2329	.1754	.0846
3	.1884	.1529	.0913
4	.1616	.1380	.0922
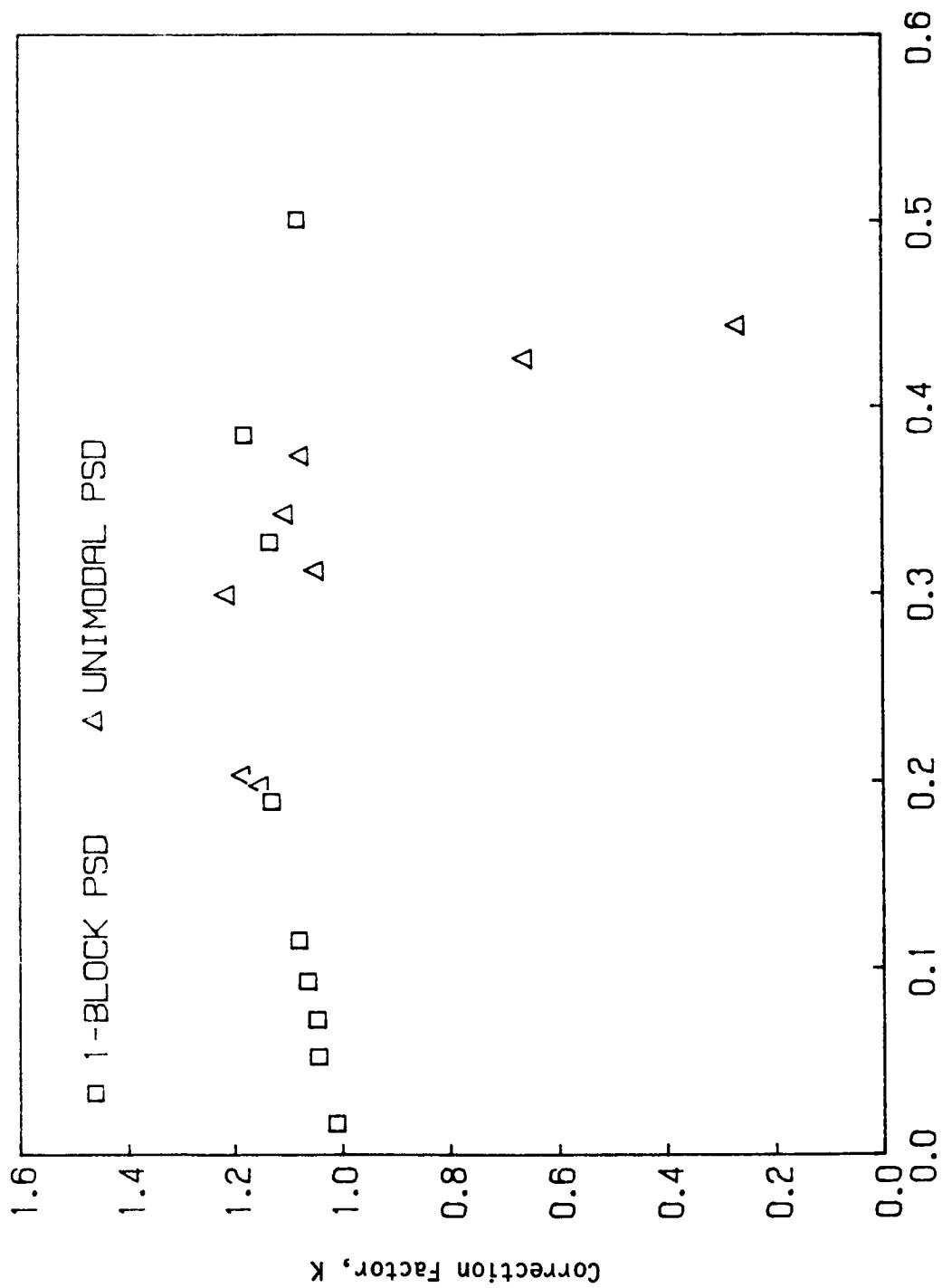
Figure E-8   Correction Factor, K vs. Vanmarcke's Parameter
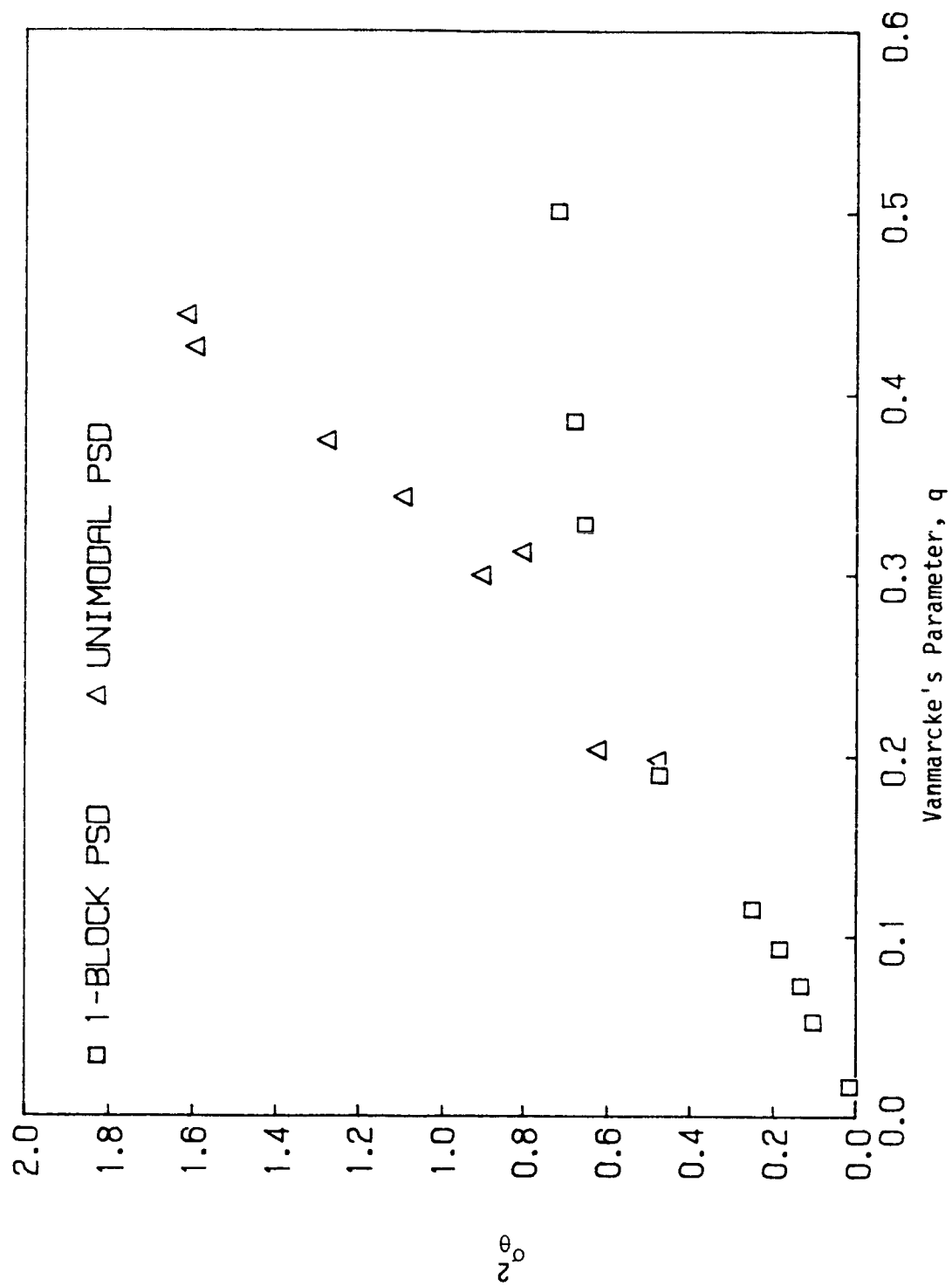
Figure E-9 σ_θ^2 vs. Vanmarcke's Parameter

131

E.4 A Second Simplification to the Step-Type Approximation

Because of the results of the previous section, showing that $V_{N^*} \neq V_T$, the following development was in an attempt to relate V_{N^*} to V_T. Assume a simple distribution for N^* of:

$$P[N^* = j] = \beta$$

$$P[N^* = j - 1] = P[N^* = j + 1] = \frac{1 - \beta}{2} \qquad (E-49)$$

Then:

$$E[N^*] = j$$

$$E[N^{*2}] = j^2 + 1 - \beta$$

$$VAR[N^*] = 1 - \beta$$

$$V_{N^*} = \sqrt{1 - \beta}/j \qquad (E-50)$$

Again assuming that Δ is gamma distributed, $G(k,\lambda)$, gives:

$$E[\Delta] = \frac{k}{\lambda}$$

$$VAR[\Delta] = \frac{k}{\lambda^2}$$

$$V_\Delta = 1/\sqrt{k} \qquad (E-51)$$

Recall the previous result for $P[N^* = o]$, equation E-27:

$$P[N^* = 0] = \Phi[\frac{k - \lambda\tau}{\sqrt{k}}] - \frac{\lambda\tau}{(k - 1)} \Phi[\frac{k - 1 - \lambda\tau}{\sqrt{k - 1}}] \qquad (E-52)$$

To fit the first extrema of $R_{XX}(\tau)$, set $\lambda\tau = k$:

$$P[N^* = 0] = \frac{1}{2} - \frac{k}{k - 1} \Phi [\frac{-1}{\sqrt{k - 1}}] \qquad (E-53)$$

Empirical data for V_Δ can be used to compute k as:

$$k = \frac{1}{V_\Delta^2} \qquad\qquad (E-54)$$

A value for $P[N^* = 0]$ can be computed from equation E-53, and a value for β from E-49. Finally, a value for $V_{N}* = \sqrt{1 - \beta}$ can be compared to the value of $V_{N}*$ computed using equation E-46 for $E[N^* = 1]$. The results of the comparison are summarized in Table E-4 for five unimodal psd's. The relative agreement between the two calculations for $V_{N}*$ indicates that equation E-46 might be used to compute $V_{N}*$ for a given psd, from which $V_{N}* = \frac{\sqrt{1-\beta}}{j}$ could be used to estimate $P[N^* = j]$, $P[N^* = j - 1]$, and $P[N^* = j + 1]$ according to equations E-49. However, a comparison of this approach with the results of the normal simplification to the step-type model, Section E.2, indicates that the distribution for N^*, computed as outlined above, is not as sharply peaked as was found to be required in Section E.2 for the step-type model to fit the extrema of $R_{XX}(\tau)$. This is shown in Table E-5 in which the value of β computed from E-49 is compared to the value computed from equation E-36 for the five psd cases of Table E-4.

Table E-4

Comparison of $V_N^* = (1 - \beta)^{1/2}$ to V_N^*, using Equation E-46

1-Block PSD

	ω_1	ω_2	V_Δ (Empirical)	k	$P[N^* = 0]$	$V_N^* = (1-\beta)^{1/2}$	V_N^* (E-46)
1	6.0	9.0	.2260	19.58	.0689	.3712	.3325
2	4.5	8.0	.2667	14.06	.0812	.4031	.3838
3	4.5	9.0	.2997	11.13	.0844	.4107	.4100
4	3.0	7.0	.3159	10.02	.0882	.4200	.4355
5	3.0	10.0	.3508	8.13	.0944	.4345	.4687

134

Table E-5

Comparison of β Values

PSD Case	β, Equation E-49	β, Equation E-36
1	0.862	0.990
2	0.838	0.969
3	0.831	0.957
4	0.824	0.939
5	0.811	0.890

REFERENCES

1. Benjamin, J.R. and Cornell, C.A., Probability Statistics and Decision for Civil Engineers, McGraw Hill, 1970.

2. Borgman, L.E., "Ocean Wave Simulation for Engineering Design," Journal of Waterways and Harbors Division, Proceedings of the American Society of Civil Engineers, No. WW4, 1969, pp. 556-583.

3. Box, G.E.P., and Jenkins, G.M., Time Series Analysis: Forecasting and Control, Holden-Day, 1976.

4. Chang, M.K., et al., "ARMA Models for Earthquake Ground Motions," Operations Research Center Technical Report ORC 79-1, University of California, Berkeley, California, January, 1979.

5. Corazao, M., "Stress Ranges Produced by Stochastic Loads," Masters Thesis, Rice University, Houston, Texas, 1981.

6. Cramer, H., and Leadbetter, M.R., Stationary and Related Stochastic Processes, John Wiley & Sons, Inc., New York, New York, 1967, pp. 128-143.

7. Crandall, S.H., and Mark, W.D., Random Vibration in Mechanical Systems, Academic Press, 1963.

8. Dowling, N.E., "Fatigue Failure Predictions for Complicated Stress-Strain Histories," Journal of Materials, Vol. 7, No. 1, March, 1972, pp. 71-87.

9. Downing, S.D., and Socie, D.F., "Simple Rainflow Counting Algorithms," International Journal of Fatigue, Vol. 4, No. 1, January, 1982, pp. 31-40.

10. Gersch, W., "Estimation of the Autoregressive Parameters of a Mixed Autoregressive Moving-Average Time Series," Institute of Electrical and Electronic Engineers Transactions on Automatic Control, AC-15, 1970, pp. 583-588.

11. Gersch, W., and Luo, S., "Discrete Time Series Synthesis of Randomly Excited Structural System Response," Journal of the Acoustical Society of America, Vol. 51, 1972, pp. 402-408.

12. Gersch, W., and Sharpe, D.R., "Estimation of Power Spectra with Finite-Order Autoregressive Models," Institute of Electrical and Electronic Engineers Transactions on Automatic Control, AC-18, 1973, pp. 367-369.

13. Gersch, W., and Foutch, D., "Least-Squares Estimates of Structural System Parameters Using Covariance Function Data," Institute of Electrical and Electronic Engineers Transactions on Automatic Control, AC-19, 1974.

136

14. Gersch, W., and Yonemoto, J., "Synthesis of Multivariate Random Vibration Systems: A Two-Stage Least Squares ARMA Model Approach," _Journal of Sound and Vibration_, Vol. 52, No. 4, June 22, 1977, pp. 553-565.

15. Gersch, W., and Martinelli, F., "Estimation of Structural System Parameters from Stationary and Non-Stationary Ambient Vibrations: An Exploratory-Confirmatory Analysis," _Journal of Sound and Vibration_, Vol. 65, No. 3, August 8, 1979, pp. 303-318.

16. Gersch, W., and Brotherton, T., "Parametric Time Domain Analysis of the Multiple Input/Scalar Output Problem: The Source Identification Problem," _Journal of Sound and Vibration_, Vol. 69, No. 3, April 8, 1980, pp. 441-460.

17. Gersch, W., and Brotherton, T., "Estimation of Stationary Structural System Parameters from Non-Stationary Random Vibration Data: A Locally Stationary Model Method," _Journal of Sound and Vibration_, Vol. 82, No. 2, March 22, 1982, pp. 215-227.

18. Gersch, W., and Kitagawa, G., "A Time Varying AR Coefficient Model for Modelling and Simulating Earthquake Ground Motion," _Earthquake Engineering and Structural Dynamics_, Vol. 13, No. 2, March-April, 1985, pp. 243-254.

19. Jenkins, G.M., and Watts, D.G., _Spectral Analysis and Its Applications_, Holden-Day, Inc., San Francisco, California, 1968.

20. Lin, Y.K., _Probabilistic Theory of Structural Dynamics_, Krieger Publishing Co., Inc., Melbourne, Florida, 1976.

21. Lutes, L.D., Corazao, M., Hu, S-L.J., and Zimmerman, J.J., "Stochastic Fatigue Damage Accumulation," _Journal of the Structural Division_, ASCE, Paper 19823, Vol. 110, No. ST11, 1984, pp. 2585-2601.

22. Newland, D.E., _An Introduction to Random Vibrations and Spectral Analysis_, Longman Group Limited, London, 1975.

23. Nigam, N.C., _Introduction to Random Vibrations_, the MIT Press, Cambridge, Massachusetts, 1983.

24. Matsuishi, M., and Endo, T., "Fatigue of Metals Subjected to Varying Stress," Presented to the Japan Society of Mechanical Engineers, Fukuoka, Japan, March, 1968.

25. Miles, J.W., "On Structural Fatigue Under Random Loading," _Journal of Aeronautical Sciences_, November, 1954, pp. 753-762.

26. Miner, M.A., "Cumulative Damage in Fatigue," _Journal of Applied Mechanics_, Vol. 12, 1945, pp. A159-A164.

27. Palmgren, A., "Die Lebensdauer von Kugallagern," Ver. Deut. Ingr., Vol. 68, 1924, pp. 339-341.

28. Pfeiffer, Paul E., Concepts of Probability Theory, Dover, New York, New York, 1978.

29. Pfeiffer, Paul E., and Schum, David A., Introduction To Applied Probability, Academic Press, New York, New York, 1973.

30. Polhemus, N.W., and Cakmak, A.S., "Simulation of Earthquake Ground Motions Using Autoregressive Moving-Average (ARMA) Models," Earthquake Engineering and Structural Dynamics, Vol. 9, 1981, pp. 343-354.

31. Reed, D.A., and Scanlan, R.H., "Time Series Analysis of Wind Loading on Hyperbolic Cooling Towers," submitted for publication in the Journal of Structural Engineering, ASCE.

32. Rice, S.O., "Mathematical Analysis of Random Noise," Bell Technical Journal, Vol. 23, 1944, and Vol. 24, 1945; reprinted in Selected Papers on Noise and Stochastic Processes, Wax, ed., Dover, 1952.

33. Samaras, E., Shinozuka, M., and Tsurui, A., "ARMA Representation of Random Processes," Journal of Engineering Mechanics, ASCE, Vol. 111, No. 3, March, 1985, pp. 449-461.

34. Sarkani, S., "Experimental and Analytical Stochastic Fatigue of Welded Steel Joints," Ph.D. Thesis, Rice University, 1986.

35. Shinozuka, M., "Simulation of Multivariate and Multi-Dimensional Random Processes," Journal of the Acoustical Society of America, Vol. 49, 1971, pp. 357-367.

36. Shinozuka, M., and Jan, C-M., "Digital Simulation of Random Processes and Its Applications," Journal of Sound and Vibration, Vol. 25, No. 1, 1972, pp. 111-128.

37. Spanos, P.-T.D., and Hansen, J.E., "Linear Prediction Theory for Digital Simulation of Sea Waves," Journal of Energy Resources Technology, ASME, Vol. 103, 1981, pp. 243-249.

38. Spanos, P.-T.D., "ARMA Algorithms for Ocean Spectral Analysis," Engineering Mechanics Research Laboratory, Technical Report EMRL-1137, The University of Texas at Austin, Texas, June, 1982.

39. Steinberg, H., Schultheiss, P.M., Wogrin, C.A., and Zweig, F., "Short Time Frequency Measurements of Narrow-Band Random Signals by Means of a Zero Counting Process," Journal of Applied Physics, 26, 1955, pp. 195-201.

40. Vanmarcke, E.H., "Properties of Spectral Moments with Applications to Random Vibration," Journal of the Engineering Mechanics Division, ASCE, Vol. 98, No. EM2, 1972, pp. 425-446.

41. Wirsching, P.H., and Light, M.C., "Fatigue Under Wide Band Random Stresses," Journal of the Structural Division, ASCE, Paper 15574, Vol. 106, No. ST7, 1980, pp. 1593-1607.

42. Yang, J.-N., "Simulation of Random Envelope Processes," Journal of Sound and Vibration, Vol. 21, No. 1, 1972, pp. 73-85.

43. Zimmerman, J.J., "Stochastic Stress History Simulation for Fatigue Analysis," Masters Thesis, Rice University, 1983.

1. Report No.	2. Government Accession No.	3. Recipient's Catalog No.
TM 100464		

4. Title and Subtitle	5. Report Date
Random Process Simulation for Stochastic Fatigue Analysis	March 1988
	6. Performing Organization Code

7. Author(s)	8. Performing Organization Report No.
Curtis E. Larsen	S-576
	10. Work Unit No.

9. Performing Organization Name and Address	11. Contract or Grant No.
Lyndon B. Johnson Space Center Houston, Texas 77058	
	13. Type of Report and Period Covered

12. Sponsoring Agency Name and Address	Technical Memorandum
National Aeronautics and Space Administration Washington, D.C. 20546	14. Sponsoring Agency Code

15. Supplementary Notes

This report was submitted to Rice University by the author in partial fulfillment of the requirements for the degree Ph.D.

16. Abstract

A simulation technique is described which directly synthesizes the extrema of a random process and is more efficient than the Gaussian simulation method. Such a technique is particularly useful in stochastic fatigue analysis because the required stress range moment, $E[R^m]$, is a function only of the extrema of the random stress process. The family of autoregressive moving average (ARMA) models is reviewed and an autoregressive model is presented for modeling the extrema of any random process which has a unimodal power spectral density (psd). The proposed autoregressive technique is found to produce rainflow stress range moments which compare favorably with those computed by the Gaussian technique and to average 11.7 times faster than the Gaussian technique. The autoregressive technique is also adapted for processes having bimodal psd's. The adaptation involves using two autoregressive processes to simulate the extrema due to each mode and the superposition of these two extrema sequences. The proposed autoregressive superposition technique is found to be 9 to 13 times faster than the Gaussian technique and to produce comparable values for $E[R^m]$ for bimodal psd's having the frequency of one mode at least 2.5 times that of the other mode. A key parameter in the autoregressive model is the correlation coefficient ρ_1 between adjacent extrema. A linear regression of ρ_1 on Vanmarcke's bandwidth parameter is presented as a practical description of ρ_1's dependence on bandwidth for both unimodal and bimodal psd's. The effect of psd shape on the expected fatigue damage rate is also investigated. For bimodal psd's the contribution of the two frequency components to the damage rate is determined for frequency ratios from 1.5 to 15. The relative contribution of the two modes is measured by a parameter b which is the ratio of the mean squared value of the high frequency component to that of the other component. It is found that both components must be considered for b values from 0.01 to 10. The effect of high frequency truncation of the psd on the expected damage rate is also studied for two unimodal psd's.

17. Key Words (Suggested by Author(s))	18. Distribution Statement
fatigue, random processes, simulation, stochastic processes, computer methods	Unclassified - Unlimited Subject Category: 65

19. Security Classif. (of this report)	20. Security Classif. (of this page)	21. No. of pages	22. Price*
Unclassified	Unclassified	150	